DETERMINATION OF THE GRAVITY DISTRIBUTION IN THE WEST AFRICAN LITHOSPHERE USING MODIFIED GEOPOTENTIAL GRAVITY MODEL

BY

EWUMI, TAOFIK OLUBUNMI
B.Sc(Hons) Physics (Ado-Ekiti), M.Sc Physics (Ibadan)
Matric. Number: 102561

A THESIS IN THE DEPARTMENT OF PHYSICS
SUBMITTED TO THE FACULTY OF SCIENCE
IN PARTIAL FULFILMENT OF THE REQUIREMENTS FOR THE AWARD OF THE DEGREE OF

DOCTOR OF PHILOSOPHY
OF THE
UNIVERSITY OF IBADAN

JUNE, 2021

DEDICATION

This research work is dedicated to Almighty God, the giver of life who has made it possible for me to complete this programme successfully and to my wife and children who were always available with adequate cooperation, understanding and encouragements throughout the period of the programme.

ABSTRACT

Exploitation of minerals and other factors including density variations reduce the stability of the lithosphere from changes in Earth's compactibility. The Geopotential Gravity Models (GGMs) are presently used to determine the stability of the continental and oceanic regions separately, but could not handle regions of the lithosphere which combine continental and oceanic regions. This study was therefore designed to develop a modified GGM that will cater for combined continental and oceanic regions.

A Two-Staged modelling method was employed. The density of the continental region was varied with that of the oceanic region to obtain a compensation factor η. This was used to normalise the density contrast, which resulted from gravity field variation. The normalised density component was then used as an input factor into the existing GGM to produce the Modified Geopotential Gravity Model (MGGM). Space coordinates within longitude 30˚W-15˚E and latitude 3˚-20˚N were used in spherical harmonic model to simulate Gravity Data (GD) for different pre-chosen coordinates. Also, measured GD of Itakpe area in Kogi State, Nigeria were obtained from the Nigerian Geological Survey Agency (NGSA), Abuja. Results were validated by comparing the values of gravity of the simulated GD using MGGM and GGM with measured gravity values. The simulated GD from MGGM, GGMs and measured GD of Itakpe served as input data into Markov Chain Monte-Carlo (MCMC) inversion process to obtain density anomalies. Density data were analysed using descriptive error estimation approach.

The modified model was: $V(z,\phi,\lambda)=\frac{GM}{r}\left[1+\frac{\eta}{4\hat{\lambda}G}\sum_{n=2}^{N}(2\gamma-1)\frac{\rho_0 gz}{K}\right]^{\frac{1}{n-1}}\sum_{m}^{n}(J_{nm}Cosm\lambda+K_{nm}Sinm\lambda).P_{nm}(Sin\phi)$

where V is the gravity potential, G is gravitational constant, γ is the number of Earth layers, g is the theoretical gravity, ρ_o is the density of the crust, k is bulk modulus and Z is the depth coordinate. V values of continental and oceanic lithospheres were obtained for latitudes $4.9358^{\circ}N$ to $12.4273^{\circ}N$and longitudes $13.4213^{\circ}W$ to $12.3502^{\circ}E$ which ranges from 85.6 to 249.7m^2/s^2 and 73.8 to 215.6 m^2/s^2, while the measured V for latitudes $5.8156^{\circ}N$ to $14.3912^{\circ}N$ and longitudes 15.0498°W to $10.4657^{\circ}E$ were 79.4 to 261.5 m^2/s^2 and 62.7 to 208.3 m^2/s^2, respectively. The density of the Earth's lithospheric segment obtained from MCMC with depth ranged from 0 to 860 Km for the continent, varied between 9.7 and 26.5 x 10^{3}Kg/m^3, while oceanic region varied between 14.6 and 33.2 x 10^{3}Kg/m^3 with a depth range of 0 to 255 Km. The obtained values of density vary slightly from the observed density of the Earth's lithosphere having values of 8.5 to 24.9 x 10^{3}Kg/m^3 and 12.7 to 30.5 x 10^{3}Kg/m^3 for continent and ocean, respectively. Average errors ranging from $\pm$0.3% to $\pm$11.4% and $\pm$0.5% to $\pm$28.5% were obtained when densities from MGGM and GGM using MCMC were compared with the density of Itakpe. These indicated that MGGM performed better than GGM.

The MGGM determined the lithospheric stability of combined continental and oceanic regions of West Africa simultaneously. This model could be extended to other regions of Africa.

Keywords: Lithospheric Stability, spherical harmonic coefficients, Gravity field, Anomaly, Geopotential

Word count: 496

ACKNOWLEDGMENTS

I sincerely appreciate God Almighty, the Alpha and Omega (known as the beginning and the ending), the great I am that I am, Jehovah El-Shaddai, The Omnipotent, Omniscient and Omnipresent, The great giver of life and The Eternal Rock of Ages for His divine presence, abundant blessings, His infinite mercies, all-the-time-provisions, unshakable protection and His unending love throughout the duration of this programme in the University.

My profound gratitude goes to my research supervisor in person of Dr. Adegoke Adedeji Adetoyinbo for His guidance and constructive critisizm during the research. I must equally acknowledge the support and knowledge contribution of my lecturers in the Department of Physics, University of Ibadan. They are Prof. J.A. Adegoke, Prof. Folorunso Ogundare, Dr O.I. Popoola, Dr F.L. Aderemi, Dr T.T. Ogunseye, Dr A. Ojoawo, Dr T.A. Otunla, Dr E.O.Joshua, Prof. Janet A. Ademola, Dr Mojisola A. Adeniyi, Dr E.O. Ogunsola, Dr E.F. Nymphas, Dr Oshakuade, Dr Ezekiel Oyeniyi and all members of staff of the department of Physics most especially the Solid Earth Physics unit. I am highly indebted to Prof. Adeniyi A. Ogunjobi in the department of Microbiology, University of Ibadan. It is your efforts that has made this work successful. I also thank Prof. F. Matthew-Ojelabi who has contributed a lot to the successful completion of this work and my goal attainment in life. My profound gratitude also goes to Prof. A.I. Mukolu, Dr M.O. Isinkaye, Dr E.B. Faweya, Dr K.A. Aduloju, Dr E.A.A Oyedele, Dr O.R. Salau, Dr G.E. Adesakin, Dr A.T. Fatigun and all members of staff in the Department of Physics, Ekiti State University, Ado-Ekiti, Nigeria.

This research is incomplete without showing gratitude to my darling wife, Mrs D.O. Ewumi, a great pillar and children Daniel Oluwaseun Ewumi, Samuel Oluwadamilola Ewumi, Emmanuel Oluwaseyi Ewumi and Ezekiel Oluwatobiloba Ewumi who God has used immensely and for the great understanding shown especially when I am away from home for this assignment to be accomplished. I am also grateful to my brother Mr Olufemi Abdul-Gaffar Adetokunbo Ewumi. I am also grateful to all my brethren, the prayer champion/warrior in the Redeemed Christian Church of God, Ropheka Mega/Area Parish, Ekute Ado-Ekiti and the Pastors in succession in charge of the

church for their spiritual contribution. I am also grateful to my spiritual mentors, Pst. Jonathan Oladele Adamolekun, Pst. ‘Dapo Longe, Pst Titi Olaofe, Pst. Tolulope Oluwatuyi (Mummy Ɣomi), Pst Olatubosun Emmanuel Oyedele, Dcns. Gloria Chinyere Otunaiya, Pst Ebenezer Kayode Ariyibi and Dcn. Ayodele Owolabi. I sincerely thank all the people that God had used to make this research a success. My God will remember you all for good in Jesus Mighty and Wonderful name Amen. Thank you all.

CERTIFICATION

This is to certify that this research work was carried out by Taofik Olubunmi EWUMI under my supervision in the Department of Physics, Faculty of Science, University of Ibadan, Nigeria.

Supervisor
A. A. Adetoyinbo
B.Sc.(Hons), M.Sc., Ph.D. (Ibadan)
Department of Physics,
University of Ibadan, Nigeria

TABLE OF CONTENTS

LIST OF FIGURES

LIST OF TABLES

CHAPTER ONE
INTRODUCTION

1.1 Background to the Research

An interesting area of Earth science is the study of gravity. Gravity is the force which tends to attract all objects towards the centre of the Earth. Gravity value changes as objects move from one position of the Earth surface to another. The rigid outer layer of the Earth is known as the lithosphere which is about 100Km (63miles) in thickness. This layer which comprises of the crust and upper mantle is usually hard and brittle. The brittle condition causes it to fracture when strongly stressed to produce a rupture. This rupture then produces an earthquake, which is the violent release of elastic energy. The energy produced emanated from the pressure build-up within the Earth subsurface region which passes through weak fault zones and escape to the Earth surface.

The Earth gravity can be expressed in form of a model. Gravity model is a mathematical representation of gravity by simple algebraic expression. It is known as any mathematical gravity equation which requires solution to a given Earth problem. Gravity models can be used to determine the distribution of gravity over a particular region of the Earth.

The West African lithosphere is a distinct sector of the African continent which combines continental and oceanic regions. Many operations performed by man were carried out on either of these regions of the Earth (continental or oceanic). Such operations which include rock blasting in quarries, drilling, mining, borehole, mineral exploitation, oil exploration and many more, alters the Earth body thereby generating density variation or mass anomaly. This variation produces stability problems. However, since mass changes, density is also altered. Thus, many gravity models in existence (GGMs) have been used to assess or measure the distribution of gravity in either the continental or oceanic lithosphere. This research work was therefore designed to determine the gravity potential distribution across the West African sector (having Latitude 3^{o} to 20^{o} N and Longitude 30^{o}W to 15^{o}E) using a modified

geopotential gravity model that can handle or cater for both continental and oceanic stability problems simultaneously.

At this junction, it is desirable to understand what stability is all about as regards Earth's operations. Stability is an important geophysical phenomenon which indicates the physical conditions of the Earth's lithosphere and also depicts the nature of subsurface structures. It shows the region of the lithosphere which are susceptible to both natural and artificial anti-Earth activities. Stability is majorly a tectonic problem which requires adequate attention and must be addressed accordingly (Johnston, 1990).

1.2 Statement of Research Problem

Several human operations generate some negative consequences and also pose a threat on the stability of the lithosphere. These operations which include rock blasting of a specified region, hydro-geological drilling, exploitation of minerals, oil exploration, mining of subsurface regions and heavy construction of sky scrapers were critically assessed using the existing geopotential gravity models (GGMs). However, the existing GGMs could not handle simultaneously, the regions of the lithosphere which combine continental and oceanic lithospheres as in the case of West Africa. Hence, a hypothesis was proposed having explored all the available gravity models in existence and a genuine question was raised. The question is that 'Is it possible to develop a robust single geopotential gravity model that will be able to address lithospheric stability issues and problems irrespective of continental or oceanic region'?

This question has generated a great debate in the world of geophysical science. From this question, analysis of the two combined regions of West Africa was proposed by creating another gravity model also known as the modified model version. The gravity distribution across the continental-oceanic segment was determined from modified model and compared with the existing GGM_S.

1.3 Knowledge Gap

Many areas of the Earth including the continents and ocean have been investigated using the existing GGM_S. This has allowed for the monitoring of the stability of the lithosphere due to changes in the Earth gravity values. The existing gravity models had

been used to solve problems of continents and oceans separately. However, there is a need to look for a more robust gravity model which can handle regions that combined both continents and ocean. Thus, one of the existing GGM_S (Wiechert, 2008) was then modified by introducing a parameter known as 'compensation factor η' to produce the Modified Geopotential Gravity Model (MGGM). This factor accounts for the ocean-continent interaction which previous models did not consider or address. Therefore, η bridges the gap between land and sea regions. These regions comprises of the onshore and offshore areas.

It is important to also know that the ocean-continent region of West African lithosphere has not been totally explored by previous existing gravity models. The West African sector was assessed using different gravity models for different regions of the sector. The MGGM tend to explore the combined ocean-continent regions of West African sector to solve stability problems.

1.4 Justification of the Research

The geophysical study of gravity distribution have been undertaken with the existing GGM_S which is required to address the problems of continental and oceanic region separately. However, little or no attention has been paid to the development of a gravity model that can cater for these two regions of the lithosphere simultaneously. Also, information about gravity distribution in continental-oceanic shelf using the existing models were not available and scanty information of density contrast and mass anomalies by past researchers were monitored and registered.

This study was therefore designed to develop a modified GGM (an improvement to the existing models) that will cater for or handle both regions of West Africa. This is achieved by introducing a compensation factor η into the existing GGM to normalize the density contrast, which resulted from gravity field variations. This input factor η which is the ratio of the compaction of the continent to that of the ocean defined in the MGGM (which existing model lack) was found to account for the ocean-continent interaction such that any natural or artificially inclined operation performed within one region will automatically affect the mass or density components of the other region.

1.5 Aim and Objectives of the Research

The aim of the research work is to determine the stability and strength of the West African lithospheric segment from subsurface mass distribution using the gravity model.

The objectives are to:

(1) Modify a model that will produce the gravity potential across the West African sector.
(2) Validate a model whose data can be compared with standard data elsewhere.
(3) Explore satellite gravity data through suites of numerical simulations.
(4) Determine the subsurface mass distribution.
(5) Determine the density contrast and mass anomaly from information on the Earths compactibility to achieve stability.
(6) Predict future Earths events and detect areas of natural disaster.

The aim and objectives stated will be achieved using the approach outlined below:

(1) Markov chain Monte Carlo method of numerical integration
(2) Bouguer formula for gravity-density relations
(3) Computed gravity data will be validated with the observed data to check the reliability of the model employed.

1.6 Area of Study

The area of study in this research work is the West African region of the African continent (Figures. 1.1 and 1.2). This region of Africa is characterized by certain tectonic features which make it distinct from other regions of the world. The West African sector is a region which links the activities of the continental margin to that of the ocean thereby bridging the gap between land and sea. The continent of Africa is categorized and partitioned into the following regions:

(i)West Africa: which is the region lying between longitude (30^{o}W and 15^{o}E) and latitude (3^{o}N and 15^{o}N). This region is characterized by variations in geo-potential values and gravity anomalies, geoidal undulations and upper crustal inhomogeneities. The anomaly pattern over the Atlantic Ocean and the gravity field or signature which suggests faults, troughs, folds in these regions will be considered in this research using

the MGGM. It comprises of Cameroon, Ghana, Togo, Republic of Benin, Nigeria, Cote D'ivoire, Guinea, Gambia, Senegal, Burkina Faso, Mali, Liberia, Gabon, Congo, Niger, Sierra Leone, Chad and Guinea Bissau.

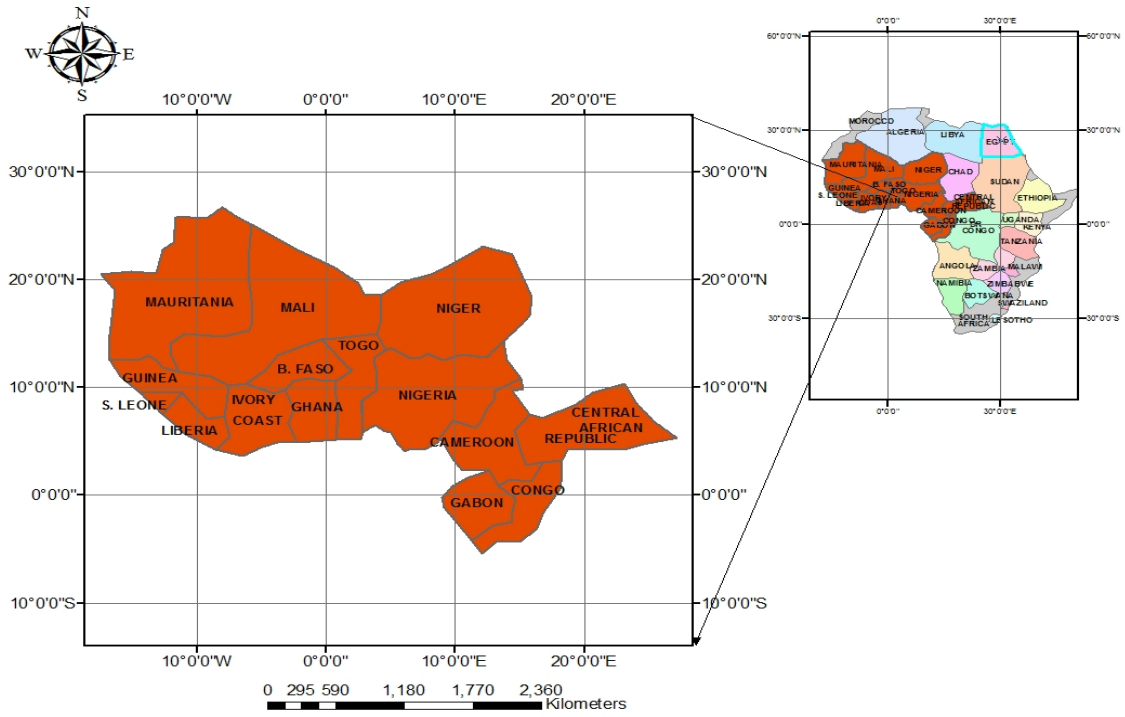

Figure 1.1: The Map of West Africa (Region carved out from world map, 2019)

Figure 1.2: The Map of West Africa (Adapted from world map, 2016)

(ii) East Africa: This covers the region of longitude (30^oE-50^oE) and latitude (15^oS-15^oN) constituting about 18 territories including the Island nations in Indian Ocean. Mount Kilimanjaro and Lake Victoria are the two striking geographical features in this region. The prominent positive anomaly which follows the East African rift system is a characteristic of this region. It comprises of Ethiopia, Kenya, Tanzania, Burundi, Somalia, Eritrea, Djibou, Malawi, Zambia, Zimbabwe, Rwanda, Uganda, Madagascar and Mozambique.

(iii) South Africa: This region lies between longitude (10^oE-50^oE) and latitude (15^oS - 35^oS). This sector which is known for the positive anomalies suggest an extension of East African rift system. It covers the region which includes Cape-town, Lesotho, Swaziland and Pretoria.

(iv) Central and North Africa: It is a region lying between longitude (20^oW-35^oE) and latitude (15^oN-30^oN). This area is also characterized by anomalies of different geological features which cannot be tied to any surficial features. It also comprises of Morocco, Algeria, Libya, Egypt, Sudan and Tunisia.

Having studied the area to be explored, we will now focus on the technique(s) adopted in solving a model problem. The question now is "What is a model"? In its simplest form, a model can be defined as a representation of certain events. It is an object or concept which represents something else. It may be physical or mathematical. A gravity model therefore, is known as any mathematical equation which require solutions to a given earth problem. This chapter explains how a model is developed (by modifying the existing model), validated and applied with respect to the Earth activities within the West African lithosphere (a region which has ocean-continent interaction). The model problem is an expression of a geo-potential equation which is desired to be calculated over the region. This geo-potential equation can be divided into sub-parts and each part is calculated separately which can then be merged together or combined to obtain the full geo-potential expression. It involves mathematical manipulation and computational analysis designed by writing a computer program. Gravity data are generated which are then used to plot 3-Dimensional contours showing the gravity anomaly pattern over the continental and oceanic regions of West Africa. To understand this, we obtain the following fundamental concepts.

1.7 Outline of the Thesis

This thesis is divided into five chapters. The introduction and background knowledge were given in chapter one. This chapter contain the statement of research problem, knowledge gap, research justification, aim and objectives while chapter two shows the relevant literature review where past researchers have contributed to knowledge and the development made in the analysis of geopotential models. The methods and techniques in details applied are specified in chapter three. The results and gravity data generated are presented and discussed extensively in chapter four while the last chapter contains the conclusion, summary, applications, contribution to knowledge and recommendations for further work based on the findings.

CHAPTER TWO
LITERATURE REVIEW

In this chapter, basic developments made by different researchers and their contributions to geopotential gravity analysis are reviewed here. A survey of relevant and related previous works on gravity studies are also provided. These previous researches necessitated that the theoretical background of this study be provided so as to understand the nitty-gritty of this research work.

2.1 Fundamental Concepts of Gravity Studies

Geopotential gravity studies had been in existence for quite a long time. Research work on gravity studies and geodetic measurements producing topographic maps (known as gravimetry) started from the 18th century. In geodesy, gravimetry appears in two specific ways: (1) To define the shape of the earth and (2) To measure the elevation of specific points to be shown on maps. The earliest gravity measurements led to the refinement of knowledge about the earth's shape from the sphere to the ellipsoid of revolution in the 17th century. However, the practical need to apply gravimetry in geodesy appeared in the mid 19th century. Gravity was then confirmed to be crucial to solving the ambiguities in precise levelling. The interpretation of gravity data was realised when geoid computation became necessary. This led to a wholly gravimetric solution of the geoids in 1952 in the USSR and in 1957 in the USA (Timar et al., 2018). Gravity geoid measurements in the USA occurred in the same year of the first spacecraft launch thereby offering a new tool for determination of the Earths shape. Nowadays, gravimetry provides the fine, high order and rank components of global gravity models. Model development started with few researchers in gravity analysis and certain limited areas were covered especially focusing on Europe and latin America. After the exploration of these regions, the existing models were then extended to the Carribeans and some part of Asian continents. This has led to the improvement in gravity model development. The research work then reviews the development and estimation of geopotential models over the past years, starting from

simple ellipsoidal normal gravity models to complex high degree 360/500 spherical harmonic expansion (Rapp, 1996). Gravity model development shows the evolutionary changes which had taken place in the mathematical models and data analysis development. With the application of these models to different regions of the world, it was now extended to Africa and especially to continental and oceanic areas but not a region that contains both simultaneously.

2.2 Review of Existing Knowledge

Several workers had contributed immensely to geopotential gravity studies. Some of these research works are listed in this section. Research gap provides a way to solving earth gravity problems. This solution requires the determination of lithospheric gravity of a known location whether oceanic or continental region. Past researchers started quality gravity work by focusing on the determination of the surface gravity of any given region or location. Surface gravity anomalies were determined using gradiometric observables (Peiliang Xu, 1992). The aim is to develop a new approach to obtain the best resolutions of mean gravity anomalies in terms of mean square errors, biases and error variances from biased estimation. To achieve this, three algorithms of ridge regression were presented and comparison was made with the least square method. The result of this finding shows that the proposed method is different from some present criteria of selection of regularization parameters used in geodetic inversion. This proposed method has not produced the desired surface gravity anomaly. Hence, the need to look for a better model that will produce accurate surface gravity values. However, recent global geopotential models were compared to terrestrial gravity field observations over New Zealand and Australia (Amos and Featherstone, 2002). This comparison of GGM-implied gravity anomalies with point free- air gravity anomalies on land geoid heights with discrete geometrical heights from collocated GPS and spirit-levelling data indicates that EIGEN-2, which uses purely champ data, is currently the best satellite-only GGM over Australia and New Zealand and an improvement on the model is achieved. It was however discovered later that EIGEN-2 model can be improved upon when more gravity models are developed and also compared.

Further development of models has led to the study of choice of global geopotential model for quasi geoids determination in Poland (Jan and Adam, 2005). This is attained if three kinds of numerical tests with use of terrestrial gravity data and GPS/leveling height anomalies were conducted. With this finding, their result shows that the best fitting global geopotential model in Poland were specified and accurate. The accuracy of this study created a great doubt in the mind of researchers and this led to further development of more gravity models require to solve regional problems. A joint geopotential model was developed by NASA Goddard space flight centre, the National Imagery and Mapping Agency (NIMA) formerly known as the Defence Mapping Agency (DMA) and the Ohio State University through collaboration to produce EGM96 (Lemoine and Smith, 2007) which represent the earth's gravitational potential. This model was developed using satellite tracking data from more than 20 satellites. It was achieved by using two different model estimation techniques i.e. quadrature and block diagonal to obtain high degree solutions. Result shows that the model EGM96 will contribute to oceanographic studies by improving the modeling of the ocean geoid using the Global Positioning System (GPS). A good idea may be obtained if we consider the geoid height of the ocean in term of its depth. A study on the evaluation of the geoid-quasigeoid separation term over Pakistan was also carried out by Sadiq et al., (2009). These researchers adopted solutions of terms involving first and second order terrain heights and their results shows that the second term of separation, which involves the vertical gravity anomaly gradient, is significant only in areas with very high terrain elevations and reaches a maximum value of 20-30m. Further investigation was also carried out on high resolution regional gravity field model of Pakistan (Sadiq, 2017). This study focuses on the development of absolute gravity model for Pakistan based on best possible residual terrain model of gravity by using residual terrain modeling technique in the remove-restore procedure for smoothing the observed gravity field. Also, the least square collocation technique was used for quality control and error estimates. In addition, lagrange and spline interpolation methods with least square adjustment were employed to predict these gravity field related parameters. The result shows that the gravity field recovered with Pakistan Gravity Model (PAKGM) is much better (about 96.16%) than both with EGM96 and EGM08 which is about 85%

only. Also, the absolute geopotential height system for Ethiopia was investigated (Bedada, 2010) which primarily aim to determine the absolute vertical reference system for the region of Ethiopia. A remove-restore approach/method was applied to eliminate longer to shorter wavelengths from the measured gravity data using EGM08 and geometrical and condensed gravity models of the SRTM data. The result obtained shows that the new model is in good agreement across 100Km baseline with a standard deviation of 0.26 This was then extended to crustal region in West Africa.

However an investigation of crustal structure and tectonics of the Calabar flank, West Africa based on residual gravity interpretation was carried out (Okiwelu et al., 2010). A 2- dimensional calculation along profiles perpendicular to the axis assessed four gravity models and a strong correlation between the rock types and residual Bouguer gravity anomaly in the flank was revealed. This further led to the evaluation of recent global geopotential models based on GPS/levelling data over Afyonkarahisar in Turkey (Ibrahim et al., 2010) where models were compared using standard deviation value and height- dependant evaluation approach. The evaluation result shows that EGM 2008 fits best to the GPS/levelling based on geoid heights than the other models with significant improvement in the study Area.

In a similar manner, gravity anomalies were interpreted in South Cameroon and Central Africa (Shandini and Tadjon, 2012) by using residual gravity map. This was done to analyse gravity data in order to delineate major structures and faults in South Cameroon. The results obtained shows that gravity anomaly map reflects faults or compositional changes which can better describe structural trends.

For the development of next generation Altimetric gravity fields, Residual Terrain Modeling (RTM) technique was investigated for gravity forward modelling (Hirt, 2013) to successfully improve high-resolution global gravity fields at short spacial scales in coastal zones. This is achieved to partially reduce the signal omission error in EGM 2008/GOCE- based height transfer in areas which are devoid of dense gravity data.

An estimation of the geopotential value for the Local Vertical Datum (LVD) of Argentina using EGM 2008 and GPS/levelling data was carried out (Tocho and Vergos, 2015). Numerical computation of mean geopotential using the least square

method to increase robustness of value was applied. It was then shown that the best possible estimation at present is 6 x $10^7 m^2/s^2$ which is improved by including proper physical heights (instead of the levelled ones). This has then led to the investigation of geopotential field anomalies and regional tectonic features in Southern Africa and Germany (Korte and Mandea, 2016), where comparison of amplitudes and characteristics of anomalies from maps were carried out based on the various available data and as measured at geomagnetic repeat stations.

Results obtained shows that a better agreement was obtained in the South African region than in Germany region indicating stronger concordance between near-surface and deeper structures in South Africa. Although the result obtained over South African region was later opposed in Saudi Arabia when gravity field anomalies from recent Gravity Ocean Circulation Explorer (GOCE) satellite-based geopotential models and terrestrial gravity data were investigated (Abdulaziz et al., 2016). The authors aimed to evaluate the free-air gravity anomalies and geoid heights determined from several recent GOCE-based GGM_S by using the corresponding gravity functions obtained from the Earth gravitational model 2008 (EGM08) over the Kingdom of Saudi Arabia (KSA). This was achieved when Spectral Enhanced Method (SEM) was applied to compensate the missed high-frequency component of geoid heights in GOCE-based GGM_S using EGM08 and a high-resolution digital terrain model based on the Shuttle Radar Topographic Mission (SRTM). The result obtained indicated an improvement over EGM08 in the medium wavelengths. Thus, the fourth and fifth releases of GOCE-based GGM_S performs much better than EGM08 and serve as the reference models for recovering the long wavelength up to SH d/o 200 and 240 respectively, when modeling the gravimetric quasi-geoid of the KSA area. About seven months later, the performance of recent global geopotential models GGM_S was evaluated over Egypt (Gad and Odalovic, 2017). It was carried out to improve our knowledge about the performance of the satellite only tracking and combining EGM_S which were generated from various satellites. A comparison technique which compares earth models EGM_S that were released between 2015 and 2017 was applied. It was then shown that there is an outstanding or superior performance of EGM2016 to the other examined GGM_S in terms of root mean square value of gravity anomaly (20.595mgal) and geoid height

(0.577m) respectively. Further investigation had led to the analysis of recent global geopotential models in the territory of Turkey (Selda & Abbak, 2017) where a numerical comparison approach between recently published GGM_S with equivalent GPS levelling data in the territory of Turkey was adopted. It was then shown that GGM_S combining Gravity Recovery and Climate Experiment (GRACE) and Gravity Field and Steady-State Ocean Circulation Explorer (GOCE) data are more accurate than the others. With this result obtained, there should be a comparison that can produce a better and more accurate result in another region.

A comparison of satellite Altimetric gravity and global geopotential models with ship borne gravity in the Red Sea (Ahmed, 2018) was carried out. Cross-validation and kriging prediction technique were adopted to ensure that the observed ship borne data and free gross error are consistent. It was then discovered that a significant improvement is procurable from the combined data set, in which the mean and standard deviation of the differences dropped from -3.60 and 9.31mgal to -0.39 and 2.04mgal, respectively. Accurate representation of the earth gravity field in the Polar Regions based on the global geopotential models were studied (Koneshov and Nepoklonov, 2018). A comparative analysis of quasi-geoid heights and gravity anomalies from the different models were carried out for the two polar regions selected within a radius of 1000Km. Results show that the accuracy of the models in the Arctic region is several times higher than in the Antarctic region.

Validation of gravity data from the geopotential field model for subsurface investigation of the Cameroon Volcanic Line (CVL) Western Africa was carried out (Marcel et al., 2018). The methodology involves upward continuation, horizontal gradient and Euler deconvolution techniques in order to evaluate gravity data derived from the geopotential field model EGM 2008 to investigate the subsurface of the CVL. Result shows a vulnerability of the CVL where special attention should be given for geoharzard prevention.

Study on the selection of optimal global geopotential models for geoid determination in Kuwait was also carried out (Mohammed El- Ashquer et al., 2019). A comparison of gravity with ground-based data using Spectral Enhancement Method (SEM) was

applied and the findings indicate that the combined GGMs, generally, fit the ground data better than the satellite-only GGMs due to the existing spectral gaps.

However, further investigation has led to an assessment of the GOCE High level Processing Facility (HPF) released global geopotential models with regional test results in Turkey (Erol, 2020). This assessment was achieved by using spectral and statistical analysis to compare gravity field mapping accuracies of the models. It was then found that the best fitting geopotential model with its optimal expansion degree improved the high frequency regional geoid model accuracy by almost 15percent. The region of assessment became a thing of concern to geophysicists who then tested the model in Europe by developing a new geopotential model tailored to gravity data (Tomislav et al., 2020). Calculation of the new geopotential model (IFE88E2) was made by using this new set of 0.5^{o} x 0.5^{o} mean free-air gravity anomalies merged with other available values of Europe. Result obtained shows an improved accuracy of the IFE88E2 model by a decrease in RMS value which reduces the slope between Denmark and Norway.

The various works done by the different researchers as reviewed in this chapter will be appreciated further if a clear understanding of how the Earth behaves are highlighted. This is because different researches performed by these researchers were based on the fundamental knowledge of the basic figures of the Earth, the internal structure of the earth, orbital parameters characterizing the earth's shape, its motion, orientation and behaviour which allows different gravity models to be developed and validated to produce desired results.

2.3 Theoretical background

An important geophysical phenomenon which indicates the physical conditions of the Earths lithosphere and also depicts the nature of subsurface structure is 'stability'. This phenomenon shows the regions of the lithosphere which are either or not susceptible to both natural and artificial anti-earth activities. Stability of the Earth's lithospheric crust is a tectonic problem that requires adequate attention (Johnston, 1990).

However, many activities performed by man such as rock blasting, hydrogeological drilling, mining, mineral exploitation, oil exploration, heavy construction of sky

scrapers among others are known to generate negative consequences which then poses a threat on the stability of the Earth lithosphere. Thus, anti-Earth activities constitute such operations (either naturally or artificially created by man) working against the initial physical conditions of the Earth. There are also, excavations (i.e. removal of hydrocarbons and replacement with brine) in the south-south Nigeria, oil exploration in the Niger Delta, geological exploration of marble deposits in Toto area in Nassarawa State and Iron ore exploitation in Itakpe, Kogi State, Nigeria. All are within the West African region.

This research work is therefore meant to determine how stable the West African lithosphere is (through gravity calculation) thereby providing an up-to-date information on the complex factors which can threaten the stability of the ground on which we are standing (Ebun-Oni, 1986). Stability of the Earth continental and oceanic lithospheres are assessed using different gravity models (Aulbach, 2000). The West African sector is a sector of the Earth which comprises combined continental and oceanic regions thereby making it distinct from other regions of the Earth.

This West African lithospheric segment is also explored using gravity models of different dimensions. The models comprises of a geopotential equation which can be represented by spherical harmonic expansion expressed to the desired degree of interest. Computed geodetic satellite parameters are also adopted in the computation which is used to describe the Earth's gravity field and anomalies of the sector. A better understanding of this research is seen if we look at the internal structure of the Earth.

2.4 The Earth's Structure and its interior

To understand the various activities within the Earth, a critical study of its internal structure is important. The first scientific idea was based on the evidence that the Earth's interior was in red-hot molten condition. This idea was considered genuine when it was observed that temperature increases with depth. Another idea shows that the interior of the Earth has a radially layered structure through the analysis of seismic waves which propagates through the Earth during Earthquakes. These layers which have 'boundaries' between them are marked by abrupt changes in seismic velocity. They are however, characterized by a specific set of physical properties determined by

the composition, pressure, temperature and density. The Earth has a mean density value of 5.52 x 10^3Kg/$m^3$and its temperature increases with depth. At shallow region within the depths of about 6-8Km, temperatures exceeding 200^{o}C have been recorded. The spherical Earth has an average radius of 6380Km. It has however become necessary to classify the Earth into the Crust, the Mantle (upper and lower), the outer and inner Cores.

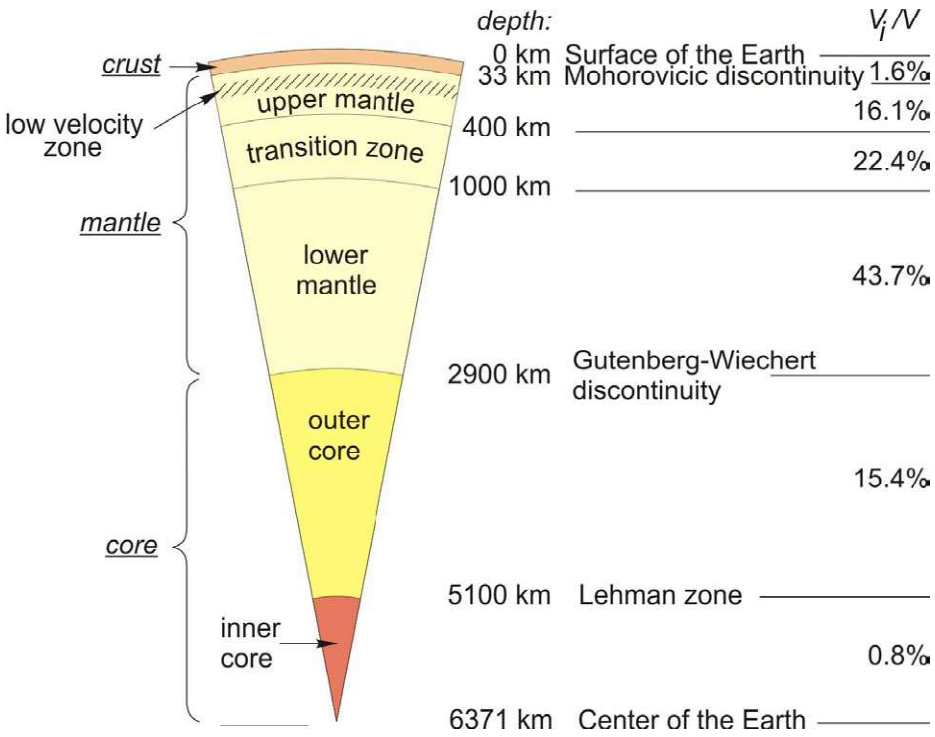

Fig 2.1: The Earth's Interior showing the different layers

2.4.1 The Crust

This is the outer top layer of the Earth having an average thickness of 33Km but its depth measures up to 70Km. Its average density is 29.4 x 10^3 Kg/m^3. At depths of a few kilometres below the Earth surface, there is a marked structural discontinuity and sharp velocity increase in the seismic waves. This seismic discontinuity discovered by Mohorovicic in 1909, estimated the range of speed of P–waves above the discontinuity to be between 5.53Km/s to 5.68Km/s. The Earth crust is made up of two regions namely the continental crust and the oceanic crust. The continental crust which is known as SIAL (made up of Silicon and Aluminum) has an average lithospheric thickness of ~100Km. (Turcotte and Schubert, 2002). It is thicker and less dense (density value range between 2.7-3g/cm^3) whereas the oceanic crust which is also referred to as SIMA (made up of Silicon and magnesium) has an average lithospheric thickness of 10Km (Schmidt and Herbert, 1998). It is thinner and denser (density value lies between 3-3.3g/cm^3). The difference in densities is as a result of their varying composition and their distinction is based on their mode of formation. As a result of this density stratification, oceanic crusts is usually subducted below the continental crusts at the subduction zone and is formed at seafloor spreading centres while the continental crust buoyantly projects above sea level and is formed through arc volcanism and accretion of terranes through tectonic processes.

2.4.2 The Mantle

This is the region of the Earth which lies between the crust and the outer core. It comprises of the upper and lower mantle. It has an average thickness of about 2,850Km and its density is about 9 x10^3Kg/m^3. The upper mantle is about 670Km thick (average depth) and both P and S waves are transmitted through the mantle layer. The uppermost part of the mantle between the Moho and a depth of 80-120Km is rigid, with increasing P- and S-wave velocities. This high seismic velocity layer together with the crust is known as the Lithosphere and is observed to consist of oxides of iron and magnesium as well as iron-magnesium silicates. The mass of the mantle is 4.1x10^{15}Kg and occupies about 83.3% volume of the total Earth.

2.4.3 The Core

This is the inner central layer estimated to have a depth of about 3400km below the mantle. It has a total mass of $1.8x10^{15}$Kg and occupies about 16.2% volume. It is made up of the outer and inner core having an average density of $25.2x10^3$ Kg/m^3. The study and interpretation of Earthquakes showed that both P and S waves were not transmitted to regions situated at distances above 105^0 of arc away from the epicentre and appear at 142^0 of arc from the epicentre. Thus, no P or S waves arrive between the epicentral distances 105^0 and 142^0 which are called a 'shadow zone'. Beyond 142^0 epicentral distance only P-waves were observed and they arrived lately, suggesting that they have been slowed down on their way through the Earth. It implies that this low seismic velocity zone contain liquid of partially molten elements.

The core-mantle boundary (CMB) is characterized by changes in body-wave velocity and a sharply defined discontinuity called 'Guttenberg discontinuity'.

A cross section of the Earth's interior showing various geologic layers and its different structural compositions are given in Fig. 2.1. Also, table 4.6 summarizes the Earth by giving the details of the different layers showing their depths, average densities, mass and percentage volume.

The outer layers of the Earth can also be divided into the 'Lithosphere' and 'Asthenosphere' while the inner layer is the 'Mesosphere'. This is based on the differences in mechanical properties and in the method of heat transfer.

2.4.4 The Lithosphere

This form a rigid outer layer down to a depth of approximately 100Km (63miles). These outer layers of the Earth show important lateral variations. It comprises of the crust and upper mantle. According to classical concepts, the lithosphere is the region which is capable of statically supporting disruptive stresses over geologically long periods. Thus, the brittle condition of the lithosphere causes it to fracture when strongly stressed. The rupture produces an earthquake, which is the violent release of elastic energy due to sudden displacement on a fault plane. The uppermost mantle between the Moho and a depth of 80-120Km is rigid, with increasing P- and S-wave velocities. The lithosphere extends to a depth range of 70-100Km under deep oceans

and 100-150Km under the continents. In terms of heat transfer, the lithosphere loses heat by conduction.

2.4.5 The Asthenosphere

This region lies beneath the lithosphere. It is a low seismic velocity zone composed of partially melted rocks which acts in a plastic manner on long time scales indicating a viscous liquid or plastic solid depending on temperature and composition. Thus, the seismic velocity often decreases thereby suggesting lower rigidity. It is about 180Km thick extending from 100-300Km (63-189miles) depth. Its upper and lower boundaries are not sharply defined. The Asthenosphere is the region of the Earth where mass flow associated with isostatic adjustment occur. It is a convecting region which is considered as the source for the mid-ocean ridge basalts (MORB). It plays an important role in plate tectonics since it makes possible the relative motions of the overlying lithospheric plate.

2.4.6 The Mesosphere

This is the innermost region which lies beneath the Asthenosphere. It is a layer which contains hot liquid metals in molten form at a very high temperature. It is evidently the inner core region with a depth of about 1300Km.

Having studied critically the internal Earth structure, the next step is to understand the orbital behavior of the Earth. This allows us to determine the Earth shape which changes due to gravity.

2.5 The Figure of the Earth

The figure of the Earth has various meanings in geodesy according to the way it is used and the precision with which the Earth's size and shape is to be defined. Thus, the figure of the Earth is a set of parameters which define the size and shape of the Earth. The concept of a spherical Earth offers a simple surface which is mathematically easy to deal with. It is a surface representing the Earth. The sphere is a close approximation of the true figure of the Earth. However, it is represented by an ellipsoid of revolution to a close approximation which ranges from modeling the shape of the entire Earth as

an oblate spheroid or Ellipsoid, to the use of spherical harmonics or local approximations in terms of local reference ellipsoids.

The Earth is flattened at the poles and bulges at the equator. Thus the geometrical figure used in geodesy to most nearly approximate Earth's shape is an oblate spheroid. An oblate spheroid or ellipsoid is an ellipsoid of revolution obtained by rotating an ellipse about its shorter axis. A spheroid which describes the figure of the Earth or other celestial body is called a 'Reference Ellipsoid'. The reference ellipsoid for the Earth is called an 'Earth Ellipsoid'.

An ellipsoid of revolution is uniquely defined by two parameters i.e. the semi major axis and flattening. The size is represented by the radius at the equator (the semi major axis of the cross-sectional ellipse) and designated by a letter **'a'**. The shape of the ellipsoid is given by the flattening, **f,** which indicates how much the ellipsoid departs from spherical. The two defining parameters are usually the equatorial radius a and the reciprocal of flattening1/f, rather than the flattening itself. For the World Geodetic System 1984 (WGS 84) spheroid used by today GPS systems, the reciprocal of the flattening 1/f is set at 298.257223563 exactly.

In practice, many reference ellipsoids have been developed over the centuries from different surveys so that flattening value varies slightly from one reference ellipsoid to another, reflecting local conditions and whether the reference ellipsoid is intended to model the entire Earth or only some portion of it. The oblate spheroidal Earth have constant radius of curvature east to west along parallels, if a graticule is drawn on the surface, but varying curvature in any other direction. For an oblate spheroid, the polar radius of curvature r is larger than the equatorial radius or a so that:

$$r = \frac{a}{b} \tag{2.1}$$

because the pole is flattened. The flatter the surface, the larger the sphere must be to approximate it. Conversely, the ellipsoids north-south radius of curvature at the equator r is smaller than the polar. Then,

$$r = \frac{b}{a} \tag{2.2}$$

where a is the distance from the centre of the ellipsoid to the equator (semi-major axis), and b is the distance from the centre to the pole (semi-minor axis).

2.6 Satellite Orbital Parameters

This research work is designed to provide the physical understanding together with a mathematical description of the resultant orbital behaviour. Orbital information is either transmitted by the satellite as part of the broadcast message or can be obtained in form of precise ephemerides (typically some days after the observation) from several sources. Earth as well as the dominant force is emphasized. Satellite orbital parameters are the physical parameters required to uniquely identify a specific satellite orbit. Thus, these parameters determine the motion, orientation and behavior of satellites. There are many different ways to mathematically describe the same orbit. However, certain schemes, each consisting of a set of six parameters, are commonly used in Astronomy and orbital mechanics to describe the motion of satellites orbiting round the Earth in an elliptical manner. These orbital parameters are emphasized as follows:

A) The two elements which define the shape and size of the ellipse are:

(i) Eccentricity (e):This give the shape of the ellipse, describing how much it is elongated compared to a circle. $0<e<1$ for Earth orbit.

(ii)Semi-major axis (a): This is the sum of the periapsis and apoapsis distances divided by two. For circular orbits, the semi-major axis is the distance between the centres of the bodies, not the distance of the bodies from the centre of mass.

B) The two elements which define the orientation of the orbital plane in which the ellipse is embedded are:

(i)Inclination (i): This is the vertical tilt of the ellipse with respect to the reference plane, measured at the ascending node (where the orbit passes upward through the reference plane).

(ii)Right Ascension/Longitude of the ascending node (Ω): This horizontally orients the ascending node of the ellipse (where the orbit passes upward through the reference plane) with respect to the reference frame's vernal point.

C) And finally, the remaining two elements are:

(i) Argument of perigee (ω): which defines the orientation of the ellipse in the orbital plane, as an angle measured from the ascending node to the periapsis.

(ii) Mean Anomaly (M): This defines the position of the orbiting body along the ellipse at a specific time (the **'**epoch**').** The anomaly is expressed as $M = (t - \tau)$

where τ is the time of perigee passage.

2.7 The Earth's Gravity Field

One of the fundamental forces which play a vital role in mechanics is the force of gravity. The Earth's geo-potential comprises of two main forces which are:

1) The force caused by the attraction due to gravitation and

2) The force caused by the Earth's rotation. Both forces act in the radial direction which is fixed to a point in size dependent on the distance. The first part is defined as the work done by gravity when a unit mass is brought from infinity to a point on the Earth surface. The second part is the work done when a unit mass is transported from a point in a rotation axis of the Earth in which the centre of gravity is chosen as a reference point. The field experienced when objects of masses are attracted by gravity towards the earth is known as the "Gravity field". From the above definition, it is observed that gravity is everywhere perpendicular to equipotential surfaces which are surfaces on which the potential is constant. The gravity field of the Earth is neither perfect nor uniform. A flattened ellipsoid is typically used as the idealized Earth so that gravity value changes from one point of the Earth to another. The strength of a gravitational field is quantitatively expressed by the force experienced when a body of mass m is placed in the field region. However, the physical exploration of the Earth's interior and subsurface structures is done using the gravitational field, which can be measured accurately at the surface using gravimeters and remotely by satellites. Since topography and all geological masses disturb or affects the gravitational field, true vertical therefore generally does not correspond to theoretical vertical (deflection ranges from 2" to 50"). Then, the gross structure of the Earth's crust and mantle (lithosphere) can be determined by geodetic-geophysical models of the subsurface. This logically implies that the subsurface materials erupted to the Earth's surface due to tectonic motion and interactions (thereby disturbing the stability of the Earth's lithosphere and causing mass anomaly and density variation) are adequately determined by gravity anomalies obtained from our geo-potential calculations.

2.8 The Geoid and Equipotential Surface

The **"geoid"** is defined as the equipotential surface of the Earth's gravity field which coincides with the mean sea level. According to C.F. Gauss, it is the mathematical figure of the Earth. The figure of the Earth is a smooth but highly irregular surface which corresponds not to the actual surface of the Earthcrust, but to a surface which can be known through extensive gravity measurements and calculations. It has evidently shown that equipotential surfaces of the Spheroidal Earth are all axially symmetric. The equation of the equipotential surface, which is assumed to be the Earth's outer surface and having the same volume as the geoid (also known as the Earth spheroid) is given as:

$$U_O = U \tag{2.3}$$

where U_O is a constant indicating the potential of the geoid.

CHAPTER THREE

RESEARCH METHODOLOGY

This chapter gives the detail of how the research was carried out. The computational approach or methods adopted in solving a model problem are also explained appropriately here. The improvement made to the existing gravity potential model is equally analysed as applied to both oceanic and continental regions.

3.1 Gravitational Potential of Spheroidal Earth

Any particle or body of a given mass m is attracted to the Earth having mass M according to Newtonian mechanics by a force:

$$F = ma \tag{3.1}$$

The object moves towards it by a small displacement dr which is the result of work W exerted by the gravitational field generated by M. So that

$$W = Fdr = madr \tag{3.2}$$

By Newton's universal gravitation:

$$F = \frac{GMm}{r^2} = ma \tag{3.3}$$

Then, work is expressed as:

$$W = \frac{GMm}{r^2}\, dr \tag{3.4}$$

The gravitational potential (denoted by U) is the amount of work necessary to bring the particle from infinity to a given distance r. Thus, we can write gravity potential as:

$$U = \int_{\infty}^{r} G\frac{m}{r^2}\, dr = G\int_{\infty}^{r} m\frac{1}{r^2}\, dr = Gm\left[\frac{1}{\infty} - \frac{1}{r}\right]$$

So that

$$U = -\frac{Gm}{r} \tag{3.5}$$

The gravity potential of the spheroidal Earth is termed the "Earth's Geo-potential". If we consider the three orthogonal coordinate system in which

$$r = r(x, y, z)$$

then (3.6)

$$r = x\vec{i} + y\vec{j} + z\vec{k}$$

It implies that gravity can be related to geopotential as;

$$g_x = -\frac{\partial u}{\partial x},\ g_y = -\frac{\partial u}{\partial y},\ g_z = -\frac{\partial u}{\partial z} \quad (3.7)$$

where U is the total geopotential. In general,

$$G = -\frac{\partial u}{\partial r} = -\nabla u \quad (3.8)$$

Equation (3.8) indicates that the gravity potential of the earth is the minus gradient of gravity.

The total geopotential at any point is the sum of the gravitational potential denoted by V and the rotational potential denoted by T so that:

$$U = V - \frac{1}{2}\omega^2 r^2 \cos^2\phi \quad (3.9)$$

where ω is the angular velocity of the Earth's rotation taken to be about Z-axis and (r, ϕ) are coordinates of a point on the surface of the Earth. To obtain an expression for V implies that the geoid will be calculated. By direct integration, the Earth's geopotential V could be obtained if the distribution of mass within the earth were known otherwise we need to derive information about the Earth's interior from the form of the geoid. To solve this problem, we use Laplace's Equation which V must satisfy at all points external to the Earth so that

$$\nabla^2 V = \frac{1}{r^2}\frac{\partial}{\partial r}\left(r^2\frac{\partial V}{\partial r}\right) + \frac{1}{r^2\sin\theta}\frac{\partial}{\partial\theta}\sin\theta\frac{\partial V}{\partial\theta} + \frac{1}{r^2\sin^2\theta}\frac{\partial^2 V}{\partial\lambda^2} = 0 \quad (3.10)$$

where r is the distance from the centre of the earth, $\theta = \left(\frac{\pi}{2} - \phi\right)$ is the geocentric co-latitude and λ is the longitude. Then, V can be expressed in a power series of r with coefficients which are spherical harmonic functions of θ and λ. A solution of the form

$$V = R(r)\ \theta(\theta)\ \phi(\phi)$$

$$V = R(r)\ S(\theta,\phi) \tag{3.11}$$

is obtained. The solution S (θ, ϕ) is known as "Surface Harmonics". If equation (3.11) is substituted into equation (3.10) and dividing throughout by R(r) (θ, ϕ), we will have

$$\frac{1}{R}\frac{d}{dr}\left(r^2\frac{dR}{dr}\right) + \frac{1}{\sin\theta s d\theta}\left(\sin\theta\frac{ds}{d\theta}\right) + \frac{1}{s\sin^2\theta}\frac{d^2s}{d\phi^2} = 0 \tag{3.12}$$

By setting μ = Cos θ and transforming the variable θ to μ, we will obtain:

$$\frac{d}{d\mu}\left[\left(1-\mu^2\right)\frac{ds_n}{d\mu}\right] + n(n+1)\ S_n = 0 \tag{3.13}$$

which is the "Legendre Equation" whose solution is given by the Legendre Polynomials:

$$S_n = P_n(\mu) = P_n(\text{Cos}\ \theta) \tag{3.14}$$

The complete solution is then written as:

$$V = \sum_{n=0}^{\infty}\left(A_n r^n + \frac{B_n}{r^{n+1}}\right) P_n \cos\theta \tag{3.15}$$

The first few Legendre Polynomials are written as follows:

P_o (Cos θ) = 1

P_1 (Cos θ) = Cos θ

P_2 (Cos θ) = ½ (3Cos^2 θ - 1)

P_3 (Cos θ) = ½ (5Cos^2 θ - 3Cos θ)

P_4 (Cos θ) = $^1/_8$(35Cos^4θ - 30Cos^2 θ + 3) etc

These are known as zonal harmonics and after solving the equation, we can obtain the gravitational potential of our spheroidal Earth as:

$$V = -\frac{GM}{r}\left[J_0P_0 - J_1\left(\frac{a}{r}\right)P_1 - J_2\left(\frac{a}{r}\right)^2 P_2 - ....\right] \tag{3.16}$$

where G is the universal gravitational constant, J_o, J_1, J_2,…… are dimensionless coefficients which are to be determined. These coefficients represent the distribution of mass within the Earth, and 'a' is the equatorial radius of the earth.

From normalization, J_o is known to be unity (i.e $J_o = 1$) so that at great distances all other terms become insignificant. This implies that we consider the potential due to a point mass M also called potential of the centered mass written as – GM/r. Since we have taken the origin of the coordinate system to be the centre of mass of the Earth, we then make J_1 identically zero so that the second term in the above expression (equation 3.16) equal to zero. Adequate attention is now focused on the J_2 term, which is the one required to give the observed oblate spheroid form of the geoid. The departure of the geoid from an ellipsoid is represented by higher harmonics with amplitudes smaller by factors of order 1000. Hence, the geopotential equation for V reduces to the expression:

$$V = -\frac{GM}{r} + \frac{GMa^2}{2r^3} J_2 \left(3\sin^2 \phi - 1\right) \tag{3.17}$$

If we consider the internal distribution of mass, then, J_2 can be expressed in terms of the principal moment of inertial of the Earth about the arbitrary coordinate axes as:

$$V = -\frac{GM}{r} - \frac{G}{2r^3}\left(A + B + C - 3I\right) \tag{3.18}$$

which is the general Mac-Cullagh's formula. It then implies that

$$I = Al^2 + Bm^2 + Cn^2 \tag{3.19}$$

Where I is the moment of inertial and l, m, n are direction cosines with respect to coordinates x, y, z.

3.2 Spheroidal Earth Rotation

If we consider the rotation of the Spheroidal Earth, then, we look at the axes which rotate with it. The centrifugal force is:

$$F_c = \omega^2 r \tag{3.20}$$

where r is the perpendicular from point P to the axis of rotation. This force act on every particle of unit mass outward along the perpendicular P.

The workdone by a centrifugal force when a unit mass move from the axis of rotation where the centrifugal potential is zero to point P is given by:

$$\omega_c = \int \omega^2 r dr = \frac{1}{2}\omega^2 r^2 \tag{3.21}$$

so that the total spheroidal Earth geo-potential is a combination of gravitational potential (due to attraction by gravity) and centrifugal potential (due to Earth's rotation). This geo-potential is written as;

$$V = -\frac{GM}{r} + \frac{G}{2r^3}(C - A)\left(3\sin^2\theta - 1\right) - \frac{1}{2}\omega^2 r^2 \cos\theta \qquad (3.22)$$

The coefficient J_2 of the gravitational potential is

$$J_2 = \frac{C - A}{ma^2} \qquad (3.23)$$

which is called the "dynamical form factor" of the Earth and is closely related to the flattening f.

3.3 The Earth's Spherical Harmonic Potentials

The Earth potential V can be represented by a spherical harmonic expansion equation of mathematical description (Heiskanen and Moritz, 1967) given as:

$$V = \frac{GM}{r}\left[1 - \sum_{n=2}^{\infty}\left(\frac{a}{r}\right)^n \sum_{m=0}^{n}\left(J_{nm}\ Cos\ m\lambda + K_{nm}\ \mathrm{Sin}\ m\lambda\right) P_{nm}\ \left(Sin\ \phi\right)\right] \qquad (3.24)$$

where J_{nm} and K_{nm} denote the zonal and tesseral coefficients of the harmonic development known from an Earth model which will be specified later in this research work. TheJ_{nm} and K_{nm} are the numerical coefficients of the model but the function $Cosm\lambda.P_{nm}(Sin\ \phi)$ and $Sinm\lambda.P_{nm}(Sin\ \phi)$ are known as "Spherical Harmonics" since they are periodic on the surface of a unit sphere. These spherical harmonics are often used to approximate the shape of the geoid. The best set of spherical harmonic coefficient is EGM 96 (Earth Gravity Model 1996) which was determined in an international collaborative project led by NIMA. EGM 96 contains a full set of coefficients to degree and order 360 (i.e n_{max} = 360), describing details in the global geoid. The number of coefficients, J_{nm} and K_{nm}, can be determined by first observing in the equation for V that for a specific value of n there are two coefficients for every value of m except for m = 0. There is only one coefficient when m=0 since Sin (0λ) = 0. There are thus (2n+1) coefficients for every value of n. Using these facts and the well known formula:

$$\sum_{I=1}^{L} I = \frac{L(L+1)}{2} \tag{3.25}$$

It follows that the total number of coefficients is given by:

$$\sum_{n=2}^{n_{max}} (2n+1) = n_{max}(n_{max}+1) + n_{max} - 3 = 130317 \tag{3.26}$$

Using the EGM 96 value of n_{max} =360.

3.4 Analysis of the Geopotential Coefficients

The numerical values of the gravity coefficients are most accurately determined from satellite tracking data. Table 4.5 is a list of satellite determined values of Zonal Harmonics of the geo-potential up to J_{21} as computed by kozai (1967) and king-Hele et al (1992) while the fully normalized Tesseral Harmonic Coefficients J_{nm} and K_{nm} of the geo-potential are tabulated later in this work. These constants depend on the earth mass distribution and hence on density at different locations of the Earth.

Infact, these harmonic coefficients provide valuable information on the mass anomalies which are expressed in terms of either gravity anomalies or geoidal undulation. These anomalies and undulations which are computed with respect to a reference provide information on the figure of the Earth associated with the crustal and upper mantle deformation (Jones, 1992). Any departure from a reference is truly indicative of the hydrostatic stresses or forces existing in the earth, especially in the crust and upper mantle (lithosphere) resulting in instability. The greater the forces in existence, the higher the crustal deformations. The advantage of satellite data over that of the terrestrial is that it gives a stronger and more accurate geo-potential value.

3.5 The Ellipsoidal Earth

As a first approximation, the Earth is a rotating sphere. It can however be regarded as an equipotential ellipsoid since the earth cannot be viewed as a perfect sphere but it is flattened at the pole and bulges at the equator so as to assume the shape approximated to an oblate spheroid known as “An Ellipsoidal Earth”. A particular ellipsoid of revolution which is called the “Normal Earth” is the one having the same angular

velocity and the same mass as the actual Earth. The equation of the equipotential surface can be obtained such that the potential U on the ellipsoid surface equal to the potential U_0 on the geoid so that the centre coincides with the centre of mass of the Earth. Thus, the reference ellipsoid is the ellipsoid which best fits the geoid. Practically speaking, the ellipsoid of revolution is considered to represent the figure that would be assumed by the geoid if the Earth were a uniform mass. The theoretical value of gravity on the rotating reference ellipsoid (Clairaut,1740) can be expressed as given in equation 3.27 as:

$$g = g_o (1 + K_1 \, Sin^2\phi - K_2 \, Sin^2 2\phi) \qquad (3.27)$$

where g_o is the gravity at the equator, K_1 and K_2 are constants which depend on the shape and rotation of the Earth. This formula which assumes a homogeneous Earth shows that g depends only on latitude ϕ and longitude λ. Since the Earth is an heterogeneous medium, then, variations/deviations from normal gravity values called "gravity anomalies or geoidal undulations" which is the difference, in metres, between the geoid reference ellipsoid will result. Thus, the geoid is the actual figure of the Earth while the ellipsoid is the theoretical shape of the Earth. Figure3.1 shows the geoidal and Ellipsoidal Earth surfaces. The land and sea topography are also indicated.

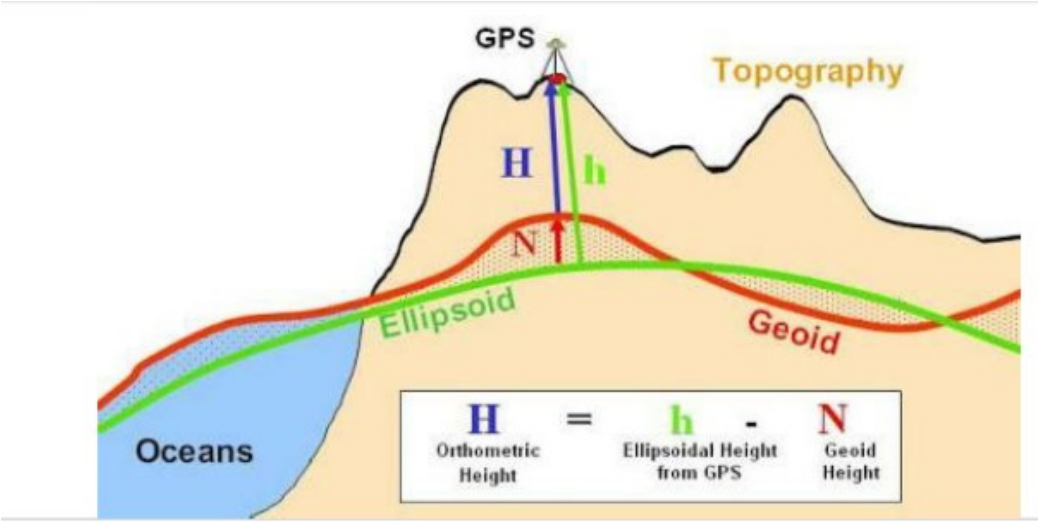

Figure 3.1: The schematic representation of the geoidal and ellipsoidal Earth surface (Encyclopedia Britannica, 2017)

The deviations of the actual gravity field from the ellipsoidal theoretical or normal field are small. The splitting of the Earth's gravity field into a normal and a small disturbing or anomalous field considerably simplifies many problems in geophysics which form the basis of this research work.

Since the gravity changes, the potential will also show a remarkable deviation ($G = -\nabla U$). If U_n represent the normal potential of the geoid, and R is the disturbing potential which is due to mass excesses and deficiencies also known as the Earth mass anomalies, then,

$$U = U_0 = U_n - R = \text{Constant} \qquad (3.28)$$

The two equipotential surfaces do not necessarily coincide as they may be separated by a distance N_0 from the geoid to the Earth's spheroid or ellipsoid. The difference in Earth potential between corresponding points on the two surfaces (geoid and ellipsoid) can be expressed as;

$$R = g_0 N_0 \qquad (3.29)$$

where g_0 is the value of gravity reduced to the geoid. Thus, if g is the gravity on the geoid and γ_o is the normal gravity on the ellipsoid, then, the gravity anomaly is given by:

$$\Delta g = g - \gamma_0 \qquad (3.30)$$

3.6 Development of the Gravity Field Model

As earlier stated, a model is a mathematical representation of algebraic expression which requires solution to any given earth problem. The model employed in this research work comprises of some parameters of a mathematical representation of the Earth's gravitational potential $V(r,\phi,\lambda)$ which can be used to map the gravity at or near the Earth's surface. These parameters can be estimated by tracking the data obtained in satellite geodesy. The estimated parameter and the corresponding mathematical representation constitute a gravity field model. In this analysis, it is desirable to choose satellites which are dominated by the geo-potential and for which other effects can be assumed in some way (Kaula,1966; Anderle,1967;Gaposchkin and Lambeck,1970). The suitable satellite so chosen is the champ grace satellite launched by GeoForschungs Zentrum (GFZ) in Potsdam, which gives the values of fully

normalized tesseral harmonic coefficients J_{nm} and K_{nm} up to degree and order 360. All values are reported formal and not calibrated. These tesseral harmonic coefficients were taken on 15th March, 2017.

To explain this model, we express the potential V of a perfectly spherical Earth as:

$$V = \frac{Gm}{R} \qquad (3.31)$$

If a satellite is set in motion around the Earth in closed orbits, the satellite will move in an elliptical orbit such that the Earth would occupy one of the foci of this ellipse. In this case, the centre of mass of the Earth will lie in the same plane as the elliptical orbit. This is the potential of the actual Earth which differs from the potential due to spherical mass distribution by a small quantity R, which is called the "disturbing potential". The potential V of the actual Earth is then given as:

$$V = \frac{Gm}{r} + R \qquad (3.32)$$

This suggests that the Earth is not a perfect sphere. Because of its rotation, the Earth is flattened and to first order, the shape is approximated to that of an "oblate spheroid" (which is a surface generated by revolving an ellipse around its minor axis) with an eccentricity of 1/298. The spheroidal surface that gives the closest overall fit to the mean sea level is called the "reference spheroid". To predict its gravitational field precisely at any point, we must know its shape and density distribution with the greatest possible accuracy. The satellite is then subjected to small disturbing forces due to the disturbing potential R. The satellite orbit being elliptical has orbital elements (highlighted earlier in previous chapter) which undergo a slow change. This change in any of the orbital elements is known as "Perturbation" in that element. Thus, the disturbing potential R produces effects on the various orbital elements of a satellite orbit which can be expressed by the equations (3.33) to (3.38)

$$\frac{da}{dt} = \frac{2}{na}\frac{\delta R}{\delta M} \tag{3.33}$$

$$\frac{de}{dt} = \frac{1}{na^2e}\left[(1-e^2)\frac{\delta R}{\delta M} - (1-e^2)^{\frac{1}{2}}\frac{\delta R}{\delta \omega}\right] \tag{3.34}$$

$$\frac{\delta M}{\delta t} = n - \frac{(1-e^2)}{na^2e}\frac{\delta R}{\delta e} - \frac{2}{na}\frac{\delta R}{\delta a} \tag{3.35}$$

$$\frac{\delta \Omega}{\delta t} = \frac{1}{na^2(1-e^2)^{\frac{1}{2}}\frac{1}{n}\sin i}\frac{\delta R}{\delta i} \tag{3.36}$$

$$\frac{\delta \omega}{\delta t} = \frac{(1-e^2)^{\frac{1}{2}}}{na^2e}\frac{\delta R}{\delta c} - \frac{\cot i}{na^2(1-e^2)^{\frac{1}{2}}}\frac{\delta R}{\delta i} \tag{3.37}$$

$$\frac{\delta \mathrm{i}}{\delta t} = \frac{1}{na^2(1-e^2)^{\frac{1}{2}}}\left[\cot i\frac{\delta R}{\delta \omega} - cosec\ i\ \frac{\delta R}{\delta \Omega}\right] \tag{3.38}$$

where all parameters are as enumerated/highlighted earlier have their usual meaning.

The effect of the geo-potential harmonic coefficients on the satellite orbit which results in perturbation (instability) produce variations in the orbital parameters. The even zonal harmonics J_2,J_4,J_6,……..J_{14} (King-Hele et al., 1992) cause secular and long-period changes in the right ascension of the ascending node **Ω** and argument of perigee ω, while long-period changes in the eccentricity e and inclination i of the orbit are more pronounced by the odd zonal harmonics J_3,J_5,J_7……..J_{21} (Khan, 1967). However, the tesseral harmonics, which define longitude-dependent variation cause short-period changes in the orbital elements and are more difficult to determine because of the necessity of a greater and more even distribution of the observations in space and time in order to detect the short period variations caused by them in the orbital elements. Due to the difficulties involved in the determination of these coefficients, many attempts have been made to compare the spherical harmonic coefficients obtained from various satellite solutions with each other and with coefficients obtained from surface gravity data so as to check their reliability. Low degree harmonics are easier to determine with reasonable accuracy than the higher degree zonal and tesseral harmonics which should be accepted with caution.

Thus, the Earth and its model known as the normal ellipsoid has three potentials of interest in geodesy. They are the Earth gravity potential (also called the Earth's Geo-potential) V, which is the sum of its normal gravitational potential U (one caused by

the attraction due to gravitation) and the disturbing potential R (caused by the Earth rotation) so that

$$V = U + R \tag{3.39}$$

This Earth potential V is approximated by a geo-potential model which is made up of a series of spherical harmonic terms and potential coefficients. For a spherically symmetric non-homogeneous earth layers, the 3-D Earth gravity potential model is represented as (Poirier, 2004; Bennard, 1998; Tscherning and Poder, 1981);

$$V(r, \phi, \lambda) = \frac{GM}{r}\left[1+\sum_{n=2}^{\infty}\left(\frac{a}{r}\right)^{n} J_n \sum_{m=0}^{n}\left(J_{nm} Cos\ m\lambda + K_{nm} \mathrm{Sin}\ m\lambda\right) P_{nm}\left(Sin\ \phi\right)\right] \tag{3.40}$$

However, a well recognized model developed by Wiechert (Equation 3.41) was considered to be the most desirable (or if possible termed as best) model amongst the many existing gravity potential models (GGM_s) since it contains adequate valuable physical parameters of the Earth which takes into consideration the depths, geometry (i.e. latitude and longitude), bulk modulus, number of earth layers etc. Although, widely accepted but it could not be applied to the oceanic-continental regions where several human activities/operations had taken place i.e. it cannot solve ocean-continent problems. It is therefore desirable to develop a more robust model which can take care of or handle activities and operations performed within the ocean-continent regions of West Africa. Such a model is expressed in equation (3.41b). Wiechert's model is given as:

$$V(z,\phi,\lambda) = \frac{GM}{r}\left[1+\frac{1}{4\pi G}\sum_{n=2}^{N}(2\gamma-1)\frac{\rho_0 g z}{K}\right]^{\frac{1}{n-1}}\sum_{m=0}^{n}\left(J_{nm}Cosm\lambda + K_{nm}Sinm\lambda\right)P_{nm}(Sin\phi) \tag{3.41a}$$

It is important to know that the geo-potential V used in this research work is a development to the existing Wiechert's representation also known as modified geopotential gravity model (MGGM). This modified model has an additional parameter η which is referred to as the "compaction factor" or "compaction ratio". It can also be referred to as compensation factor/ratio. This factor is now introduced to the existing Wiechert's geopotential model which can be represented as:

$$V(z,\phi,\lambda)=\frac{GM}{r}\left[1+\frac{\eta}{4\pi G}\sum_{n=2}^{N}(2\gamma-1)\frac{\rho_0 gz}{K}\right]^{\frac{1}{n-1}}\sum_{m=0}^{n}(J_{nm}Cosm\lambda+K_{nm}Sinm\lambda)P_{nm}(Sin\phi) \quad (3.41b)$$

The normalizing factor 'η' takes care of the compaction difference between the oceanic and continental regions of West Africa situated between longitude 30°W-15°E and latitude 3°N-20°N where anti Earth activities were carried out. Thus, η enables the modified gravity potential model to be applicable to both oceanic and continental regions of West African sector. This dimensionless factor accounts for ocean-continent interaction which is the contributing factor of this research work that other previous models fail to consider or address. The compaction factor has a value 2.43 which is defined as the ratio of the weight of fully compacted continent having value 6280N to the weight of partially compacted ocean having value 2584N. If an assumption is established such that the weight of fully compacted continent is equal to the weight of partially compacted ocean, then, η will take unity value and equation (3.42) results into equation (3.41). Equation (3.42) is a potential expression which comprises of an infinite series of spherical harmonics where all parameters take their usual meaning. z, ϕ and λ are polar coordinates. r is the geocentric radial distance which is also referred to as the semi-major axis of reference ellipsoid with value 63,712m, ϕ is the geocentric latitude, λ is the geographic longitude. G is the Newton's universal gravitational constant having value $6.673 \times 10^{-11}Nm^2/kg^2$, M is the mass of the Earth which is $5.975 \times 10^{24}kg$, a_e is referred to as the mean equatorial radius of the earth equal in magnitude to 6,378km. $\boldsymbol{\gamma}$ is the number of earth layers of the lithosphere. P_{nm} are the fully normalized associated Legendre functions. If m = 0, they are generally written as $P_n(Sin\phi)$ and are called Legendre Polynomials which are latitude dependent. The functions $Cosm\lambda\ P_{nm}(Sin\phi)$ and $Sinm\lambda\ P_{nm}(Sin\phi)$ are the surface spherical harmonics. For m =0, the functions are called Zonal Harmonics but if $m \neq 0$, they are referred to as Tesseral Harmonics. J_{nm} and K_{nm} are the constant coefficients of the various spherical harmonics occurring in the expansion of R which are known as the "Geo-potential Coefficients" of degree n and order m. These J_{nm} and K_{nm} values are extracted satellite data used in the computation of the desired geopotential V. These fully normalized harmonic coefficient values are obtained from the website http://www-app2.gfz-

potsdam.de/pb1/media/champ/eigen-cg03c/eigen_cg03c_coef. However, it can also be extracted as geodetic parameters for a Smithsonian Institution Standard Earth obtained from The Smithsonian/NASA Astrophysics data system with website http://adsabs.harvard.edu/abs/1966SAOSR.200.....L. NASA is the National Aeronautics and Space Administration which is a recognized body in charge of satellite data acquisition. This satellite gravity data can also be obtained from "The Nigerian Geological Survey Agency" in Abuja, Nigeria. They are constants depending on the Earth's mass distribution. GM is the product of the Earth's gravitational constant G and its mass M. N is the maximum degree and order of the available coefficients. The Legendre Polynomial and associated Legendre functions are given by the following expressions respectively:

$$P_n(Sin\phi) = \frac{1}{2^n}\sum_{k=0}^{r}(-1)^k \frac{(2n - 2k)!\ Sin^{n-2k}\phi}{k!\ (n - k)!\ (n - 2k)!} \qquad (3.42)$$

where r is the greatest integer $\leq \frac{n}{2}$ and

$$P_{nm}(\sin\phi) = \left[\frac{2(2n + 1)!\ (n - m)!}{(n + m)!}\right]^{\frac{1}{2}} \frac{Cos^n\phi}{2^n} \sum_{k=0}^{r}(-1)^k \frac{(2n - 2k)!\ Sin^{n-m-2k}\phi}{k!\ (n - k)!\ (n - m - 2k)!} \qquad (3.43)$$

where r is the greatest integer $\leq \frac{(n-m)}{2}$

Another way of expressing the fully normalized associated Legendre Polynomial is:

$$P_{nm}(Sin\phi) = \sqrt{k}(2n + 1)\ \frac{(n-m)!}{(n+m)!} P_{nm}(Sin\ \phi) \qquad (3.44a)$$

By using the model (equation 3.41b), gravity potentials and anomalies will be computed from the harmonic coefficients found by satellites and compared with measured gravity anomalies (Bjerhammar,1981;Kohnlein,1982;Rapp,1988).

3.7 Validity of the Gravity Model

To validate a model, it implies that we need to solve our model problem which is the required solution of the geo-potential equation and produce results which are comparable with standard work elsewhere. Thus, a good model work should be able to solve both local and global problems when their correlation is checked or assessed. Generally speaking, the validity of gravity models can be checked in two basic independent ways (Anderle, 1993) which are:

(A) By a direct comparison of the gravity field model with areas where detailed ground data are available and

(B) A Comparison between the model geoid and the geoid as measured directly by satellite altimeter experiments.

In this research work, the mathematical geo-potential model is tested if it can solve a given local or global problem by comparing and finding the close correlation between the model in question and the problem. Thus, the first approval was employed where free air gravity maps of the West African region which was computed from a spherical harmonic representation of satellite data is compared with the free air gravity map of Itakpe in kogi State, Nigeria (In-situ data of continental region) as well as the free air gravity map of Niger delta area also situated in Nigeria (In-situ data of oceanic region). However, it was also compared with the standard, universal Earth models also known as the global geopotential model computed by Khan using surface terrestrial data (Erol et al.,2009; Ustun and Abbak, 2010) which will be shown in the latter figure. A global geopotential model is a set of spherical harmonic coefficients which describe the long wavelength characteristics of the geoid and gravity field on a global scale. These are computed through the analysis of satellite orbits, and higher resolution models are produced with the combined use of terrestrial gravity and satellite altimetry data. The correlation is considered quite satisfactory. Thus, a close correlation in gravity data shows that the deviation between the gravity values and their contoured maps is extremely small. Average error was minimized.

In the validation of Earth gravity model (EGM) with external data, it should be considered that the terrestrial data represent the full spectrum of the gravity signal, whereas the Earth gravity model contains only low frequencies and high wavelength. Therefore, it is good enough to decompose the available terrestrial data using an appropriate filtering algorithm with suitable parameters which can make sense before comparing with the EGM signal at this point (Erol et al., 2010).

Thus, validity of gravity field model in this research work is done by comparing the data generated from modified geo-potential equation (3.41b) side by side with the results obtained from existing geo-potential equation (3.41a) produced by Wiechert as well as the data of Itakpe (continental region). It was also carried out for Niger delta area (oceanic). This simply implies that the gravity anomalies which have been computed from spherical harmonic expansion and whose coefficients are extracted from satellite data are compared with the measured gravity anomalies. This simply implies that the geoid heights supplied by a global geopotential model are in close fit to the geometrically derived geoid heights so that a reasonable correlation is obtained. The tesseral harmonics define the longitude-dependent variation while the latitude variation is expressed in the associated legendre polynomial as given by the complete geopotential equation. This validation is complete if the geo-potential values obtained are compared with the global geopotential values. Table B1 (see Appendix B) shows the geopotential validation by comparing the data obtained from modified model (MGGM) and existing model (GGM) with the In-situ or observed data of Itakpe area in kogi state, Nigeria where human operations have engaged.

3.8 Gravity Field (Geopotential) Computation

The Earth's gravity field (also known as the geopotential gravity) can be computed from the analysis of our model which is can be written in equation form as:

$$V(z,\phi,\lambda)=\frac{GM}{r}\left[1+\frac{\eta}{4\pi G}\sum_{n=2}^{N}(2\gamma-1)\frac{\rho_0 gz}{K}\right]^{\frac{1}{n-1}}\sum_{m=0}^{n}(J_{nm}Cosm\lambda+K_{nm}Sinm\lambda)P_{nm}(Sin\phi) \quad (3.44b)$$

where $P_n(\text{Sin}\phi)$ and $P_{nm}(\text{Sin}\phi)$ are the Legendre polynomial and associated Legendre polynomial respectively as represented by equations (3.35) and (3.36) earlier taking into consideration the values of r.

In this computation, the flattening of the Earth **f** (which gives the Earth figure) is taken to be 1/298.26. This is the recommended and adopted ellipsoidal reference as given by the International Union of Geophysics and Geodesy (IUGG) in 1967. Other internationally adopted Astronomical constants are:

The Semi-major axis of reference ellipsoid r = 63,712m

Mean Equatorial radius of the Earth a_e = 6,378,155m ≈ 6,378km

Mass of the Earth $M_e = 5.975 \times 10^{24}$ Kg

Earth gravitational constant G =$6.673 \times 10^{-11} Nm^2/kg^2$ (or in $kg^{-1}m^3s^{-2}$)

so that $\mu = GM = 3986013 \times 10^8 m^3/s^2$ and $J_2 = 10827 \times 10^{-7}$

Few parameters of concern in the computation include:

ϕ which is the geocentric latitude and λ is the geographic longitude of computational point, J_0, J_1, $J_{2,.....}$ are dimensionless coefficients which are determined because they represent the distribution of mass within the Earth. J_2 is known as the dynamical form factor of the Earth and is closely related to the flattening f.

The zonal harmonics up to J_{21} as computed by Kozai (1978) were used in the computation as starting values, with fully normalized coefficients of the spherical harmonic expansion of degree and order 360^0. To solve our model problem (equation) with the adopted values for J_{nm} and K_{nm}, a computer program was written to generate the potential gravity across the West African sector of the African continent. The program is written in MATLAB platform (refer to Appendix A). The variations of latitude and longitude values were also carried out which was achieved by keeping the latitude fixed over some varying values of longitude. The latitude and longitude intervals were in a grid of 2.

3.9 Geoidal Undulations

We consider a spherically symmetric rotating Earth. Let the gravity of the geoid be given as g_g, we can obtain from gravity, the geoidal departure from a reference ellipsoid (Wahr, 1997). This departure of the geoid from the spherical Earth is known as "Geoidal Undulations" denoted by N. Geoid heights and gravity anomalies can easily be computed from a set of geopotential coefficients using the algorithms of either Rapp (1982) or Rizos (1979).

In the computation, the geoidal undulation at a point (r, ϕ, λ) is obtained from the expression:

$$N = -\frac{GM}{rg_0}\left[1+\frac{\eta}{4\pi G}\sum_{n=2}^{N}(2\gamma-1)\frac{\rho_0 gz}{K}\right]^{\frac{1}{n-1}}\sum_{m=0}^{n}(J_{nm}Cosm\lambda + K_{nm}Sinm\lambda)P_{nm}(Sin\phi) \tag{3.45}$$

where g_o is the theoretical gravity on the ellipsoid at (r, ϕ, λ). Mathematical computation of geoidal heights using MATLAB platform can be done (see Appendix A2) considering the variations of longitude and latitude over the West African sector.

In general, the global or large-scale features of the geoid are expressed by a spherical harmonic expansion of the gravitational potential. Thus, computation of the geoid undulation i.e. the height of the geoid above the reference ellipsoid (or spheroid) of the West African sector is done by means of the Geopotential coefficients. The harmonic coefficients in the expansion provide information in terms of either gravity anomalies or geoidal undulations.

Having obtained the geoidal height data of Itakpe (a region within West Africa) using the existing geopotential model (GGM) developed by Wiechert and the modified version (MGGM), which has been validated by comparing with the available in-situ/observed data. The next step is to know what gravity anomaly implies.

3.10 Gravity Anomalies

The geophysical use of gravity is to learn about the Earth's interior. We need to remove the effects of the Earth's irregular and non-elliptical surface. In principle, it implies that the observed gravity is compared to that of ellipsoidally-produced theoretical gravity values at each observation station. This difference is termed "Gravity Anomaly". The free-air gravity anomaly is the difference between the observed gravity, without terrain-related corrections, and the theoretical gravity. The complete Bouguer anomaly is the difference between the observed gravity with the complete Bouguer correction and the theoretical gravity (Li and Gotze, 1996). The gravity anomalies denoted byΔg at any point (r, ϕ, λ) is obtained from equation (3.46):

$$\Delta g = -\frac{GM}{r^2}\left[1+\frac{\eta}{4\pi G}\sum_{n=2}^{N}(2\gamma-1)\frac{\rho_0 gz}{K}\right]^{\frac{1}{n-1}}\sum_{m=0}^{n}\left(J_{nm}Cosm\lambda + K_{nm}Sinm\lambda\right)P_{nm}\left(Sin\phi\right) \tag{3.46}$$

where all parameters are as defined earlier. The gravity anomalies are computed over the West African sector where there are variations in longitude and latitude values. It is quite interesting to know that all these gravity equations differ from one another when we consider the parameters starting the equations. The geopotential carries the expression $\frac{GM}{r}$, geoidal height has $-\frac{GM}{rg_o}$ and gravity anomaly has $-\frac{GM}{r^2}$ as the initializing factor. This will invariably account for the data obtained at the end of the day. Table B3 (see Appendix B) shows the gravity anomaly data of Itakpe region as obtained from GGM, MGGM and In-situ.

It is important to note that the unit of gravity anomaly is milligals (mGal). It can however be related to the standard unit of m/s^2 if we know that;

1000mGals = 1Gal and 1Gal = $0.01 m/s^2$.

The gravity anomaly contour map of West Africa is presented in Fig. 3.7

Equations (3.44b) to (3.46) are the general mathematical expressions representing the geopotential gravity, geoidal undulation and gravity anomaly models over the region desired to be explored. By applying these models, gravity data are generated and contour maps in Figures 4.1 to 4.4 are obtained respectively.

3.11 Gravity Data Generation and Interpretation

The differences in the Earth's gravitational field at specific locations on the Earth surface can be measured using gravity method which is known to be a non-destructive geophysical technique. This is meant to determine the distribution of mass in the crust and mantle (i.e. lithosphere). We can obtain the gravitational potential and acceleration when we integrate over any specified distribution of mass (Turcotte and Ockendon,1977). In this case, a unique relationship between the gravity, geoid anomalies and lithospheric distribution of density may be of considerable use. Such relationship is expressed by a Bouguer formula for the gravity anomaly Δg given as:

$$\Delta g = 2\pi G\sigma(x,y,z) \qquad (3.47)$$

where G is the gravitational constant. The crustal density distribution is:

$$\sigma(x,y) = \int_0^h \Delta\rho\ (x,y,z)\ dz \qquad (3.48)$$

where $\Delta\rho$ is the density anomaly also known as the density contrast. This Bouguer formula is valid if the density variation is considered on a large horizontal scale where h<<a. a is the radius of the Earth and h is the depth.

A power series expansion for the gravitational acceleration and potential caused by slowly varying density changes was derived by Ockendon and Turcotte (1998) using the technique of marched asymptotic expansion. They find that if the density distribution is in isostatic equilibrium, then, the gravitational potential anomaly ΔU is given by eqn. (3.49):

$$\Delta U = -2\pi G\ \delta(x,y) \qquad (3.49)$$

where the dipole density distribution is given as:

$$\delta(x,y) = \int_0^h z\Delta\rho(x,y,z)dz \qquad (3.50)$$

It is clear that the success of this method is dependent on the different earth materials which possess different bulk densities and mass anomalies which produce variations in the measured gravitational field (Mickus 2002). These variations can then be interpreted by a variety of analytical and numerical (computer) methods to determine the depth, geometry or location and density which causes the gravity field variations. Gravity data specifying the Earth's geopotential values are calculated from the model using series of numerical computer simulated approach or program. This geopotential calculation is achieved up to degree 360 using a high technology super power

computer system under the Matrix Laboratory (MATLAB) platform which has the ability to store maximum data. These computations were carried out on an intel hp computer where a detailed computer program is written. The fully normalized satellite geopotential harmonic coefficients are also utilized in the computation taking into consideration the longitude and latitude variations within the region of coverage (West Africa). This research work have also figured out different traverse sections within this region where anti-earth activities is intended to be monitored which are Tr 1 (-20^{o}W to 25^{o}E, 5^{o}N), Tr 2(-20^{o}W to 25^{o}E, 10^{o}N), Tr 3 (-20^{o}W to 25^{o}E, 15^{o}N), Tr 4 (-20^{o}W to 25^{o}E, 20^{o}N), Tr 5(-20^{o}W to 25^{o}E, 25^{o}N), Tr 6 (-20^{o}W to 25^{o}E, 30^{o}N), Tr 7 (-20^{o}W to 25^{o}E, 0^{o}N) and Tr 8 (-20^{o}W to 25^{o}E, -5^{o}N) . The interval between the longitude will be 5degrees, i.e. -30^o, -25^o, -20^o, -15^o, -10^o, -5^o, 0^o, 5^o, 10^o, 15^o, 20^o and 25^{o}E while the latitude values varies between 5^{o}N and 20^{o}N respectively. The gravity field values computed are highlighted in table 4.1 below. These values are then used to generate the gravity anomaly contour maps around the West African coastal region for various degrees n and orders m using either surpher 10 or grapher 4 software. These maps can then be interpreted appropriately.

The table B4 shows a combined data of geopotential V(r,ϕ,λ), geoidal height N and the gravity anomaly Δg using the MGGM when latitudes are varied and longitudes are fixed at 5^0 interval during the computation.

However, Table B5 shows a combined gravity data of West African region. The gravity data includes the geopotential, geoidal height and gravity anomaly values computed at various latitude and longitude using the existing GGM model given by Wiechert.

3.12 Interpretation of Gravity Anomalies Data

The major purpose of the gravity technique is to obtain valuable information about the Earth's subsurface region based on its diverse human (artificial) and tectonically-imposed natural activities. To interprete gravity data, then, our interest is, in determining the subsurface variations of mass and this process usually requires that the

density of the material of interest or the density contrast between the material of interest and the surrounding material be known. The density of the Earth's lithosphere can be determined in many ways but before then, we look at the various geophysical techniques that can be used to interpret gravity anomaly data. Some of these methods are specified in sections 4.2.1 to 4.2.3.

3.12.1 Analytical Method

The essence of obtaining gravity anomalies is to locate and determine the distributions of buried masses within the Earth's body. The total mass which produced such anomaly can be calculated. However, the mass distribution cannot be determined uniquely since gravity is a potential function. Hence, assumptions must be made in order to calculate the mass distributions. Some physical parameters can be obtained directly under somewhat simplifying conditions if either the density or shape of the body is assumed or known. For relatively complex structures, both the density and shape can be assumed, especially when control points are available. With the use of digital computers, the resultant model readily improves thereby producing values of higher degrees and order and accuracy of data taken into consideration. The analytical method is further classified into both direct and indirect methods suitable for analyzing subsurface earth structures producing gravity anomalies, which have the wavelengths and amplitudes of the observed. The major difference is that while direct analytical methods attempt to solve equations which represent the anomaly, indirect methods make use of hypothetical models for which corresponding attractions are computed and compared adequately with the observed. This hypothetical models which ranges from simple mathematical expressions describing the bodies, for which the attraction can be computed by direct integrations (for example, a sphere, a rectangular object, a horizontal slab), to complex structures having irregular shapes or consisting of numerous layers with different density contrasts (as obtained in continental margins and archipelagoes) for which attractions are computed by either two- or three-dimensional numerical methods. A clear and precise model must therefore incorporate

known seismic, borehole and other available geophysical information. After each computed anomaly, the model is adjusted until it adequately matches and suite the observed anomaly. Applying Gauss' theorem, direct methods are used to determine the total mass without specifying its size or shape. For irregular unknown mass distributions, direct methods usually refer to inverse methods, where integral equations are solved which satisfy the observed anomaly. In inverse methods, either the shape of the body is assumed and the density distribution solved for, or the density contrast(s) assumed and the shape determined. While indirect methods make use of wide ranges of density and layer assumptions, the inverse methods usually provide more rapid solutions for simplified models.

3.12.2 Monte Carlo Inverse Method (Numerical Approach)

The most general method for solving nonlinear inverse problems requires a complete exploration of the model space. Monte Carlo methods have become important in the analysis of nonlinear inverse problems where no analytical expression for the forward relation between data and model parameters is available, and where linearization is unsuccessful. In such cases a direct mathematical treatment is impossible, but the forward relation materializes itself as an algorithm allowing data to be calculated for any given model. Monte Carlo methods can be divided into two categories which are the sampling method and the optimization method. It is good to know that while Monte Carlo sampling is useful when the space of feasible solutions is to be explored, and measures of resolution and uncertainty of solution are needed, the Monte Carlo optimization method is a powerful tool when searching for globally optimal solutions amongst numerous local optima. The practical use of Monte Carlo method has today become a reality through application of algorithms running on high-speed computers. Monte Carlo methods of inversion are basically numerical processes that produce or generate so-called pseudo-random numbers (Press, 1971) which is a series of numbers that appear random if tested with any reasonable statistical test. This method usually

operate within the scope of obtaining some 'best' model which is a model maximizing the probability density $\sigma_M(m)$ or minimizing some misfit function S(m).

If the forward problem is not excessively non-linear, the functions $\sigma_M(m)$ and/or S(m) are well behaved and usually have a single extremum, which can be obtained by using the gradient methods. These gradient methods use the local properties of the function at a current point m_n to decide on a direction of search for the updated model m_{n+1}. For highly nonlinear problems, there is a considerable risk that gradient methods will converge to secondary solutions. For model spaces with more than a few parameters, it is more economical to select points in the model space randomly than to define a regular grid dense enough to ensure that at least one point will be in the optimal area. Any method which uses a random (or pseudo-random) generator at any stage is named Monte Carlo, in homage to the famous casino. The interest of these methods is that they can solve problems of relatively large size in a fully nonlinear form (i.e. without any linearization). It becomes an efficient and only useful feasible alternative method to more direct methods for numerical evaluation especially in three dimensional space. Thus, the Monte Carlo analysis of inverse problems made attempts to randomly explore the space of possible Earth models from the considerable advances in computer technology. This research work produce interest and also shows how to interpret the resulting ensemble of gravity Earth model, especially when extra constraints are imposed on the system (Haddon and Bullen, 1969; Anderssen, 1970;Wiggins,1972;Kennett and Nolet,1978). In addition, uniform random search techniques will be used for model optimization. This genetic algorithm have been applied to a wide range of geophysical problems (Stoffa and Sen,1991;Gallagher et al.,1992;Wilson and Vasudevan,1994) in estimating seismic attenuation structure in the Earth, seismic surface wave studies, magnetotelluric studies, estimation of mantle viscosity and plate rotation vectors. Here, the Earth density structure will be estimated using this same algorithm.

The main reason for the usefulness of Monte Carlo methods in inverse problem analysis is that they are essential practical tools for dealing with probability distributions. Thus, any probability distribution can be represented by a group of

associated Monte Carlo algorithms. In this way, Monte Carlo algorithms provide a way of manipulating probability densities and even the densities that cannot be expressed mathematically in closed form. The analysis using Monte Carlo inversion method involves the following procedures:

3.12.2.1 Search for the domain of Admissible Models

Assume that we have some a priori information on the parameter space, which can be set in the simple form as

$$m_{inf}^{\alpha} \leq m^{\alpha} \leq m_{sup}^{\alpha} \qquad (\alpha \in I_M) \qquad (3.51)$$

The Monte Carlo method of inversion consists in using a pseudo-random number generator to generate random models inside the region defined by equation 4.5 (Press, 1968, 1971), in computing for each one of these models, say m, the corresponding predicted data, $d_{cal} = g(m)$, and in using some quantitative criterion of comparison between d_{cal} and d_{obs} to decide if m is acceptable or not. The computations are stopped when the number of accepted models is sufficient to suggest that the model space has been conveniently explored.

The density of the Earth's mantle as well as the velocity of seismic waves, as a function of radius r, using as data measured eigen periods of the Earth's vibration, some measured travel times of seismic waves, the total Earth's mass, and the Earth's moment of inertia were investigated (Press, 1968).

The parameters to be evaluated were the density ρ(r), the velocity of longitudinal waves α(r), and the velocity of transverse waves β(r). These functions were considered at 23 different values of r (the remaining values were defined by interpolation). This makes a total of 23 x 3=69 parameters:

$m = (m^1,\ldots,m^{69}) = (\rho(r^1),\ldots,\rho(r^{23}),\alpha(r^1),\ldots,\alpha(r^{23}),\beta(r^1),\ldots,\beta(r^{23}))$.

Approximately five million models were randomly generated and tested. Of these, six were acceptable which gave predicted data values close enough to the observed values).

3.12.2.2 Non-Linear Computation of Variances and Covariances

It is assumed here that, for any model **m**, we are able to compute the posterior probability density function in the model space, $\sigma_M(m)$. This section is concerned with problems where:

i) The number of components of the vector m, say NM, is large (infact, NM $\geq$4).

ii) For a given m, the computation of $\sigma_M(m)$ is inexpensive (so we can compute $\sigma_M(m)$ for a great number of models).

Let us write the posterior probability density in the model space as:

$$\sigma_M(m) = \rho_M(m)\ L(m), \qquad (3.52)$$

where $\rho_M(m)$ represents the prior information in the model space and L(m) is termed the 'likelihood'. For instance, if d_{obs} ($i \in I_D$) represents the observed data values and σ_D the estimated mean deviations, assuming double exponentially distributed observational errors gives:

$$L(m) = \exp\left[-\sum_{i \in I_D} \frac{\left|g^i(m) - d^i_{obs}\right|}{\sigma^i_D}\right]$$

If C_D represents the covariance operator describing estimated errors and error correlations, assuming a Gaussian error distribution gives:

$$L(m) = \exp\left[-\frac{1}{2}(g(m) - d_{obs})^t C_D^{-1}(g(m) - d_{obs})\right]$$

Our purpose here is to compute the mathematical expectation

$$(m) = \frac{1}{v}\int_M dm \quad m \quad \sigma_M(m) \tag{3.53}$$

and the posterior covariance operator is given as:

$$C_M = \frac{1}{v}\int_M \mathrm{dm} \quad \mathrm{m} \quad \mathrm{m}^t \ \sigma_M(\mathrm{m}) - \langle m\rangle\langle m\rangle^t \tag{3.54}$$

where v is the norm of $\sigma_M(m)$:

$$V = \int_M \mathrm{dm} \quad \sigma_M(\mathrm{m}) \tag{3.55}$$

Using Equation (4.6) we can rewrite

$$v = \int dm\, \rho_M(\mathrm{m})\ \mathrm{L(m)} \tag{3.56}$$

$$\langle m\rangle = \frac{1}{v}\int_M \mathrm{dm}\ \rho_M(\mathrm{m})\mathrm{m} \quad \mathrm{L(m)} \tag{3.57}$$

$$C_M = \frac{1}{v}\int_M dm\, \rho_M(\mathrm{m})\mathrm{m} \quad m^t\ \mathrm{L(m)} - \langle m\rangle\langle m\rangle^t \tag{3.58}$$

Introducing the components of (m) and C_M, we arrive at the final equations:

$$\mathrm{V} = \int_M dm \quad \rho\mathrm{M(m)} \quad \mathrm{L(m)} \tag{3.59}$$

$$\langle m^\alpha\rangle = \frac{1}{v}\int_M dm \quad \rho_M(m)m^\alpha \quad L(m) \tag{3.60}$$

$$C_M^{\alpha\beta} = \frac{1}{v}\int_M dm\, \rho_M(m)m^\alpha m^\beta \quad L(m) - \quad \langle m^\alpha\rangle\langle m^\beta\rangle \tag{3.61}$$

We see thus that to compute the mean model value $\langle m\rangle$or the components of the covariance operator C_M, we have essentially to perform integration over the model space. If the dimension of the space is large (say more than 4) it is well known that Monte Carlo method of numerical integration should be preferred to more elementary methods using regular grids in the space, because the number of points needed with

regular grids grows too rapidly with the dimension of the space. Section (3.2.1) introduces the basic method of Monte Carlo numerical integration.

3.12.2.3 The Monte Carlo Method of Numerical Integration

Let ϕ(m) be an arbitrary scalar function defined over a discrete, s-dimensional space M(m$\in M$).Assume that we need to evaluate the sum

$$I = \int dm \;\; \phi(m) = \int dm^1 \ldots \int dm^s \;\; \phi(m^1, \ldots, m^s) \qquad (3.62)$$

over a given domain M$'$ $\in$ M.

If M' has finite volume, the simplest method of evaluating I numerically is by defining a regular grid of points in M', by computing ϕ(m) at each point of the grid, and by approximating the integral in (4.16) by a discrete sum. But as the number of points in a regular grid is a rapidly increasing function of the dimension of the space (N α const^s), the method becomes impractical for large-dimension spaces (say s$\geq$ 4). The Monte Carlo method of numerical integration consists in replacing the regular grid of points by a pseudo-random grid generated by a computer code based on a pseudo-random number generator.

Although it is not possible to give any general rule for the number of points needed for an accurate evaluation of the sum (because this number is very much dependent on the form of $\phi(m)$). For a well behaved function ϕ(m), this number can be smaller, by some orders of magnitude, than the number of points needed in a regular grid.

Let us note p(m) as an arbitrary probability density function over M that we choose to use for generating pseudo-random points over M; (p(m) = constant is the simplest choice, but more astute choices can improve the efficacy of the algorithm).

Defining $\psi(m) = \frac{\phi(m)}{p(m)}$

The sum we wish to evaluate can be written as:

$$I = \int_M dm \;\; p(m) \; \psi(m) \qquad (3.63)$$

Let $m_1,...m_N$ be a suite of N points collectively independent and randomly distributed over M' with a density of probability p(m). We define

$$\psi_n = \psi(m_n) \tag{3.64}$$

$$I_N = \frac{1}{N}\sum_{n=1}^{N}\psi_n \tag{3.65}$$

$$V_n = \frac{N}{N-1}\left[\frac{1}{N}\sum_{n=1}^{N}\psi_n{}^2 - I_N{}^2\right] \tag{3.66}$$

It can easily be seen that the mathematical expectation of I_N is

$$\langle I_N \rangle = \int_{M'} dm \quad p(m)\ \psi(m) = I \tag{3.67}$$

So that I_N is an unbiased estimate of I. Using the central limit theorem it can be shown (bakhvalov, 1977) that, for large N, the probability of the relative error $|I_N - I| / |I|$ being bounded by:

$$\frac{|I_N - I|}{|I|} \leq \frac{K\sqrt{V}}{|I|\sqrt{N}} \tag{3.68}$$

where V is the unknown variance of ψ(m), is asymptotically equal to

$$p(k) = 1 - \frac{2}{\sqrt{2\pi}}\int_k^{+\infty} dt \exp\left[-\frac{t^2}{2}\right] \tag{3.69}$$

For large N, a useful estimate of the right-hand member of (3.68) is

$$\frac{k\sqrt{v}}{|I|\sqrt{N}} \simeq \frac{\sqrt[k]{V_N}}{|I_N|\sqrt{N}} \tag{3.70}$$

where I_N and V_N are defined by equations (3.65) and (3.66).

This method of numerical integration is used as follows: first, one selects the value of the confidence level, p(k), at which the bound equation (3.68) is required to hold (for instance, p(k)=0.99). The corresponding value of k is easily deduced using equation (3.69) and the error function tables ($k \simeq 3$ for p(k)= 0.99). A pseudo-random number generator is then used to obtain the point m_1, m_2,…..……distributed with the probability p(m), and, for each new point, the right-hand member of the equation (3.68) is estimated using equation (3.70). The computations are stopped when this

number equals the relative accuracy desired (for instance, 10^{-3}). The typical statement that can then be made is as follows: "The value of I can be estimated by I_N, with a probability of p(k) (e.g 99%) for the relative error being smaller than $\in$ (e.g. 10^{-3})".

Comparison of equations (3.59) – (3.61) with equation (3.63) suggests using the function $\rho_M(m)$ as density of probability of generating random points in the model space, i.e. identifying ρ_M (m) with p(m) of equation (3.63). The effect of this choice will be to sample the regions of the space more densely where a priori we expect significant values of the integrands, so the convergence of the method can be reasonably good. In addition, the identification of ρ_M (m) with p(m) allows a nice simplification of the formulas.

Explicitly, the unbiased estimators of $\langle m^\alpha \rangle$ and $C_M^{\alpha\beta}$, after generation of N points, are

$$\langle m^\alpha \rangle = \frac{1}{Nv}\sum_{n=1}^{N} m^\alpha \qquad L(m_n) \tag{3.71}$$

$$C_M^{\alpha\beta} = \frac{1}{Nv}\sum_{i=n}^{N} m^\alpha m^\beta \qquad L(M_n) - \langle m^\beta \rangle \langle m^\beta \rangle \tag{3.72}$$

where

$$v = \sum_{i=0}^{N} L(M_n) \tag{3.73}$$

and where it is assumed that the points m_1, m_2.....have been generated with the probability density ρ_M (m).

The generation of random points may be stopped as soon as the criterion of relative precision is verified.

While computing $\langle m \rangle$ and C_M, it is desirable to keep in the computer memory the models which have obtained high values for σ_M(m). They will approximately represent the domain of acceptable models as defined previously. If these models are reasonably close to $\langle m \rangle$, we can have some confidence in that the probability density function σ_M (m) is not very asymmetric or multimodal.

3.12.3 Numerical/Computational Method

An algorithm is used to generate random number in the computer, which in turn are used to select the random density (ρ) values that characterize a given model. In the generation of the models, mass M, and moment of inertia of the Earth I, about the polar axis, which are also known as the moments of the density distribution are the basic data which must constrain all models. A set of models is constructed from a uniform probability density within the bound and slope constraints which results in the generation of density models. Each of the resultant density model is tested against the mass and moment of inertia of the Earth. From the misfit properties of the ensemble of models, the robustness of the density profile in different portions of the Earth can be assessed. These data suffer in that they are incomplete and uncertain owing to observational errors and lateral variation in the crust and upper mantle. Aside from the unsolved formal problem of uniqueness of inversion of geophysical data, the many models proposed from this set of data provide empirical evidence of the lack of uniqueness. The method based on random selection of the density (ρ) values with depth variation to the depth of the asthenosphere taken to be about 650km is used in the models. The mass, M and moment of inertia, I, are computed for the density distribution. At this stage, the computation, which is the model space, is then compared with the observed model to test whether the model is successful or not. If the model is unsuccessful, another set of parameter are selected repeatedly until a model test successfully. The computation is done on a Pentium system using MATLAB 8.2 and NUPLOT as the 3-D software.

A knowledge of the density distribution within the Earth is important for many aspects of understanding the internal structure of the Earth. In particular, the density is a primary piece of information for unravelling the mineralogical constitution of the Earth. The 3-D variation of density is important in relation to the shape of the geoid and the possibility of density variations accompanying the Earth heterogeneity in gravity modeling. These models for the Earth density distribution have ultimately been derived by linearized inversion from models whose origins include a number of physical arguments to supplement the limited range of direct information (Bullen, 1975).

As earlier stated, the major constraints are obtained from the mass and the mean moment of inertia of the Earth about the polar axis. The mass is the second moment of the radial density distribution given as:

$$M = 4\pi \int_0^r dr\ r^2 \rho(r) \qquad (3.74)$$

where r_e is the mean radius of the Earth, 6378Km, and M is the mass of the Earth, 5.9736 x 10^{24}Kg.(Yoder, 1995; Cazenave, 1995; Dickey, 1995). The mean moment of inertia is a scaled fourth moment of the density distribution expressed as:

$$I = 4\pi\frac{2}{3}\int_0^r dr\ r^4 \rho(r) \qquad (3.75)$$

and the currently accepted value in terms of the mass of the Earth is $I = 0.3307144Mr_e^2$

.

However, additional information on the radial density distribution comes from the free oscillations of the Earth. The frequencies of the spheroidal and radial normal modes are influenced by the density distribution through self-gravitation effects induced during the Earth deformation associated with the mode.

Presently, the mean density of the crust used in the Bouguer anomaly reduction is 2.74g/cm^3. (Woollard,1988). However, the crust is hydrostatically supported by the mantle in accordance with the Airy concept of isostasy. Following this mechanism of isostatic compensation, the mass of mantle material displaced must be equal to that of the overlying crust ($\Delta H_m \sigma_m = H_c \sigma_c$), and the surface elevation will be dependent on the thickness of the crustal column (H_c) and the density contrast between the crust and mantle($\Delta\sigma = \sigma_m - \sigma_c$).The critical factor is the thickness of the actual crust, which probably extends well below the mohorovicic discontinuity and possibly to the seismic low-velocity zone at about 150Km.

Thus, the gravity equation can be used to evaluate anomalies in terms of the mass distribution associated with the crust and upper mantle. This is then used to obtain the density distribution within the Earth subsurface region. Tables B6 and B7 (see

Appendix B) shows the density data distributed across the West African region for various latitude and longitude values. This is obtained alongside their depths.

However, it is also possible to obtain the density distribution using the model for various geographical locations in West Africa if we insert their latitude and longitude values. Table B8 summarizes the range of density distribution over all the West African countries and their geographic location.

This simply implies that density calculations can be made from known density model if appropriate geographic locations of latitude and longitude are inserted during numerical computations. Appropriate density data generated from the model can now be compared with available terrestrial density data of the location where anti-Earth activities has occurred and tectonic events are prevalent. It can also be compared with the available satellite data. For more adequate reliability of the model, density values must conform with the expected trend and close to reality so that the associated errors are minimized. Density comparisons are done for In-situ/observed and models i.e. MGM and MGGM. However, different existing density models are equally compared with the density model obtained from our Monte Carlo method used in the calculation process for both oceanic and continental areas of West African region (also known as the density model validation). The density model used in this research work is a time varying equation which can be expressed as:

$$\rho'(t) = \frac{\partial \rho}{\partial t} = \frac{3}{8\pi} \cdot \frac{GM}{r^2} \left[1 + (\gamma + 1) \frac{\rho_0 g z}{Cos\Phi} \right]^{n-1} e^{-2t} \qquad (3.76)$$

This time-series density equation can be used to determine the density value of any given location (including areas which had been derailed by human activities both in the oceanic and continental regions of West Africa) at a particular point in time. The interesting part is that density calculations are made before and after such human activities (i.e. anti-earth operations) are performed. Without any doubt, it is expected that a change in density values will be observed and this density calculation makes the research work interesting. Many areas of interest within the West African region where density calculations can be done include the South-south Nigeria where excavation

have taken place, Niger delta oil field region where exploration or exploitation of valuable hydrocarbon occurs, Iron ore and marble deposit regions in Ajabanoko area in Kogi State and Toto area in Nasarawa State respectively where geological explorations had begun. Although, this research work focus on landslide area in Itakpe, Kogi state Nigeria which existed as a result of the excavation in the south-south region of Nigeria where oceanic is linked with continental within the West African sector. The next section gives the different earth gravity equations which takes into consideration various physical parameters of interest.

3.13 The Earth Density Models

Many density equations are in existence which specify the density of the lithosphere and especially the density of regions that are affected by natural and artificial human activities within the continental and oceanic sector. It is important to note that density calculations are made from known density equation. The density model used in this research is obtained from Monte-Carlo calculation where equations (4.1) and (4.2) relates gravity to density. This density model is validated by comparing the model with the existing density models. The various density models are thus listed in the expressions defined as:

1.) $\rho(z) = \frac{1}{\mu}\frac{GM}{r} - \frac{3}{4}\rho_o K^2 gz$ (Sunket, 2002)

2.) $\rho(z) = \rho_o[1+ (\frac{R_o}{R})^3 (\frac{<\rho>}{\rho_o} -1)]$ (Bennard, 1997)

3.) $\rho(z) = \frac{\rho_o}{\frac{1-\rho}{k}}$, $\frac{1}{k} = \frac{-1}{\rho^2 g}\frac{dp}{dr}$ (Williamson-Adams, 2011)

4.) $\rho(z) = \frac{Rak\eta}{g\alpha\Delta T H^3}$ (Bullen, 1998)

5.) $\rho(r) = \frac{2}{3}(\frac{R}{r})\rho$ (Buffet, 2003)

6.) $< \rho >= \frac{3}{R^3}\int_o^R \rho r^2\, dr$ (Spengler, 2006)

7.) $\rho = \frac{4\pi G\rho_o}{3} R[\,(1-\frac{T_o}{R})^3 - 1]$ (Murnaghan, 2013)

8.) $\rho(r) = \frac{3}{2\pi}\frac{P(r)}{G(R^2-r^2)}$ (Sin mλ + Cos mλ) (Pollack, 1995)

9.) $\rho(r) = \frac{3g}{4\pi Gr}(r^3 - R^3)$ (Poirier, 2000)

10.) $\rho = \frac{5E}{8\pi}\frac{1}{GMR^2}$ (Hemley, 2012)

11.) $\rho = \frac{3g}{4\pi}\frac{1}{Gr}$ (Hirose, 2007)

12.) $\rho(z) = \frac{3M}{4\pi R^3}\frac{1}{Z-r}\text{Cos}\, m\lambda - 1$ (Lay et al., 2005)

13.) $\rho(P) = \rho_o exp(\frac{p}{k}), \quad \rho = \ln(\frac{\rho}{\rho_o})^k$ (Musset, 1993)

14.) $\rho(P) = \rho_o(\frac{k_o P}{k_o})^{-1/k}$ (Boehler, 1996)

15.) $\rho(P) = \rho_o\, exp\,(\int_o^z \frac{\alpha g}{C_p}\,\text{dz})$ (Hernlund et al., 2005)

16.) $\rho(z) = \rho_o \exp(\lambda t)$ (Van Hun et al., 2008)

where all parameters take their usual meaning. ρ_o is the earth surface density =2.80 x 10^3Kg/m^3, k is the bulk modulus = 400 GPa, g_o is the theoretical gravity (which varies), γ is the number of earth layers, z= R-r is the depth coordinate, R_o= surface radius, r=depth radius, <ρ> =Earth mean density whose value is 5.515 x 10^3Kg/m^3, P is the depth pressure, C_p is the specific heat at constant pressure, M is the mass of the Earth.

The corresponding density data for few existing models are compared for both oceanic and continental regions/locations of interest. This is the area where anti-earth activities had occurred or engaged within the West African sector.

3.14 Applications of the Gravity Field Model

As earlier stated, the model is a mathematical representation of the Earth's gravitational potential V (r, ϕ, λ) which can be used (1) to map the gravity either at or near the Earth's surface. This geopotential equation is a 3-Dimensional model which can be used to map the gravity of the West African lithospheric region. The geo-potential equation is used to determine the variations in the Earth's gravitational field at different locations over the West African sector (where ocean-continent interaction occurs) which is the area of concentration in this research. This Earth's gravity field values at various region (2) produces valuable information on the different Earth materials embedded in the subsurface region of the Earth and having different bulk densities and hence, mass anomalies. This implies that material bulk densities can be related to the Earth's gravitational field values by equations which will be expressed later. For any mass buried in the Earth, the effective density is the difference between the density of the buried object itself and that of the surrounding material. This quantity which is termed as "density contrast" is an important physical parameter which can be obtained from the model and form the basis on which gravity geophysical technique lies. This is because the interpreter of gravity data is interested in determining this subsurface variations of mass caused by human activities (such as mineral and oil exploration, hydro-geological drilling, mining, rock blasting and heavy construction of sky scrapers) in the lithosphere and this process requires that the density of the material of interest or the density contrast between the material of interest and the surrounding material be known. A good idea of the gravity field model also shows the quantity of sub-surface materials erupted to the Earth surface through diverse anti-Earth activities thereby creating mass deficiencies in the Earth's body which resulted into instability of certain sector in respect to another. (3) The various natural tectonic events such as Seafloor spreading areas, subduction zones, rift systems, oceanic and deep marine trenches, volcanoes and Earthquakes, Island Arcs, fracture regions, faults and folds can be expressed through rigorous calculations of gravity models. Basically, this gravity field model is used to determine tectonic regions of Earth depressions and elevations particularly the unstable portion of the Earth's lithosphere. (4) Thus, the orbital perturbation (created by satellite motion) allowed us

to determine the figure of the Earth thereby obtaining information concerning its shape. This model has made it possible to map out those areas, within the West African sector, that are tectonically unstable and mass deficient. It is a 3-Dimensional model of the West African lithospheric region. We can then summarily apply the gravity field model as:

(1) To map the gravity either at or near the Earth's surface region

(2) To obtain valuable information and determine the location of subsurface structures

(3) To determine the density distribution of materials in the Earth subsurface region

(4) To determine the regions of tectonic events and natural disasters

(5) To determine the Earth's figure and shape created by orbital perturbations

CHAPTER FOUR

RESULTS AND DISCUSSION

This section focuses on the results obtained from numerical computation. Scientifically, the results presented are referred to as generated data. These results are represented concisely and analysed so that data can be plotted on gravity profiles. Also, 3-dimensional gravity contour maps are obtained as well as the surface maps which can be interpreted accordingly. The results obtained in this research are as presented and discussed in the sections below.

4.1 Gravity Data Presentation

Data presentation is the organization of results obtained into tables, graphs or charts, so that logical and statistical conclusions can be derived from the collected measurements. Data may be presented in three major ways: Textual, Tabular or Graphical. Therefore, gravity data is a representation of the observed operations performed on or beneath the Earth subsurface region i.e. the lithospheric segment which could either be continental or oceanic areas as the case may be. It is useful in exploring regions of different geological structures. The Earth gravity results were obtained from the model after computation using program language. These earth gravity results could be geopotential, geoidal undulation or gravity anomaly which produces different gravity values.

Table 4.1 present the results obtained when geopotential $V(r,,\lambda)$ in m^2/s^2, geoidal height N(m) in metres and gravity anomaly Δg in mgals are generated (from numerical computation) across the continental region of West African sector by using the modified gravity model. This gravity data are obtained for varying latitude and longitude sections.

Table 4.1: The geopotential, geoidal height and gravity anomaly values at various latitude ϕ and longitude λ section computed using MGGM over the West African (continental) Region.

Latϕ(deg)	Long λ (deg)	V (r,ϕ,λ)	N(m)	Δg(mGals)
6.025	5.027	96.98	58.6	81.22
6.047	5.036	75.82	72.5	-10.91
6.082	5.042	138.31	-22.4	11.36
6.094	5.051	69.07	96.2	27.45
6.113	5.067	-35.33	35.3	-38.69
6.138	5.073	82.83	79.1	52.77
6.149	5.089	108.22	66.9	64.05
6.157	5.096	-41.15	-54.7	83.13
6.162	5.104	72.63	-20.8	-57.08
6.183	5.115	85.76	-88.3	49.87
6.197	5.128	-18.85	-12.5	91.71
6.200	5.136	139.94	58.6	-68.26
6.206	5.143	83.03	39.5	-85.24
6.213	5.150	91.55	-77.2	75.21
6.222	5.164	-17.11	-14.4	41.89
6.236	5.178	-42.05	55.9	-95.03
6.241	5.182	127.25	71.7	56.79
6.245	5.195	79.46	83.6	-12.33
6.250	5.207	86.84	61.8	84.46
6.254	5.216	105.97	84.9	57.75
6.259	5.229	-39.89	-28.6	98.12
6.263	5.231	96.91	59.2	-67.14
6.264	5.248	-12.83	83.4	56.22
6.272	5.252	131.09	44.1	-81.41
6.279	5.267	112.57	-33.7	60.68

Table 4.1 continued

Latϕ(deg)	Long λ (deg)	V (r,ϕ,λ)	N(m)	Δg(mGals)
6.285	5.279	126.23	77.9	89.25
6.305	5.284	79.81	36.5	-37.48
6.381	5.293	90.06	-18.3	70.46
6.413	5.307	205.74	39.4	61.91
6.472	5.318	82.19	102.8	-43.27
6.524	5.326	138.33	97.7	84.83
6.566	5.330	92.24	46.7	61.18
6.597	5.342	64.75	29.2	42.32
6.604	5.356	-30.29	39.0	-59.94
6.639	5.368	114.86	-66.4	43.77
6.682	5.372	-22.26	-38.1	-22.65
7.005	5.389	89.59	-63.6	53.93
7.314	5.395	56.66	35.8	86.71
7.593	5.404	-14.06	58.5	-69.47
7.728	5.416	69.18	-92.2	55.77
7.911	5.429	-37.09	-48.6	-41.39
8.136	5.438	65.86	63.8	62.03
8.394	5.443	-58.97	57.4	97.36
8.482	5.455	115.19	-12.7	-55.24
8.605	5.469	70.52	-59.5	64.87
8.719	5.478	141.11	27.1	-71.42
8.753	5.482	97.34	75.6	35.39
8.762	5.493	62.96	-44.9	63.15
8.781	5.506	87.23	98.6	-51.25
8.800	5.517	155.93	36.2	88.19
8.814	5.529	85.61	-91.4	-43.73
8.826	5.538	90.74	28.6	57.29
8.839	5.541	76.52	94.5	63.07
8.845	5.552	149.94	-32.4	38.15
8.857	5.560	223.16	-51.4	-52.33

Table 4.1 continued

Latϕ(deg)	Long λ (deg)	V (r,ϕ,λ)	N(m)	Δg(mGals)
8.862	5.573	135.38	47.1	-79.25
8.873	5.589	96.79	29.6	65.04
8.885	5.597	48.04	-23.9	-47.28
8.896	5.604	126.96	78.7	-65.93
8.907	5.612	81.75	-13.2	78.94
8.912	5.628	90.64	31.6	57.58
8.929	5.635	79.28	64.5	93.11
8.931	5.641	225.83	-20.2	-64.24
8.946	5.653	132.46	57.3	87.08
8.953	5.669	-24.13	40.8	60.78
8.965	5.674	106.08	62.5	92.27
8.972	5.682	101.51	-85.9	-46.83
8.984	5.690	85.16	47.1	-57.81
8.996	5.705	72.97	92.4	36.17
9.015	5.713	138.31	38.6	58.43
9.027	5.729	165.63	-14.5	-47.79
9.036	5.735	93.88	45.3	61.19
9.042	5.748	64.75	85.8	-15.02
9.058	5.752	138.26	69.7	58.43
9.063	5.769	149.94	80.2	-66.74
9.071	5.774	65.48	-41.6	-10.69
9.086	5.783	74.62	76.9	72.68
9.094	5.791	160.17	31.5	56.62
9.105	5.802	82.88	66.4	84.03
9.116	5.816	95.34	82.3	-69.11
9.128	5.822	121.91	75.1	-47.36
9.132	5.837	69.13	59.9	93.92
9.145	5.845	124.55	16.2	-10.81
9.159	5.853	93.41	-26.5	-29.57
9.162	5.869	186.79	53.7	73.14

Table 4.1 continued

Latϕ(deg)	Long λ (deg)	V (r,ϕ,λ)	N(m)	Δg(mGals)
9.174	5.875	157.52	30.4	48.52
9.183	5.880	84.66	88.8	67.54
9.196	5.897	51.83	-32.1	96.62
9.207	5.904	-19.04	47.6	59.82
9.215	5.913	156.32	82.5	84.66
9.228	5.926	85.85	-39.3	95.62
9.239	5.938	97.46	-52.4	103.45
9.246	5.946	87.07	-47.2	94.71
9.252	5.951	30.18	82.6	75.16
9.265	5.963	-27.75	56.0	87.35
9.278	5.972	79.85	73.8	-91.68
9.283	5.986	-22.51	38.2	65.37
9.296	5.995	94.52	83.5	42.92
9.304	6.006	-12.77	51.9	-74.22
9.315	6.014	186.38	-69.4	23.19
9.327	6.023	-59.36	97.3	62.27
9.336	6.038	214.44	58.2	-78.65
9.348	6.047	85.75	46.2	69.44
9.359	6.059	-25.98	123.7	51.59
9.362	6.062	127.54	-37.5	-24.17
9.373	6.076	73.27	-82.9	49.21
9.385	6.088	92.73	92.6	-64.65
9.391	6.095	-25.13	75.2	-85.43
9.406	6.104	139.81	65.4	43.18
9.415	6.113	68.94	-41.5	-74.68
9.422	6.127	-43.11	-11.3	52.55
9.436	6.139	225.48	174.1	64.46
9.447	6.141	72.01	58.9	-82.06
9.458	6.156	-28.35	67.4	-31.29

From Table 4.1, the latitude ϕ of the continent varies between 6.025^0N and 9.458^0N while the longitude λ varies between 5.027^0W and 6.156^0E. The geopotential has a minimum value at $98.3m^2/s^2$ and attains a peak value at $482.5m^2/s^2$. This geopotential value increases eastward initially to $162.6m^2/s^2$ at a height of 238m and then begin to drop drastically to a value of $24.8m^2/s^2$ at a depth of 74m. This low value of gravity potential indicates that mineral exploitation had occurred in that region or location and certain quantity of mass had been removed from the earth lithospheric segment. Usually, continental areas are associated with high geopotential values. According to this table 4.1, geopotential values are appreciably low which corresponds to high mineralized zones. These gravity values begin to increase, indicating that such area had being explored and certain human operations were carried out in that location. The data presented were acquired over low longitude.

Geoidal height data for continental lithosphere (Itakpe area) located within the West African region at latitude 7.453^0N to 9.226^0N and longitude 6.431^0E to 8.457^0E varies from -51.6m to a maximum value of about 498.7m at latitude 7.532^0N to 9.136^0N and longitude 6.714^0W to 8.514^0E with an average height of about 272.3m at latitude 7.592^0N and longitude 6.514^0W. The gravity height or undulation increases in value to a height of about 301.6m as we move towards the South-western direction. However a decrease in gravity height value to about 12.8m is experienced in the southward direction at latitude 7.481^0N and longitude 6.527^0W. The geopotential data for the continental lithosphere of West African sector can be presented on combined graphs known as geopotential gravity profile plots (Fig. 4.1).

4.2 The Geopotential Profiles

Gravity geopotential profiles are presented in Figures 4.1 and 4.2. It is observed that geopotential variations are quite distinct for both oceanic and continental region within the West African sector since their weights are also different. This has become prominent when gravity is related to the subsurface mass anomaly distribution as expressed in the bouguer formula (Equation 3.47). However, any anti-Earth operation performed by man within the oceanic region can produce an overall effect on the

continental sector within the West African region. The gravity geopotential value reduces due to human activities in the region.

Figure 4.1 is the combined gravity potential profile or chart obtained from the density results of Table 4.1

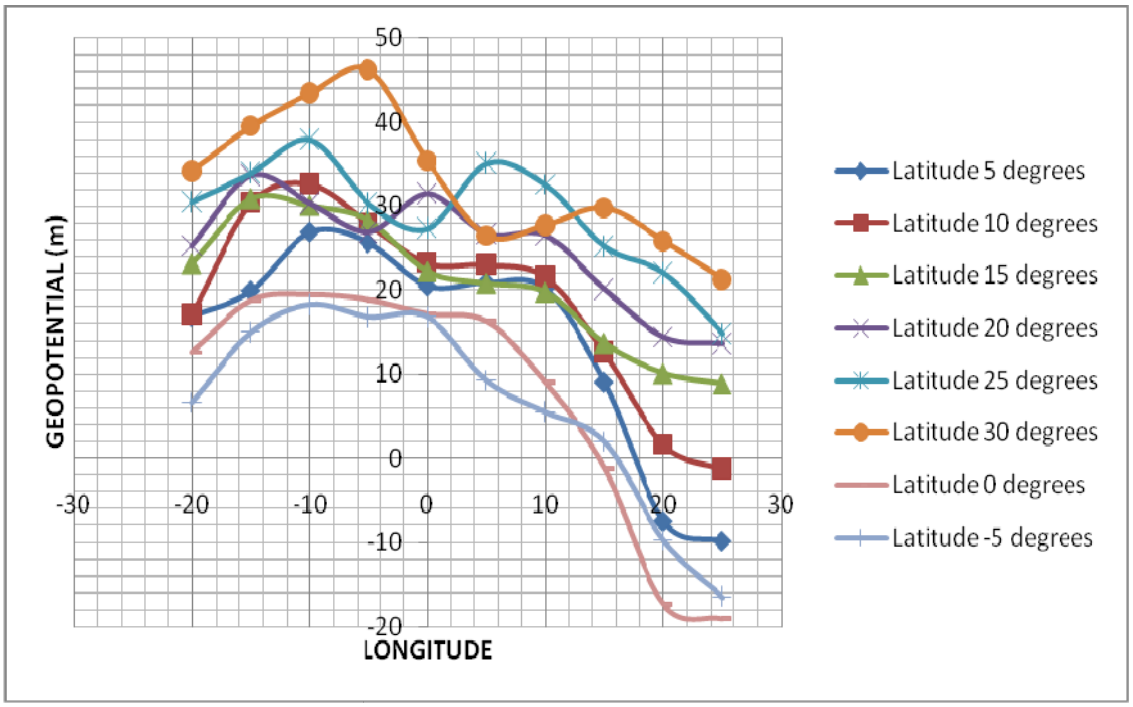

Figure 4.1: The combined Plots of density values against Longitude at various Latitude values using the modified gravity geopotential model for continental lithosphere

From Figure 4.1, the combined plots of gravity field values against the longitude at different latitude using the modified geopotential gravity model for continental lithosphere of West African sector is obtained. The Figure shows that there is an increase in the gravity field values with an increase in latitude. The least latitude of -5degree has the minimum gravity field plot ranging between -162.8m^2/s^2 and 71.4m^2/s^2 at longitude values between -20^{0}W and 25^{0}E. The next gravity field profile with latitude 0degree has a minimum gravity field value of -194.6m^2/s^2 with a peak value at 133.2m^2/s^2 at longitude which coincides with the -5degree latitude profile. Just immediately above it is the 5degree latitude profile having an increase in gravity field value from 165.6m^2/s^2 to about 273.8m^2/s^2 which then reduces to 200.7m^2/s^2 at longitude of -2^{0}W. This gravity field remains constant to longitude 10^{0}E and then reduces drastically to about -90.5m^2/s^2. Gravity field profile with latitude 10degree has a gravity field value ranging between 168.4m^2/s^2 and -12.6m^2/s^2 at longitude varying between -20^{0}W and 20^{0}E. There is sharp reduction in this value of gravity field. Profile with latitude 15degree maintains a gravity field value of 231.5m^2/s^2 at longitude between -15^{0}W and -5^{0}W and then observe a reduction in gravity field value to a minimum of about 86.7m^2/s^2. The 20degree latitude profile has an initial gravity field value of 250.9m^2/s^2 at longitude -20^{0}W which increases to a value of about 342.6m^2/s^2 at longitude -12^{0}W. This gravity field then reduces to 268.5m^2/s^2 at longitude -5^{0}W and then begin to experience an increase in gravity field value again to 322.4m^2/s^2 at longitude 2^{0}E. The 25degree latitude profile was observed to have a twice increase in gravity field value from 310.6m^2/s^2 to 380.3m^2/s^2 at longitude between -18^{0}W and -10W and also from 270.8m^2/s^2 to 358.5m^2/s^2 at longitude variation between -2^{0}W and 5^{0}E. At 5^{0}E, the gravity field value then reduces to 146.7m^2/s^2. The 30degree latitude profile has a sharp increase in gravity field value from 340.8m^2/s^2 to about 462.3m^2/s^2 peak value at longitudes between -20^{0}W to -5^{0}W and then begin to experience a reduction in gravity field value at longitude between -5^{0}W and 5^{0}E from 462.3m^2/s^2 to 264.7m^2/s^2. The modified gravity field values, gravity model (MGGM) gave a precise and accurate value of gravity field value for the continental lithosphere within the West African sector. At this point, it is equally desirable to look at what will be experienced at the oceanic lithosphere. Table 4.2 is a comprehensive data showing the gravity field

$V(r,\phi,\lambda)$, geoidal height N(m) and gravity anomaly Δg at various latitude and longitude values over oceanic lithosphere using the modified GGM.

It is deduced that low latitude gravity potential profiles are associated with high mineralized zones while the high latitude profiles shows low mineralized deposits. The implication of this is that mineral exploitation in high mineral deposits will result in low density values. This may be found in continental lithospheres.

Table 4.2: The geopotential, geoidal height and gravity anomaly values at various latitude ϕ and longitude λ section computed using MGGM over the West African (oceanic) Region.

Latϕ(deg)	Long (deg)	λ	V (r,ϕ,λ)	N(m)	Δg(mGals)
4.825	5.934		125.35	87.6	-21.52
4.836	5.947		26.22	36.9	68.79
4.839	5.951		89.87	94.4	-45.22
4.847	5.963		-18.64	61.2	15.48
4.851	5.977		79.07	-22.0	32.31
4.856	5.986		93.55	85.8	-16.14
4.862	5.992		34.98	103.3	-12.78
4.866	5.998		122.01	67.5	54.33
4.872	6.007		30.56	-10.7	34.65
4.875	6.015		166.79	-71.9	63.77
4.880	6.022		82.83	127.4	-34.86
4.884	6.037		99.71	43.5	-52.83
4.889	6.041		126.54	205.7	23.56
4.893	6.049		68.76	-55.2	37.89
4.896	6.053		79.45	-67.3	13.34
4.907	6.064		-57.33	-98.0	82.61
4.909	6.072		83.32	45.7	76.85
4.915	6.079		92.59	89.9	16.92
4.921	6.083		38.06	123.8	67.46
4.928	6.095		-27.33	-34.6	23.14
4.934	6.102		69.56	67.5	56.89
4.939	6.108		41.07	-54.2	88.73
4.946	6.113		73.95	89.5	42.67
4.950	6.119		-90.51	42.8	81.98
4.953	6.126		109.99	67.6	33.27
4.958	6.132		86.84	34.4	55.42
4.961	6.139		37.24	76.2	43.95

Table 4.2 continued

Lat ϕ(deg)	Long λ (deg)	V (r,ϕ,λ)	N(m)	Δg(mGals)
4.967	6.143	70.41	77.8	34.26
4.971	6.147	98.45	49.6	73.47
4.982	6.158	56.15	34.8	95.42
4.986	6.164	101.56	-28.4	34.89
4.993	6.179	80.37	45.6	45.22
4.999	6.185	106.08	76.1	65.84
5.006	6.189	-87.52	-35.2	44.76
5.012	6.193	68.45	45.3	62.29
5.025	6.199	57.38	67.6	57.50
5.037	6.202	89.18	-45.8	76.12
5.044	6.215	64.17	-39.7	34.86
5.049	6.224	93.95	27.0	45.42
5.056	6.231	32.86	67.9	31.97
5.061	6.245	79.31	-45.4	15.29
5.067	6.249	**151.77**	31.2	49.38
5.073	6.351	86.66	-43.8	20.24
5.082	6.368	43.65	-26.1	66.75
5.095	6.374	87.93	53.5	85.69
5.106	6.386	138.22	35.6	77.73
5.113	6.392	-44.86	-19.3	96.28
5.118	6.398	16.22	23.7	83.97
5.124	6.405	169.56	-32.0	55.95
5.138	6.417	78.59	-38.5	36.74
5.146	6.429	62.21	43.2	68.45
5.155	6.433	81.08	62.7	-57.48
5.162	6.438	163.11	95.6	43.71
5.169	6.445	92.06	42.1	53.28
5.173	6.457	183.72	59.8	26.73
5.185	6.472	97.07	75.3	-16.52
5.192	6.488	72.39	94.9	18.93

Table 4.2 continued

Latϕ(deg)	Long λ (deg)	V (r,ϕ,λ)	N(m)	Δg(mGals)
5.197	6.493	126.58	87.6	-58.16
5.204	6.507	78.48	65.4	65.24
5.213	6.512	-95.42	-41.2	-50.21
5.218	6.529	47.69	89.5	-18.66
5.222	6.536	89.75	56.8	-34.74
5.225	6.540	76.03	47.3	-37.48
5.236	6.548	143.67	-56.0	-39.52
5.240	6.553	66.95	78.1	67.25
5.247	6.557	85.72	63.6	41.61
5.251	6.565	94.68	86.2	87.29
5.258	6.571	81.56	-45.5	-56.38
5.263	6.576	162.17	67.8	-45.70
5.269	6.582	72.73	-78.4	34.34
5.276	6.585	85.19	87.7	45.32
5.284	6.593	120.83	78.1	-23.85
5.287	6.606	55.16	67.9	43.42
5.292	6.617	94.29	-43.2	49.66
5.305	6.625	203.61	-36.4	-51.19
5.313	6.638	74.95	39.8	43.87
5.321	6.641	88.19	23.5	-47.32
5.326	6.649	143.94	50.1	40.63
5.330	6.654	62.81	56.5	35.84
5.337	6.663	91.69	52.8	26.42
5.342	6.679	139.22	-45.2	44.18
5.349	6.685	84.04	-41.4	-35.77
5.351	6.692	105.38	-37.3	22.16
5.358	6.701	73.05	76.7	-29.75

Table 4.2 continued

Latϕ(deg)	Long λ (deg)	V (r,ϕ,λ)	N(m)	Δg(mGals)
5.367	6.707	84.62	85.9	34.86
5.374	6.715	60.92	-58.8	-65.32
5.379	6.723	93.58	76.9	-33.16
5.383	6.729	51.72	71.5	-60.74
5.386	6.731	97.49	64.0	-28.04
5.392	6.739	83.55	-82.3	74.95
5.395	6.742	148.02	-87.7	92.53
5.408	6.748	84.67	77.2	68.81
5.413	6.754	55.24	59.6	89.29
5.417	6.759	76.08	-56.8	69.98
5.423	6.765	109.09	71.7	93.76
5.429	6.778	64.87	48.4	-55.24
5.436	6.784	93.66	97.1	-81.87
5.441	6.789	82.61	63.5	-96.38
5.448	6.793	120.77	84.9	-36.53
5.527	6.797	79.15	29.4	-37.85
5.549	6.805	-53.28	22.8	-46.22
5.563	6.816	92.03	-49.6	55.83
5.582	6.828	104.17	-35.3	49.66
5.614	6.837	38.53	26.8	44.39
5.639	6.841	65.71	34.2	35.97
5.647	6.859	219.34	89.0	-23.46
5.651	6.864	31.45	63.5	-23.74
5.665	6.882	135.29	34.7	-19.32
5.689	6.897	78.54	28.1	-19.95
5.693	6.916	96.66	57.6	84.38
5.704	7.033	83.42	94.4	63.41

From Table 4.2, latitude ϕ of the oceanic lithosphere varies between 4.825^0N and 5.704^0N while the longitude λ varies between 7.033^0E and 5.934^0E respectively. The geopotential has a minimum value at -126.8m^2/s^2 and a peak value at 297.9m^2/s^2. This geopotential value increases eastward initially to about 33.6m^2/s^2 at a depth of -86m and then begin to reduce to a value of -105.3m^2/s^2 at a depth of -92m. This low gravity potential value experienced shows that certain operations such as oil exploration and replacement with brine (salt solution) had occurred in that region. It is known that oceanic areas are associated with moderately low geopotential values due to the topography of the region. Although, magnetic minerals and large oil deposits can be obtained underneath the ocean base where geopotential gravity values are high. However, geoidal height data for oceanic lithospheres (Niger delta and South-south Nigeria) also located within the West African sector at latitude 5.732^0N to 4.826^0N and longitude 7.154^0E to 5.866^0E varies from -229.5m to a value of about -516.7m minimum at latitude 4.286^0N and longitude 6.917^0E with an average height of about 378.6m at latitude 4.853^0N and longitude 6.726^0E. Gravity height reduces in value to a height of about -282.5m as we move towards the South-eastern direction. This decrease in geoidal height value is associated with the tremendous exploration of oil within the region.

Gravity anomaly values of the oceanic lithospheres varies from location to location as we move towards the South-eastern direction. It ranges between a minimum value of -75.88mgals to a peak value of about 200.65mgals at latitude between 5.424^0N and 5.793^0N and longitude ranging between 7.114^0E and 6.839^0E. The combined gravity plots for oceanic lithosphere is now shown in Figure 4.2 using MGGM.

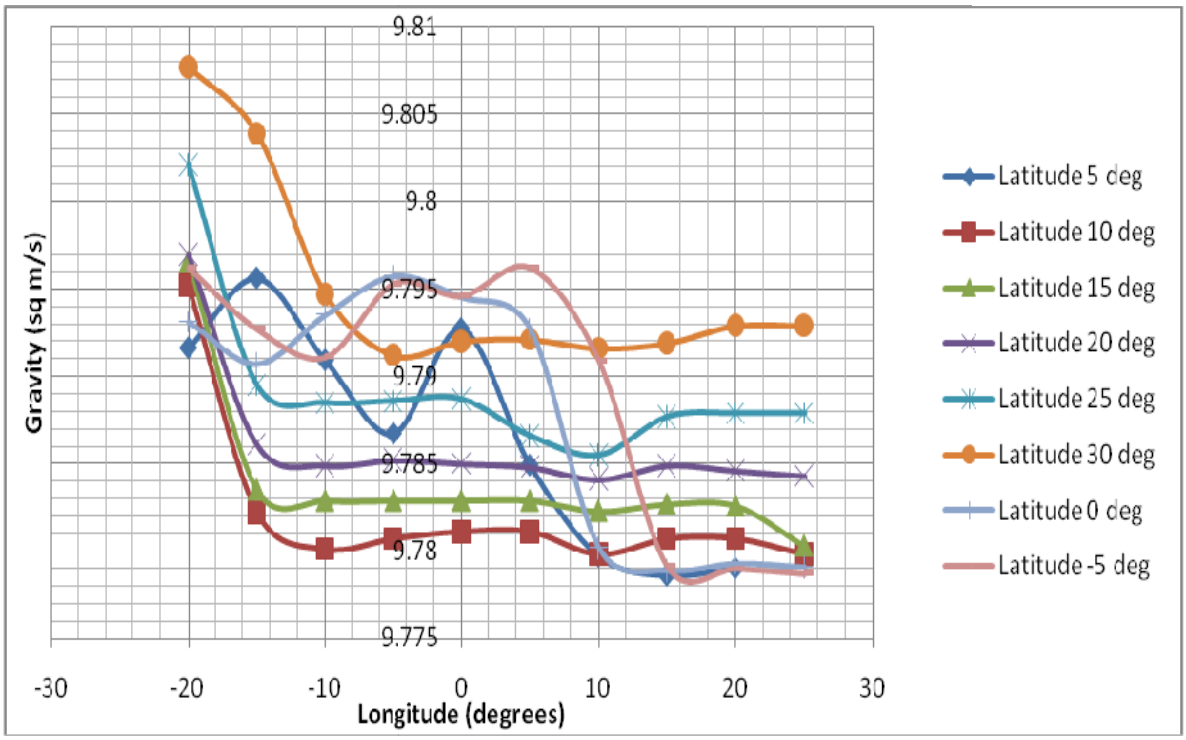

Figure 4.2: Graph of combined plots Showing Gravity Variation With Longitude at various Latitude values using the modified gravity geopotential model for oceanic lithosphere

A plot of gravity anomaly variation using modified geopotential gravity model (MGGM) against longitude at various latitude values over the oceanic lithosphere of West Africa shows that there is a decrease in gravity values as the longitude is traced from West to Eastward direction. Here, the least latitude profile of -5degree has the highest gravity values. A gravity value of 9.796sqm/s at longitude -20^0W decreases to 9.791sqm/s at longitude -10^0W and then begin to reduce to a value of about 9.778sqm/s. The next gravity profile of latitude 0 degree has a minimum gravity value of 9.779sqm/s and a peak value of 9.795sqm/s. Gravity value only increases between longitude -15^0W and 4^0E. At latitude 5 degree, gravity profile decreases from 9.803sqm/s to 9.790sqm/s between longitude -20^0W and -15^0W and then maintain a constant value of gravity to a longitude of 10^0E before inccreasing again to 9.795sqm/s. This reduction in gravity value indicates a shallow region in the oceanic lithosphere where certain quantity of subsurface material has been explored. Hence, there is a change in mass content of this oceanic lithosphere. Also, latitude profiles from 15 degree to 25 degree shows similar pattern except for a slight variation in gravity values in sqm/s. Having generated the goepotential, geoidal height and gravity anomaly data for both the continental and oceanic regions of West Africa, the summary of the data will now be presented in Table 4.3

Table 4.3 shows the geopotential values obtained from model and the observed/In-situ for both continental and oceanic lithospheres taking their latitude and longitude values into consideration.

Table 4.3: Summary of the geopotential data, location and model type

Geopotential data:	Area/location	Model/In-situ	Latitude	Longitude
85.6-249.7(m^2/s^2)	Continental	Model	4.9358°N-12.4273°N	13.4213°W-12.3502°E
73.8-215.6(m^2/s^2)	Oceanic	Model	5.1983°N-20.4013°N	6.2847°E-8.9936°E
79.4-261.5(m^2/s^2)	Continental	Observed	5.8156°N-14.3912°N	15.0498°W-10.4657°E
62.7-208.3(m^2/s^2)	Oceanic	Observed	6.3922°N-18.5749°N	7.5416°E-9.2748°E

From Table 4.3, the MGGM gives geopotential values ranging between $85.6m^2/s^2$ minimum to a peak value of $249.7m^2/s^2$ for continental lithosphere at latitude 4.935^0N to 12.427^0N and longitude 13.421^0W to 12.350^0E. This indicates an increase in geopotential value which tend to reduce with increased artificial anti-earth operations performed by man. This MGGM model produced geopotential values of $73.8m^2/s^2$ minimum which increases to $215.6m^2/s^2$ for the oceanic lithosphere at latitude 5.198^0N to 20.401^0W and longitude 6.284^0E to 8.993^0E. However, this is quite different for the observed or in-situ data. The observed gravity results which is the already measured available data also known as in-situ data has geopotential values ranging between $79.4m^2/s^2$ and $261.5m^2/s^2$ at latitude 5.815^0N to 14.391^0N and longitude 15.049^0W to 10.657^0E for continental lithospheres while the oceanic lithosphere produces a minimum geopotential value of $62.7m^2/s^2$ and a peak value of $208.3m^2/s^2$ at latitude 6.392^0N to 18.574^0N and longitude 7.541^0E to 9.274^0E. Geoidal height values for oceanic lithosphere (south-south Nigeria) at latitude 5.678^0N to 8.331^0N and longitude 6.952^0W to 5.938^0E has gravity values which varies from -249.7m to -168.2m for modified model while gravity heights values from in-situ data varies from -254.3m to -122.1m at latitude which coincides with that of the modified model.

4.3 Gravity Data Validation

This section is desired to validate the geopotential gravity data generated by the different models. We can achieve this by comparing the gravity results obtained from MGGM with the results obtained from GGM given by Wiechert and the observed in-situ gravity data. This will allow any reseacher in the area of geophysical science to determine the improvement made by the new model. Table 4.4 gives the geopotential values computed from MGGM, GGM, which are then validated by comparing the data generated with in-situ or observed gravity data for continental lithosphere. This may also be done for the oceanic lithosphere and variations in gravity values may be seen.

Table 4.4: The Geopotential values computed from Modified Model (MGGM) over Itakpe and compared with existing GGM (Wiechert, 2008) and observed/In-situ data.

Latitude (deg)	Longitude (deg)	Geopotential (m^2/s^2) Wiechert W/A (GGM)	Geopotential (m^2/s^2) Itakpe W/A	Geopotential (m^2/s^2) West Africa (MGGM)
6.264	5.027	96.67	88.55	93.84
6.267	5.033	85.01	69.27	77.26
6.269	5.039	68.33	46.13	59.22
6.273	5.044	116.83	92.49	86.91
6.281	5.051	24.83	-35.28	95.85
6.285	5.057	59.24	21.75	-33.36
6.291	5.062	-40.53	59.23	38.22
6.298	5.069	62.02	48.96	-25.42
6.304	5.073	49.73	57.14	69.45
6.310	5.078	-86.50	-24.82	-46.73
6.316	5.084	62.43	37.87	52.89
6.322	5.089	198.76	49.03	-27.55
6.328	5.095	79.45	56.14	68.64
6.331	5.101	-28.85	-46.27	33.90

Table 4.4 continued

Latitude (deg)	Longitude (deg)	Geopotential (m^2/s^2) Wiechert W/A (GGM)	Geopotential (m^2/s^2) Itakpe W/A	Geopotential (m^2/s^2) West Africa (MGGM)
6.335	5.107	57.16	29.63	42.11
6.342	5.116	-16.25	-38.39	-22.58
6.347	5.121	59.03	67.84	42.56
6.353	5.128	81.15	53.94	75.86
6.359	5.134	-47.33	-28.56	-31.64
6.364	5.139	-39.02	-46.83	-57.02
6.370	5.145	56.84	27.91	43.27
6.376	5.152	-23.89	-39.68	-10.55
6.381	5.160	-31.90	-57.42	-49.99
6.388	5.167	45.61	63.17	76.84
6.395	5.173	34.45	29.53	47.24
6.402	5.178	62.89	55.02	82.09
6.409	5.184	-20.14	-36.97	-29.12
6.414	5.190	-39.02	-16.94	-27.83
6.417	5.196	98.22	68.19	75.34
6.423	5.204	52.97	41.53	62.69

Table 4.4 continued

Latitude (deg)	Longitude (deg)	Geopotential (m^2/s^2) Wiechert W/A (GGM)	Geopotential (m^2/s^2) Itakpe W/A	Geopotential (m^2/s^2) West Africa (MGGM)
6.428	5.211	67.04	88.16	59.32
6.435	5.217	61.36	92.54	78.07
6.442	5.222	80.65	73.03	94.21
6.449	5.226	-57.90	-46.25	-30.41
6.456	5.234	61.26	73.84	88.15
6.463	5.240	23.07	18.09	46.23
6.467	5.248	-42.56	-54.92	-39.71
6.472	5.253	98.59	85.73	79.67
6.478	5.259	62.03	51.48	46.15
6.485	5.267	91.67	83.19	96.52
6.491	5.272	73.14	59.26	68.99
6.494	5.275	-30.92	-48.17	-23.22
6.501	5.282	-67.10	55.86	-31.69
6.509	5.286	98.33	72.51	84.45
6.513	5.294	56.24	49.06	68.38
6.517	5.298	42.81	28.93	31.62

Table 4.4 continued

Latitude (deg)	Longitude (deg)	Geopotential (m^2/s^2) Wiechert W/A (GGM)	Geopotential (m^2/s^2) Itakpe W/A	Geopotential (m^2/s^2) West Africa (MGGM)
6.524	5.305	69.77	53.46	-33.64
6.528	5.312	53.68	49.88	61.74
6.535	5.316	67.06	82.15	42.93
6.542	5.324	39.28	55.09	27.35
6.547	5.329	85.26	91.73	103.63
6.553	5.337	93.63	79.46	65.51
6.560	5.341	79.31	88.52	94.32
6.564	5.348	46.90	56.38	67.29
6.569	5.353	81.44	99.26	92.53
6.572	5.356	79.66	52.07	63.64
6.576	5.362	84.50	92.34	59.22
6.583	5.369	48.14	63.28	75.39
6.588	5.374	72.43	85.35	64.16
6.595	5.378	52.67	49.06	38.99
6.601	5.385	83.15	95.72	62.65
6.609	5.397	46.97	75.31	58.04

Table 4.4 continued

Latitude (deg)	Longitude (deg)	Geopotential (m^2/s^2) Wiechert W/A (GGM)	Geopotential (m^2/s^2) Itakpe W/A	Geopotential (m^2/s^2) West Africa (MGGM)
6.614	5.403	97.93	65.64	84.31
6.620	5.409	106.37	87.91	79.53
6.627	5.414	46.43	53.24	61.82
6.632	5.420	35.12	48.75	56.35
6.638	5.426	92.57	76.19	84.98
6.643	5.435	115.25	82.04	91.27
6.649	5.441	56.09	49.73	62.85
6.655	5.447	84.86	119.62	108.50
6.662	5.453	82.35	74.17	93.43
6.669	5.459	79.50	65.23	58.16
6.673	5.465	43.40	52.86	74.35
6.679	5.472	86.25	93.77	82.63
6.691	5.477	79.38	65.42	78.43
6.695	5.491	65.46	89.03	92.83
6.702	5.496	93.74	105.26	84.69
6.706	5.503	62.80	75.49	59.23

A close comparison shows that the geopotential results obtained from the MGGM has a correlation with the observed data than the existing GGM. The geopotential value at latitude 6.291^0N and longitude 5.062^0W shows a tremendous high value of $159.23m^2/s^2$ for observed and $138.22m^2/s^2$ for GGM while the existing GGM has a low geopotential value of $-40.53m^2/s^2$ which is a wide deviation from the in-situ data. This geopotential value increases to a value of about $209.46m^2/s^2$ for observed and $238.55m^2/s^2$ for MGGM while the GGM shows a slight increase to a value of about $82.97m^2/s^2$. However, low geopotential values of $56.11m^2/s^2$ and $42.93m^2/s^2$ were observed at latitude 7.531^0N and longitude 6.068^0W for the in-situ and MGGM data respectively while the GGM produces a high geopotential value of $207.85m^2/s^2$ at the same latitude and longitude. Average Error for MGGM model type varies between +0.15% to +9.67% while the average error for GGM model type produces a value ranging from +0.32% to +17.45% for continental lithosphere.

Geopotential contour map of West African sector (Itakpe) using the modified gravity model (Eqn. 3.44) are shown in Figure 4.3 Potential data varies from a least value of $43.27m^2/s^2$ to a high value of $1.5.26m^2/s^2$. High gravity values were observed at low longitudes between 5.145^0E and 5.496^0E and low latitudes ranging between 6.376^0 and 6.702^0N respectively.

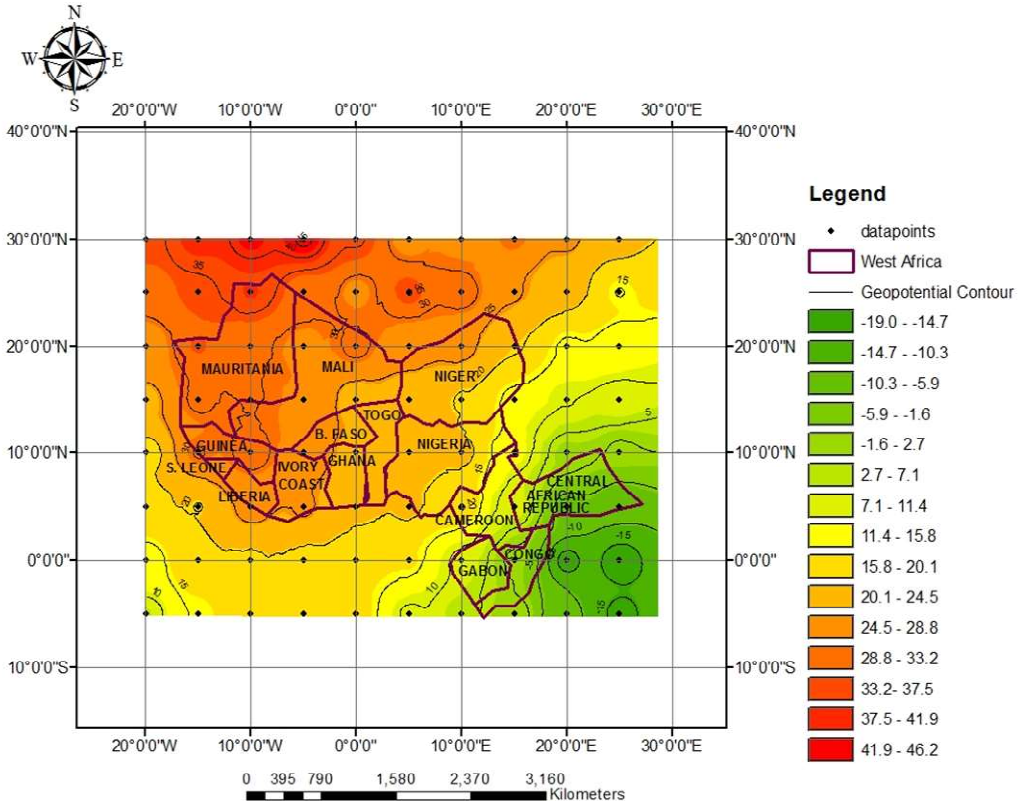

Figure 4.3: The Geopotential contour Map of West African continental Region using modified geopotential gravity model.

Figure 4.4 shows the geoidal height gravity contour map of Itakpe area (a continental region) from global geopotential model while Figure 4.5 is the gravity height map of the same location from the observed data. Geoidal height at low latitude 6.285^0N to 6.673^0N and longitude 5.057^0E and 5.465^0E values varies between 122.9m and 163.2m for the GGM and 113.3m and 156.1m for the modified model. Geoidal height values of the In-situ data varies between 139.7m and 178.4m Gravity height was initially high at low latitude and longitude but decreases slightly towards the south-east direction to a value of 85.3m and then begin to increase towards the south-west direction.

Figure 4.6 is the gravity anomaly contour map of West African sector. The gravity anomaly values vary between 9.778sq m/s and 9.801sq m/s.

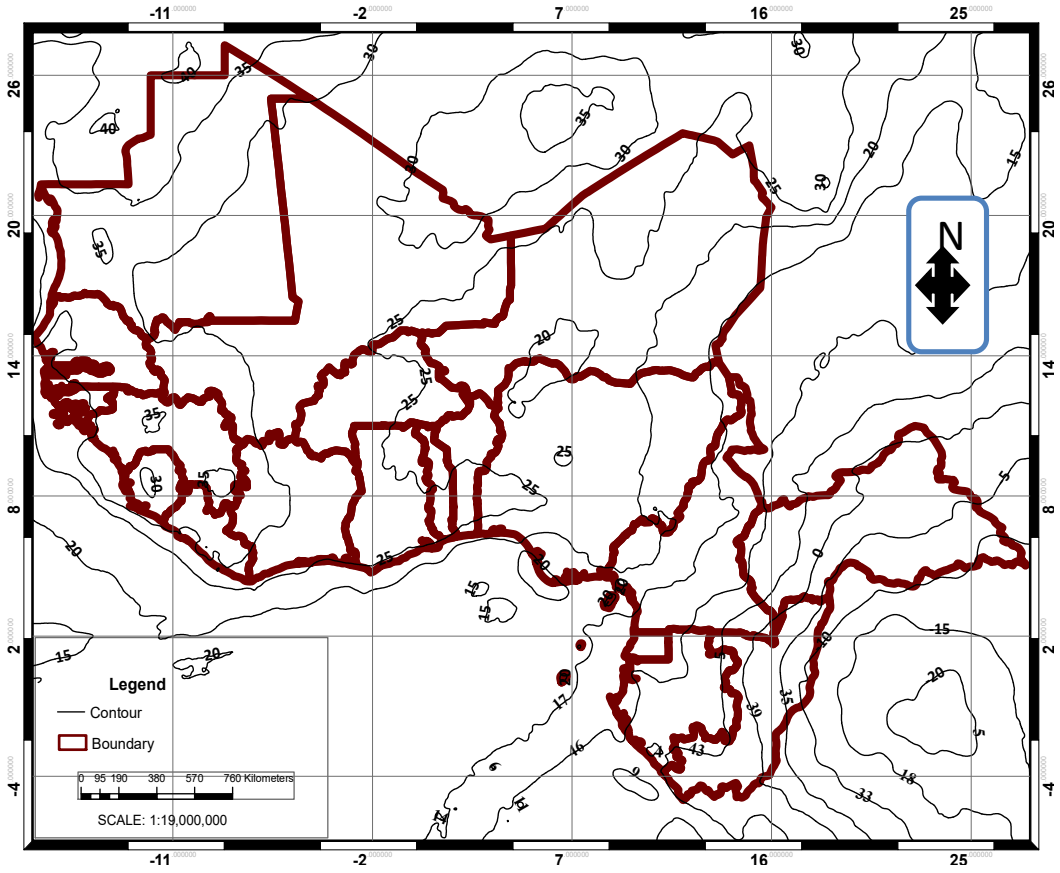

Figure 4.4:Geoidal Height of West African Region obtained from global geopotential Model showing the contours

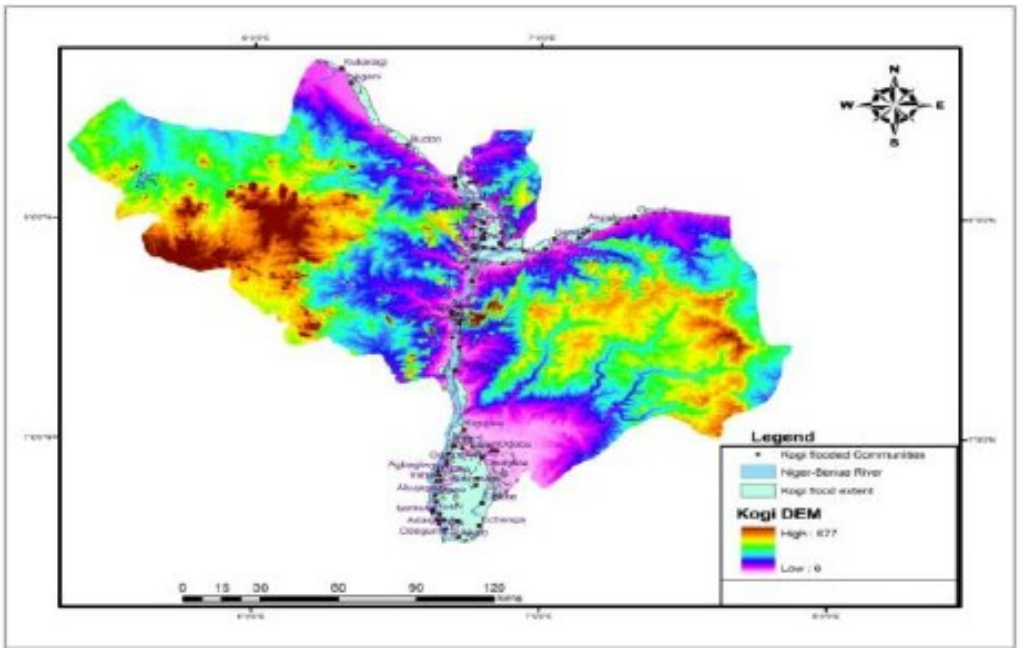

Figure 4.5: Geoidal Height contour map of Itakpe (a continental region) in Kogi State, Nigeria obtained from the existing geopotential Model (Wiechert, 2008)

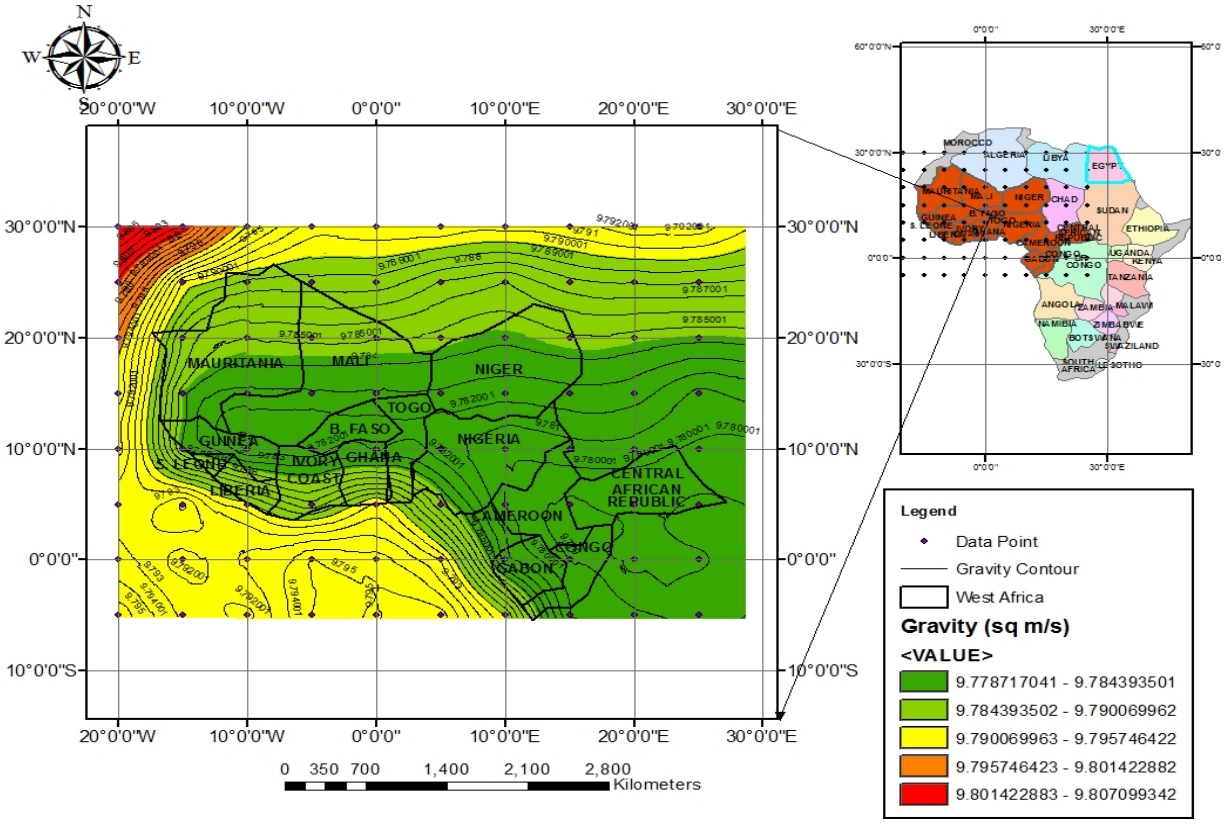

Figure 4.6: Gravity Anomaly contour map of West African Region

4.4 Gravity Data Interpretation

Interpretation of gravity data is the presentation of gravity results which can be obtained in form of a 3-dimensional contour maps by using the inverse square approach. These 3-dimensional contour maps are obtained for the geopotential distribution, geoidal undulations and gravity anomalies which were computed using the modified geopotential gravity model across the West African region. Usually, gravity contour maps are presented over the sector at low degree (30,30), intermediate degree (30,30) to (120,120), high degree (120,120) to (250,250) and complete degree (360,360). These maps are termed free air gravity contours maps which shows a detailed version of the maps referred to the equilibrium figure with a flattening f = $\frac{1}{298.26}$.

4.4.1 The Free Air Gravity Maps

The free air gravity maps are the gravity contour maps which represent the anomalous gravity trend over the West African region where various tectonic and anti-Earth activities had occurred. These maps are obtained from the geopotential computation by using our modified gravity equation. These free air gravity maps are usually partitioned into low-degree (30, 30) field, intermediate-degree (30, 30) – (120, 120) field, high-degree (120, 120) – (250, 250) field and complete degree (360, 360) field depending on the wavelength components of anomalous gravity. However, the wavelengths of probable interest in this research work are the low degree and order field (30, 30) which is isolated by subtracting it from a complete to degree and order 360. The resulting free air gravity map will produce contours which show a series of linear positive and negative gravity anomalies spanning the West African region which lies between latitude 3^{o}N -20^{o}N and longitude 30^{o}W and 15^{o}E.

We now proceed to look at the 3-dimensional gravity contour maps produced by the generated gravity results. Figures 4.3, 4.4 and 4.5 shows the gravity contour map of West Africa with the least degree i.e. low degree (30,30) field, the free-air gravity anomaly map over West Africa at high degree (120,120) to (360-360) field and the geoidal undulations map at complete degree (360,360) field respectively.

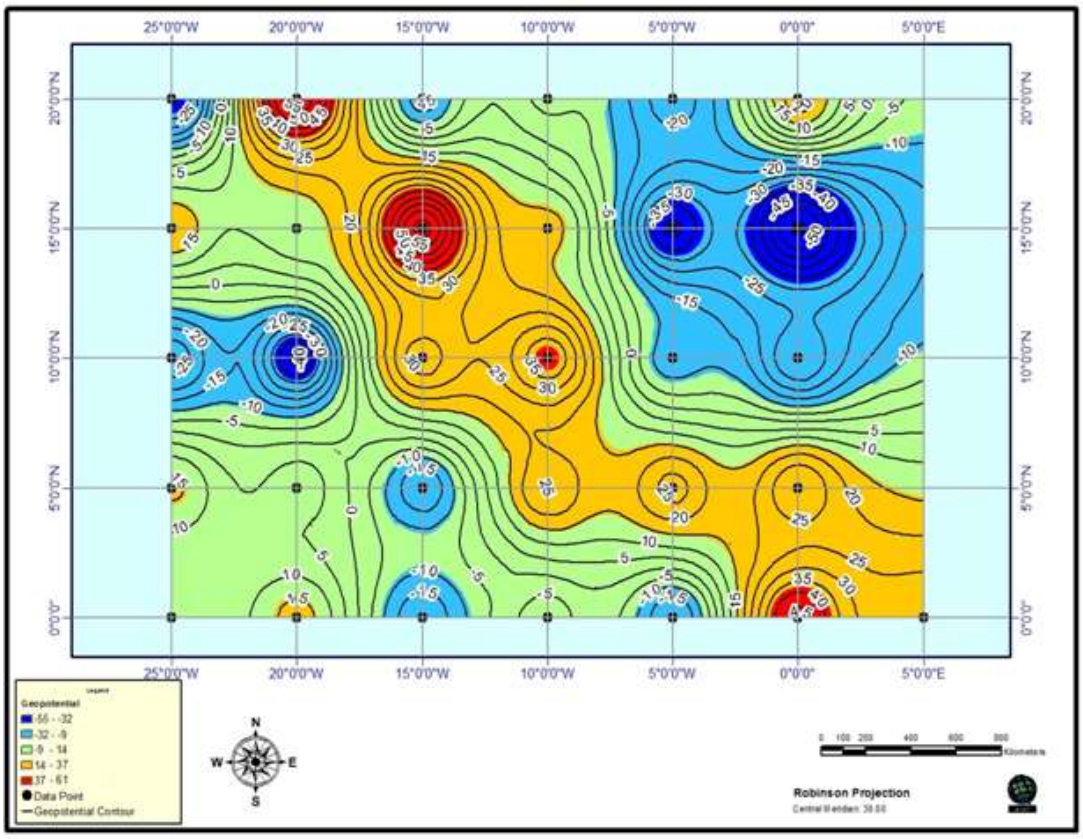

Figure 4.7: The Geopotential gravity contour map of West African Sector at Low Degree (30, 30) Field measured in m^2/s^2.

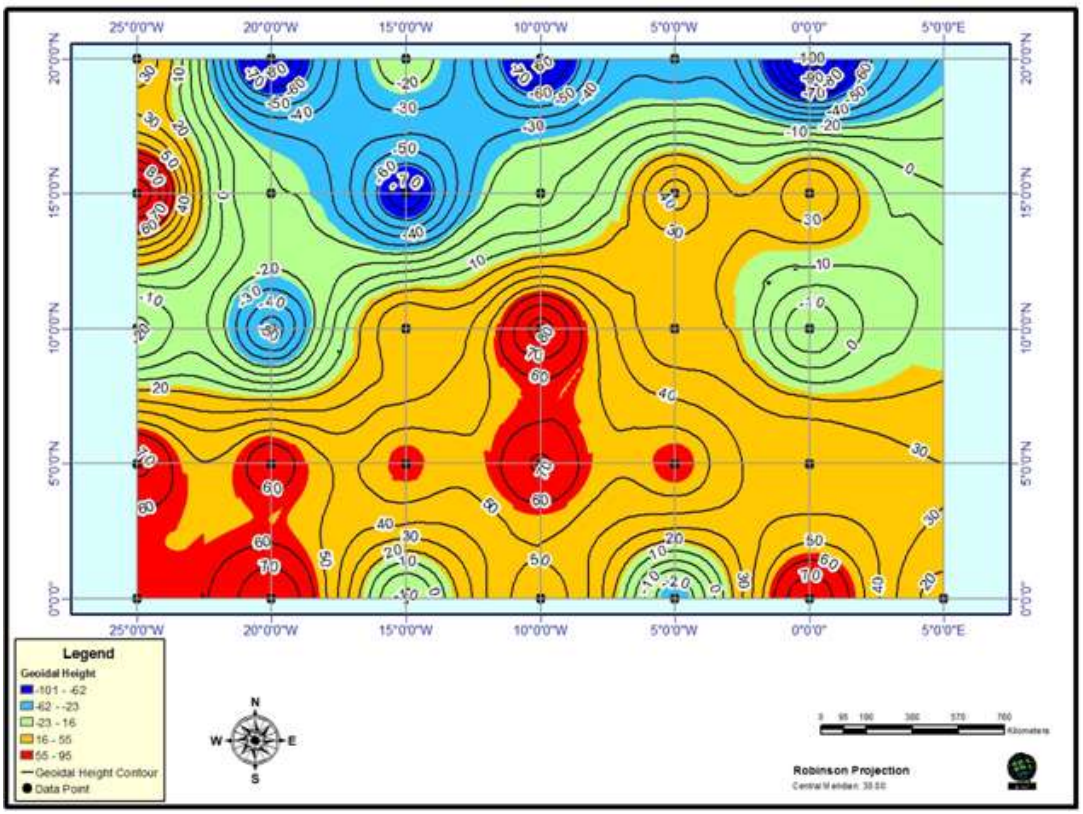

Figure 4.8: Geoidal Undulation (N) of the West African Region at Low Degree (30, 30) Field in metres.

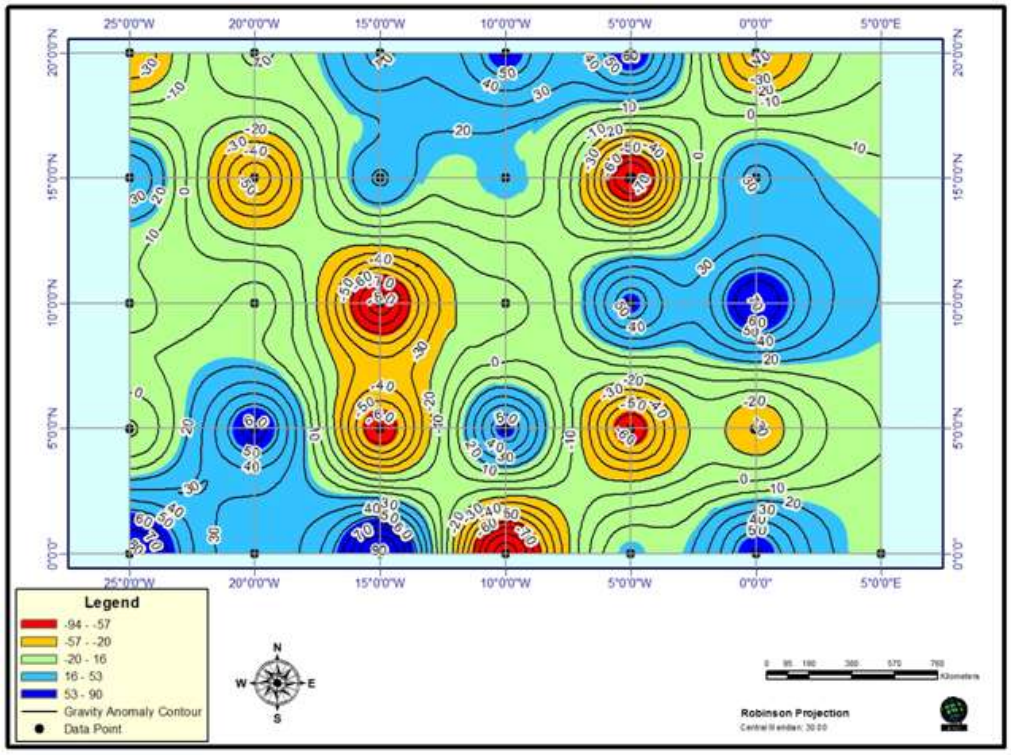

Figure 4.9: Free-air Gravity Anomaly contour map over West Africa at Low Degree (30, 30) Field model in mGals.

4.4.1.1 The Low Degree (30, 30) Field

In Figure 4.3, the gravity potential contour map which is based on the coefficients up to (30,30) field represent adequately only the long wavelength component of anomalous gravity which exhibits many of the broad features on the contour map which could not be tied to any crustal surface features. Thus the long wavelength portrayed the anomalous mass which is deep seated down the lithosphere. The geopotential computation and satellite representation of the gravity field up to this degree has outlined regional areas of anomalous gravity such as the positive gravity anomaly bordering on the southwest coast of Africa. This low degree map has high gravity values associated with latitudes between 20^0W and 20^0E. Although there are low gravity sections of distinct partitions at longitudes 15^0W, 5^0E and 15^0E respectively. High geopotential data with value ranging between 80 and 120m^2/s^2 are observed in this low degree field.

Figure 4.4 shows the geoidal undulations of West African region at low degree (30,30) field in metres. Gravity height values varies between -84.2m (oceanic region) and 96.9m (continental sector). High gravity height values are shown on blue and red regions of the contour while and yellow partitions on contour maps indicate low geoidal height. Low gravity height value varies between -84.2m to 16.5m while high value varies between 16.5m to 96.9m

Figure 4.5, shows the free-air gravity anomaly contour map which is now presented over West Africa at low degree (30,30) degree field measured in mgals.

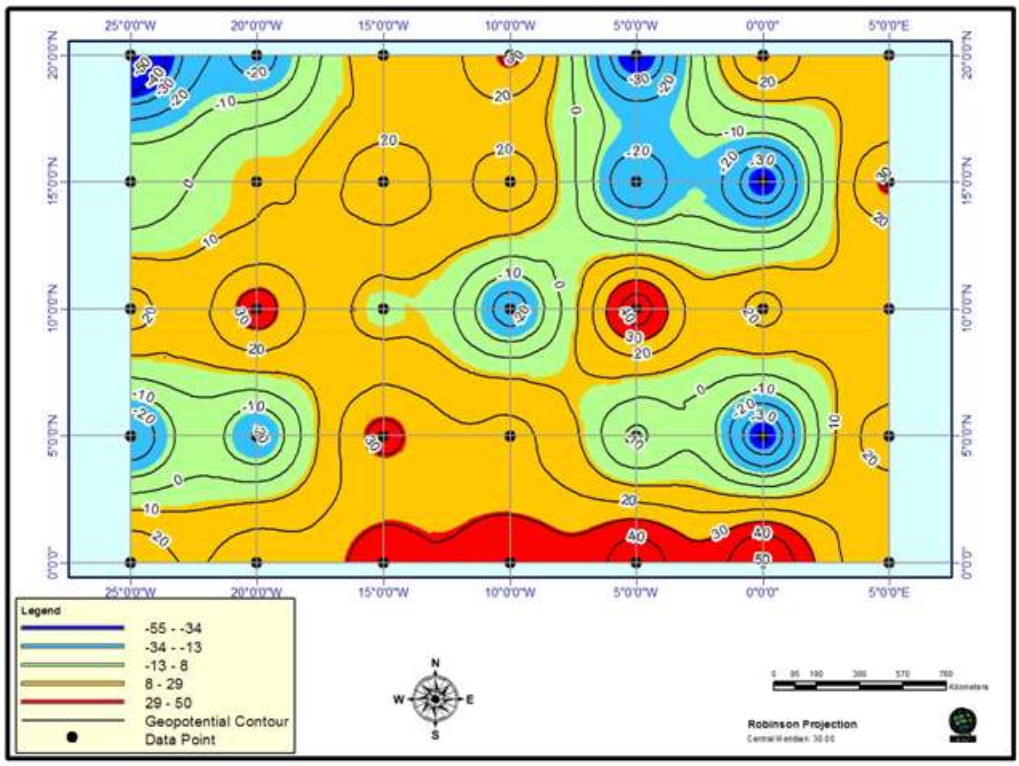

Figure 4.10: Goepotential map of West African Sector at Intermediate Degree (30, 30) to (120, 120) Field in m^2/s^2.

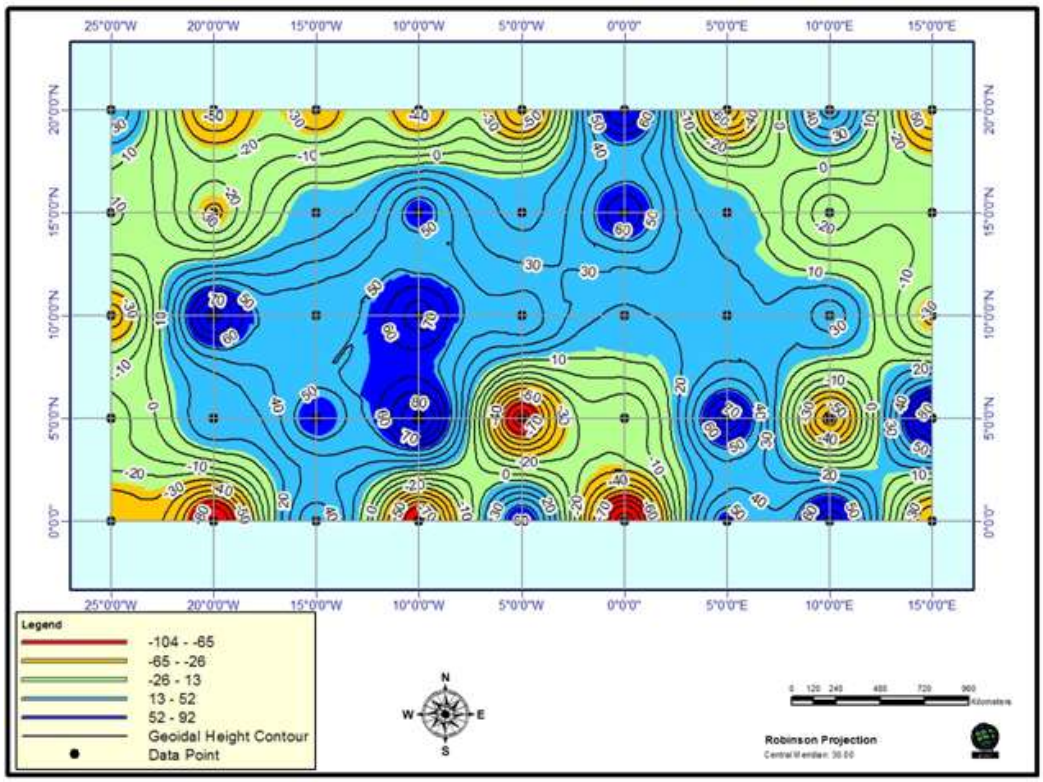

Figure 4.11: Geoidal Undulation of West African Region at Intermediate Degrees (30, 30) to (120, 120) Field in metres.

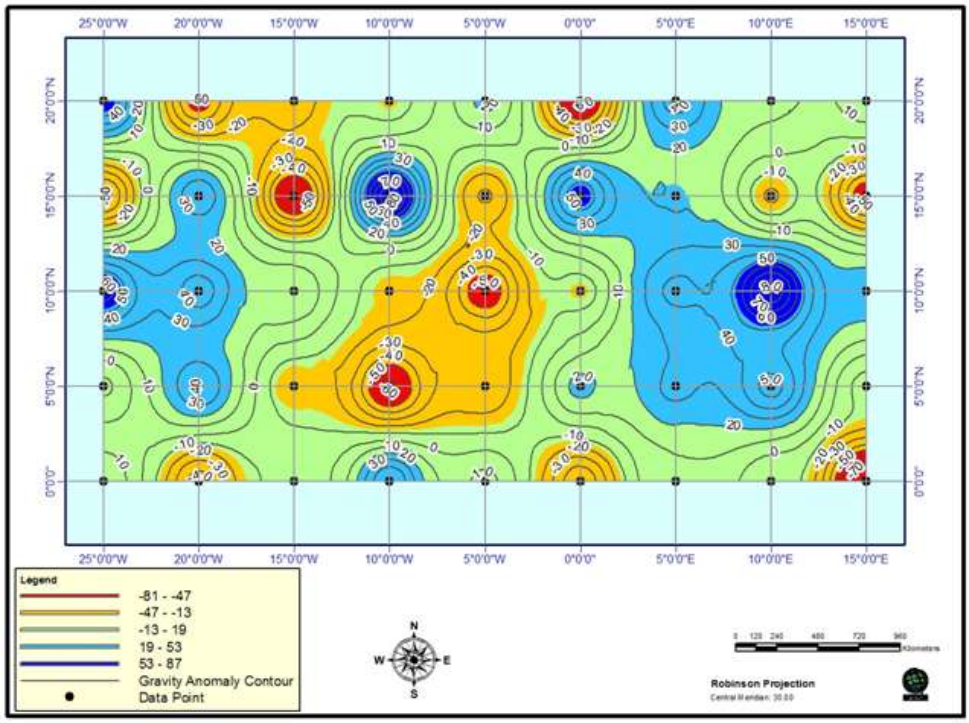

Figure 4.12: The Free-Air Gravity Anomaly map over West Africa at Intermediate Degree (30, 30) to (120, 120) Field measured in mGals.

4.4.1.2 The Intermediate Degree (30,30) to (120,120) Field

The computation of field models within the intermediate degree utilizes coefficients in the range (30-60), (60-90) and (90-120). This can be seen in Figures 4.10, 4.11 and 4.12 respectively which specifies the geopotential, geoidal heights and gravity anomalous variations. The gravity contours maps in this field represent anomalies of half wavelength to a depth of about 115km. There are variations in the anomalies different from the anomalies for the low degree field. The anomaly pattern over the West African region produces inhomogeneities in the continental regions and this extend towards the ocean.

Geopotential value reduces across the border line between oceanic and continental margins of West African sector while a sharp increase in gravity undulations and anomaly are observed.

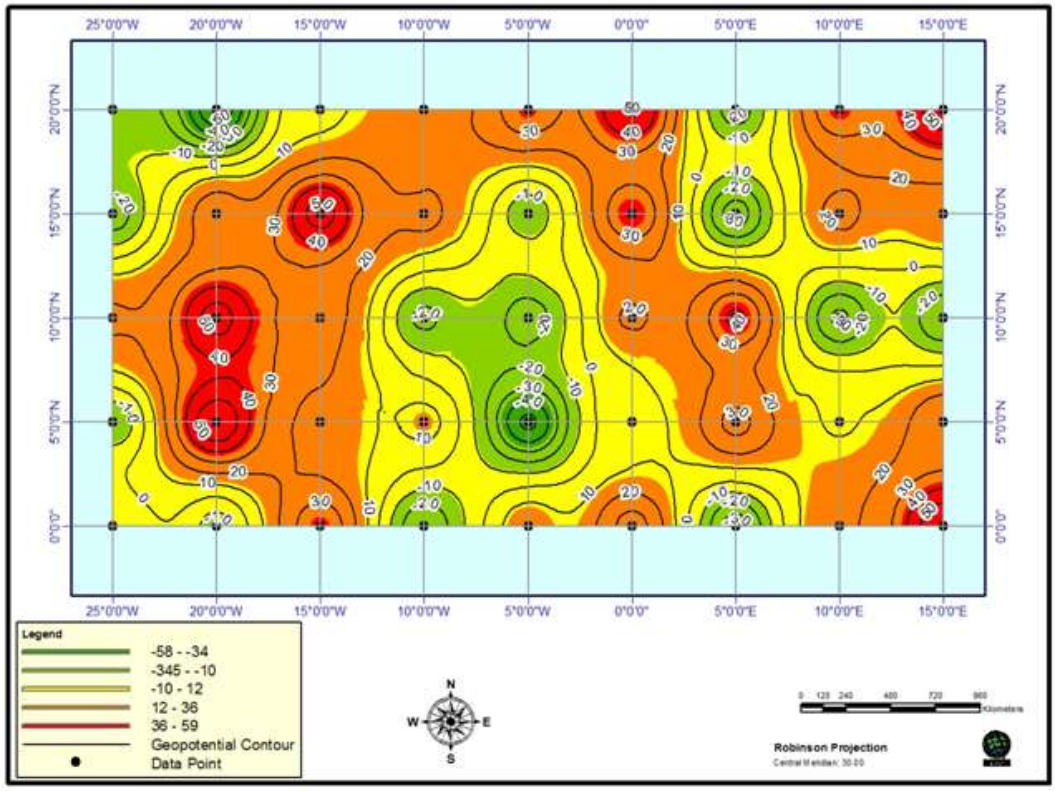

Figure 4.13: The Geopotential contour map of West African Region at High Degree (120, 120) to (250, 250) Field in m^2/s^2.

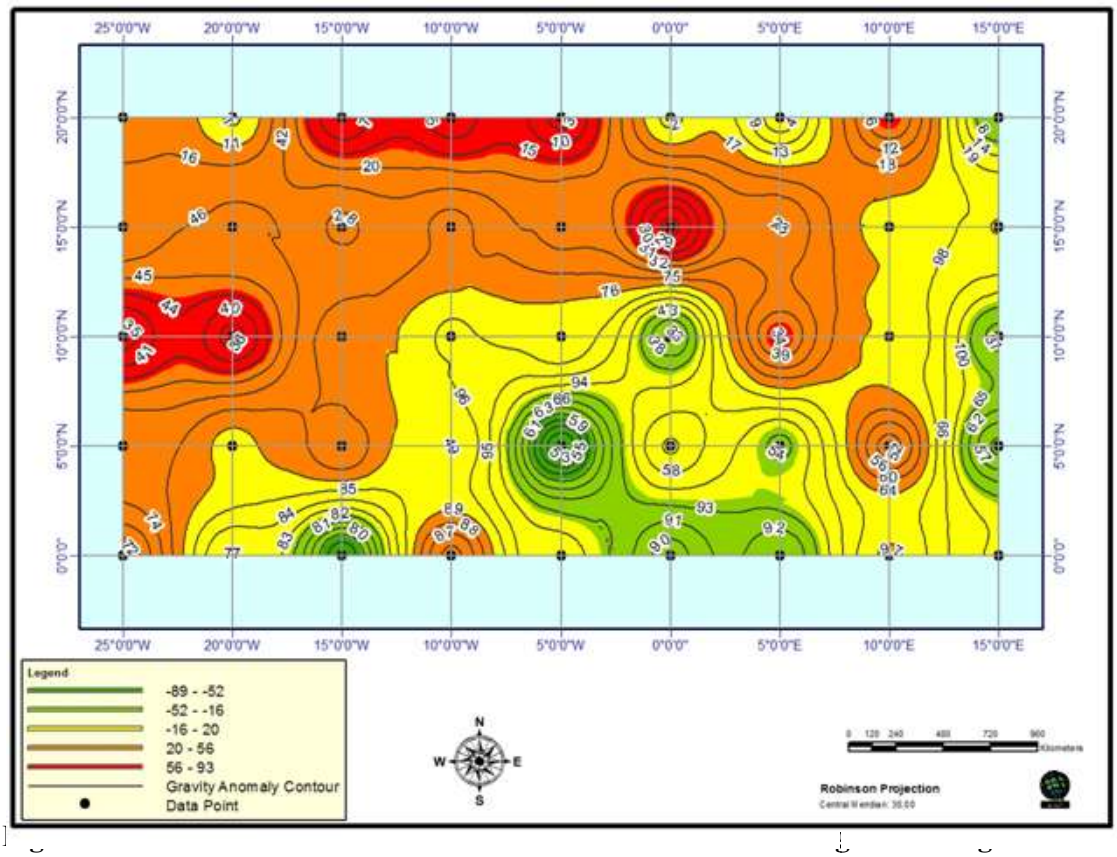

Degree (120, 120) to (250, 250) Field in metres.

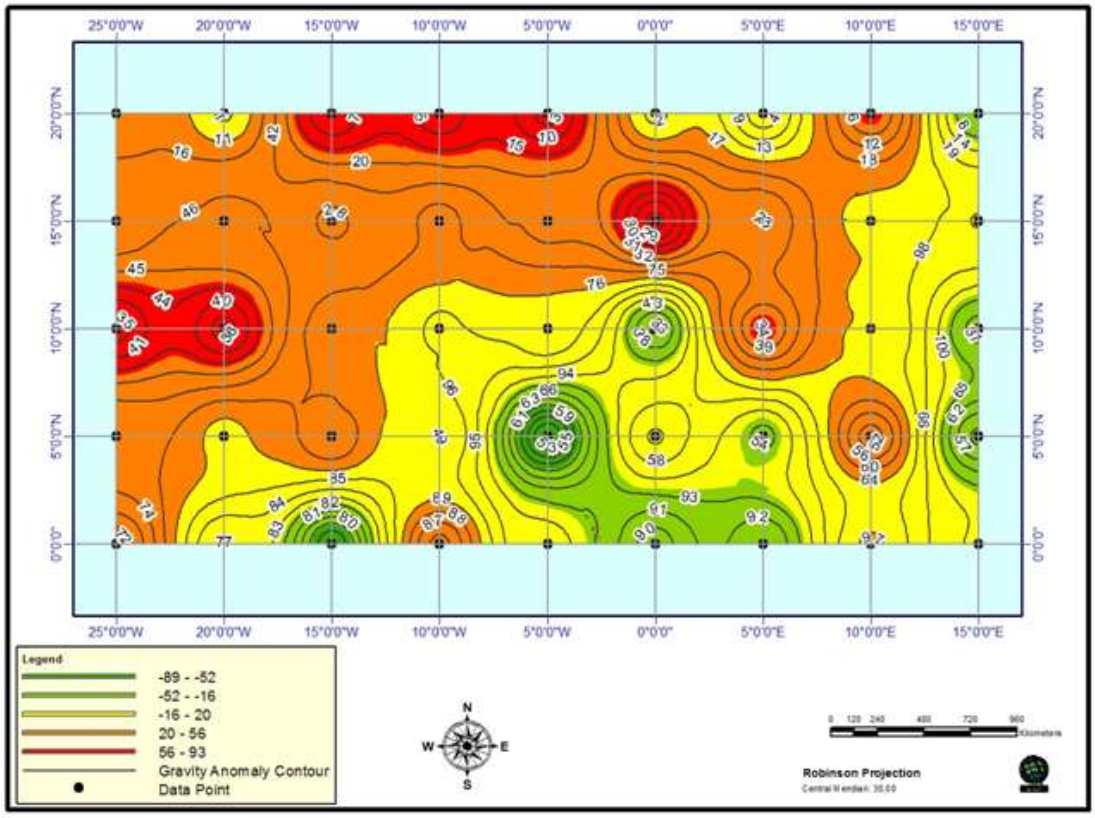

Figure 4.15: The Free-air Gravity Anomaly map of West African Region at High Degree (120, 120) to (250, 250) Field in mGals.

4.4.1.3 The High Degree (120, 120) – (360, 360) Field

In Figure 4.13, the gravity contour maps in this field range represent anomalies of half wavelength from a depth between 1500Km to 2500Km. The computation of the field models which utilizes coefficients in the range (120-150), (150-180), (180-210), (210-240), (240-270), (270-300), (300-330), and (330-360) was achieved and from the computed anomalies of the field models, gravity anomaly maps of half wavelengths to a reasonable depth of about 80km was obtained. However, this research work does not require an area of concentration beyond the lithospheric region. The tectonic activities in this region of the Earth are extracted from the available integrated geophysical information of meaningful geopotential values. The positive anomaly area over the Mid-Atlantic ridge are characterized by anomalous geophysical relations such as subnormal mantle velocity, high heat flow along the crest of the ridge and pronounced magnetic anomaly which are indicative of higher than normal density values which gives abnormal mass distributions. The computed anomalies of model utilizing the high degree and order fields with coefficients (180-210), (210-240), (240-270) and (270-300) on the gravity contour maps shows basically same features except for slight additional anomalies. However, the models which utilizes coefficients (300-330) and (330-360) exhibit many of the broad features of the complete field. The anomaly pattern over the West African sector produces earth inhomogeneities more pronounced in the Atlantic border. The field is not well defined over the Archean nucleus of Liberia, Guinea, Sierra Leone and Gambia but has a gravity signature which is suggestive of the Sassandra fault (Lesquer et al, 1984). Although gravity around the area extending from 8^{o}W to 30^{o}W is not well defined by gravitational field models, the anomalies become more pronounced in areas spanning Cameroun, Nigeria, Republic of Benin, Togo, Ghana and Cote D'ivoire. These anomalies which extend from Eastern to North-Eastern parts could be correlated with a variety of elongated geological features and crustal deformations such as faults, folds, dolerite dykes, troughs and horst of variable age (Guiraud et al, 1987).

Figure 4.17 is the geoidal undulations over West African region at complete degree field. This figure is a detailed version of the field which shows the spacial distribution of gravity contours at various latitude and longitude sections.

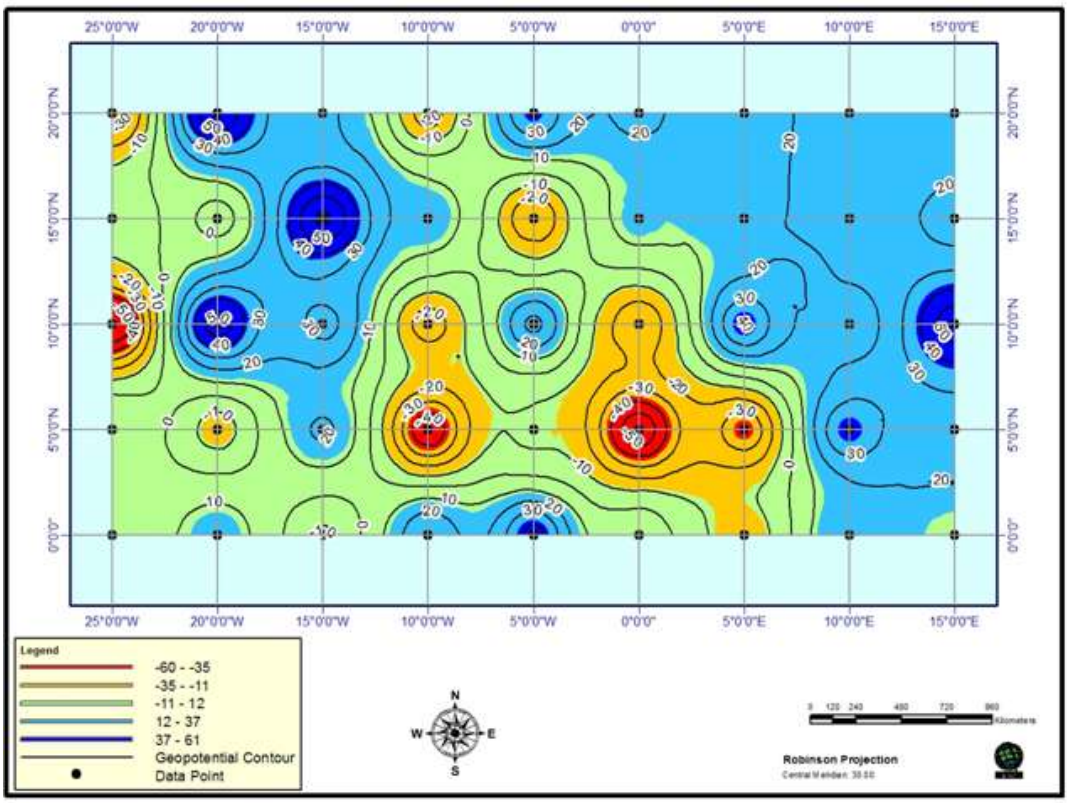

Figure 4.16: The Geopotential contour map of West African Sector from the complete Degree (360, 360) Field model.

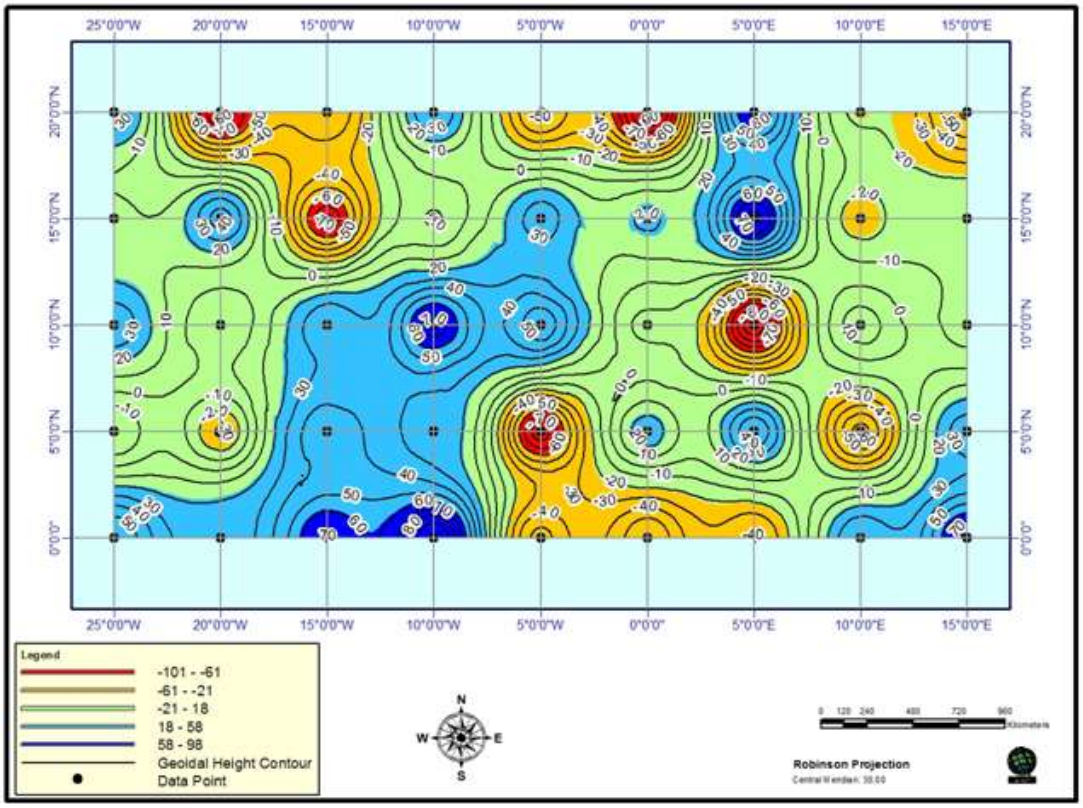

Figure 4.17: Geoidal Undulation gravity map of West African Region for the complete Degree (360, 360) Field model.

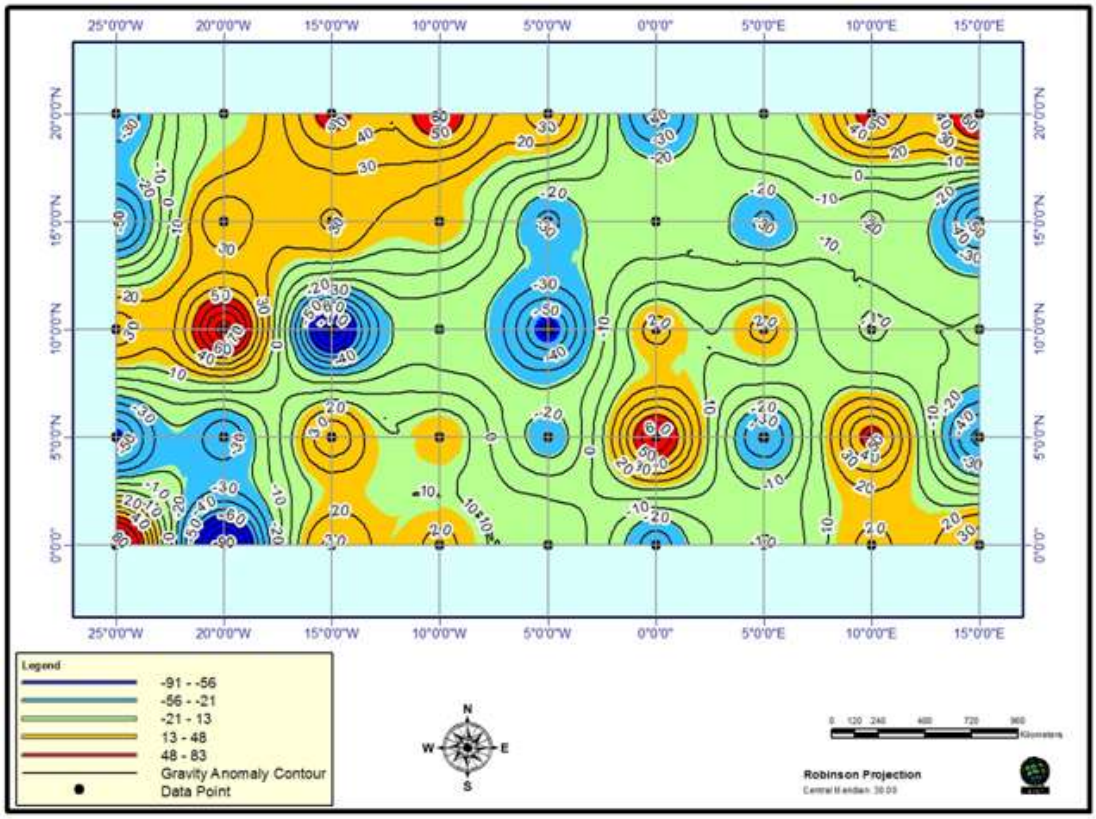

Figure 4.18: The Free-air Gravity Anomaly contour map of West African Region for the complete Degree (360, 360) Field model.

4.4.1.4 The Complete Degree (360, 360) Field

Figure 4.17 shows the gravity contour maps which specify the geoidal undulations of the lithosphere in metres. The lithospheric depth can be interpreted for the complete degree field. A free air gravity map can be computed from the complete (360, 360) field model which shows the gravity anomalies referred to an ellipsoid with a flattening f = $\frac{1}{298.26}$ which is computed from the Kozai zonal and Gaposchkin tesseral harmonic coefficients complete to degree and order 360. This map which shows a detailed version of the earth anomalies represent the integrated effect of a number of shallow mass anomalies located in the upper mantle or crust. In this case, there is also a contribution from surface topography whose effect appears to be only of secondary importance. Thus, the correlation of the global variations of topography with those of the gravity field appears to be low (Jeffreys,1952). Generally speaking, the correlation between gravity and surficial tectonic features is always difficult to assess unless the low degree and order anomalies are removed from the complete (360, 360) field. This complete field is adequately characterized by anomalies of low wavelength. The 3-dimensional gravity contour maps can be specified.

Figures 4.7 to 4.18 show the gravity contour maps of geopotential, geoidal height and gravity anomaly in 3-dimensions at low, intermediate, high and complete degrees. The maps with respect to region or location and their gravity data are summarized in section 4.5

4.5 The 3-D Gravity Contour Maps of West Africa

The 3-dimensional gravity contour maps for the various degrees are obtained ranging from low degree (30, 30) field to complete degree (360, 360) field. These are given in figures 4.7 to 4.18. These maps show the gravity anomaly pattern in the lithospheric crust. The gravity variations for different sections as we move from continental region to oceanic region are clearly indicated in the maps. Low gravity values are obtained in areas where exploration, mining and anti-earth operations are performed and this is

indicated in areas where contours are spaced in the map. However, regions of high mineral deposits show high gravity values contours are adequately well defined. The geopotential values observed in Figure 4.7 at low degree (30,30) field varies between -10m^2/s^2 and 45m^2/s^2 while the value varies for high degree (120,120) – (250,250) between 68m^2/s^2 and 145m^2/s^2 respectively. A high geopotential value is observed for the complete degree (360,360) and it varies between 102m^2/s^2 and 200.7m^2/s^2 as we move from continental to oceanic region in W/Africa. The map shows a relatively high geopotential around the northwestern part of the West African sector while the southeastern flank is characterized by relatively low geopotential. The high potential zone falls within the yellowish-red colour band whereas, the low potential zone has a greenish-light yellow colour band.

Geoidal height values become prominent as we move from ocean to continent. Geoidal height data ranges between -26.5m to 248m as we move from ocean to continent. Variations in geoidal height data show that the Earth does not have uniform gravity values. Thus, the Earth is an heterogeneous medium with different structural geologic composition.

The geopotential gravity contour map of west African region at low degree (30,30) field shows a gravity value of 20, 25, 30, and 40m^3/s^3 at latitude 10^0N and longitude -25^0W. Also, gravity potential component of similar value are experienced at latitude 2^0N and longitude -4^0W respectively.

However, it is of great importance to obtain a table of zonal harmonics of the geopotential adopted in the computation. These harmonic given by Kozai, 1967 and King Hele et al., 1992 are satellite derived parameters known as geopotential coefficients which were utilized in the geopotential computation. They are dimensionles constants which are specified in the model. Table 4.5 is the list of zonal harmonic coefficients which ranges from J_1 to J_{21}. A detailed version which combines both zonal and tesseral harmonics are given in Table B7.

Table 4.5: The Zonal Harmonics of the Geopotential (kozai, 1967) and (King-Hele et al, 1992)

Coefficient	Kozai	King-Hele et al
J_0	1623.96×10^{-6}	
J_1	0	
J_2	1082.628×10^{-6}	1082.68×10^{-6}
J_3	-2.538×10^{-6}	-2.532×10^{-6}
J_4	-1.593×10^{-6}	-1.61×10^{-6}
J_5	-0.230×10^{-6}	-0.22×10^{-6}
J_6	0.502×10^{-6}	0.71×10^{-6}
J_7	-0.361×10^{-6}	-0.41×10^{-6}
J_8	-0.118×10^{-6}	0.13×10^{-6}
J_9	-0.100×10^{-6}	0.09×10^{-6}
J_{10}	-0.354×10^{-6}	0.09×10^{-6}
J_{11}	0.202×10^{-6}	-0.14×10^{-6}
J_{12}	-0.042×10^{-6}	-0.31×10^{-6}
J_{13}	-0.123×10^{-6}	0.29×10^{-6}
J_{14}	-0.073×10^{-6}	-0.18×10^{-6}
J_{15}	-0.174×10^{-6}	
J_{16}	0.187×10^{-6}	
J_{17}	0.085×10^{-6}	
J_{18}	-0.231×10^{-6}	
J_{19}	-0.216×10^{-6}	
J_{20}	-0.005×10^{-6}	
J_{21}	0.145×10^{-6}	

Table 4.5 shows the zonal harmonic coefficients adopted in the geopotential computation. A close study of the harmonic coefficients shows that the odd zonal harmonics J_1, J_3, J_5, J_7, ...J_{21} adopted in computation are utilized in computing the geopotential at low and intermediate degree fields which causes a long-period changes in the eccentricity e and inclination i of the earth orbit while the even zonal harmonics J_2, J_4, J_6, J_8, ...J_{14} can be utilized in obtaining the geopotential at high degree field. This causes a secular and long-period changes in the right ascension of the ascending node Ω and argument of perigee $\boldsymbol{\omega}$. The tesseral harmonic coefficients define the longitude-dependent variation and causes a short-period changes in the earth orbital elements. A comprehensive list of the combined Zonal and Tesseral harmonic coefficients are given in Appendix B (Table B7).

The coefficients represent the distribution of mass within the earth subsurface lithospheric region. These mass distribution can be assessed if we consider the different Earth layers.

Table 4.6 shows the different Earth composition with various geological layers. The depth of each layer (in kilometers) starting from the surface to the innermost region, their average densities, mass and percentage volume are shown in Table 4.6

Table 4.6: The different Earth composition showing geologic layers

Layer	Depth (km)	Average Density x 10^3 Kg/m^3	Mass x 10^{12} Kg	%	Volume x 10^9 Kg	%
Earth crust	10 – 70	29.4	15	0.3	5.1	0.5
Mantle	70 – 2850	9.00	4088	68.4	902.9	83.3
Outer Core	2850 – 5100	10.50	1747	29.2	166.4	15.4
Inner Core	5100 – 6380	14.53	125	2.1	8.6	0.8
Total		5.52	5975	100	1083.0	100

The outer layer known as the earth crust has a depth variation of about 10-70km with average density of 29.4x 10^3Kg/m^3. The mass of the crust is 15x 10^{12}Kg and occupies about 0.3% volume of the total earth. The next layer is the mantle which has a thickness of about 2780km and an average density of 9x10^3Kg/m^3. Its mass is 4.1x10^{15}Kg and occupies about 83.3% volume of the total earth. Directly below the mantle is the outer core which is 2,250Km deep while the inner core is 1,300Km thick. Their average densities are 10.5x 10^3Kg/m^3 and 14.53x10^3Kg/m^3 with percentage volume of 15.4% and 0.8% respectively. The earth body has a total depth of 6380Km and an average density value of 5.52x10^3Kg/m^3.

Since the earth lithosphere comprises of both the continental and oceanic regions, density distribution data for both regions of the lithosphere are obtained using the model. Observed density values are also tabulated.

Table 4.7 shows the density values in kg/m^3 with the depth range, the location and model type.

Table 4.7: A Table showing the summary of the density data, depth range, location and model type

Density data:	Depth Range	Area/location	Model/In-situ
(9.7-26.5) x 10^3Kg/m^3	0-860Km	Continental	Model
(14.6-33.2) x 10^3Kg/m^3	0-255Km	Oceanic	Model
(8.5-24.9) x 10^3Kg/m^3	0-860Km	Continental	Observed
(12.7-30.5) x 10^3Kg/m^3	0-255Km	Oceanic	Observed
Average Errors: $\pm$0.28% to $\pm$11.43%		Model Type:	MGGM
$\pm$0.47% to $\pm$28.53%			GGM

In Table 4.7, the density values vary as we move from location to location. This variation in density is also associated with the depth starting from the earth surface which is 0Km. At depth of about 860Km from the earth surface, the density of the continent increases from a minimum value of $9.7x10^3Kg/m^3$ to a peak value of $26.5x10^3Kg/m^3$ using the MGGM. For the same model, the density value of about $14.6x10^3Kg/m^3$ was observed at few depths beneath the ocean surface while a density value of about $33.2x10^3Kg/m^3$ was experienced at a depth of 255Km. This is quite different for the observed data of the continental lithosphere which vary in density value from $8.5x10^3Kg/m^3$ to $24.9x10^3Kg/m^3$ at a depth of about 860Km. The oceanic region has a minimum density of $12.7x10^3Kg/m^3$ which increases to $30.5Kg/m^3$ to $24.9x10^3Kg/m^3$ which increases to $30.5Kg/m^3$ at a depth of about 255Km. An average error determined for MGGM is +0.28% to +11.43% while the existing GGM produces an average error of +0.47% to +28.53%. Table B4 (see Appendix B) gives the comprehensive density results generated for both continental (Itakpe area) and oceanic (South-south Nigeria) regions of West African sector.

Results obtained show that with the inclusion of the compaction factor η, gravity anomaly pattern over the Atlantic and continental regions of West Africa becomes well defined which reveals the extent of anti-earth operations performed by human in these regions. This is also the case of natural activities and events which are uncontrollable by man. The compaction factor η produce a link between these two regions and it indicate that any anti-earth operation performed in the oceanic region will yield a great effect on the continental body and vice-versa. This is obtained from the changes in Earth density calculation before and after the activities. Density data also reveals that valuable Earth materials of sub-surface location has been depleted or explored due to several human operations which are anti (or opposing) in nature to the body of the earth. Thus, time series density calculations must be made from time to time (refers to equation 4.26) which gives the density values of the specified location. It is however expected that changes in density values are observed before and after the anti-earth operations.

CHAPTER FIVE

ANALYSIS, SUMMARY AND CONCLUSIONS

In this section, we present the summary of the research work.

5.1 Analysis of the Research

The modified geopotential gravity models (MGGM) has been used to determine the distribution of potential earth gravity over the continental and oceanic regions of the lithosphere separately. This has allowed for the prediction of lithospheric stability and strength of the two regions, most especially, those areas where anti-earth activities had prevailed or engaged as well as areas of natural disaster. However, past research work had failed to consider a more robust gravity models that can handle the lithospheric stability issues irrespective of oceanic or continental region. Hence, the need to include a compaction factor η that could define the gravity field variation properly and normalize the lithospheric density contrast. Thus, this factor η produce a great link that bridges the gap between the oceanic and continental regions of West Africa which was the region of focus in this research. This gravity field variation has been used to determine the subsurface mass anomaly distribution using bouguer equation or relation. Information of the earth internal structure and compactibility have also contributed to the determination of its stability. Stability phenomena indicate the physical conditions of the earth's lithosphere and also consider the nature of subsurface structure. In other to achieve the effective performance of the modified gravity potential model, derived parameters Jnm and Knm extracted from satellite are dimensionless constant coefficients of the various harmonic potential occurring in the expansion of the model. The space coordinates (i.e longitude and latitude which covers the West Africa region have been employed in the computation using the model. This modified geopotential gravity model MGGM has been able to produce a more reliable gravity data whose error value is minimized (i.e. extremely low) when compared with the error value generated by the existing GGMs. This may be achieved through model validation.

5.2 Contribution to Knowledge

The use of gravity models to solve lithospheric problems had become necessary in order to address Earth stability issues. In time past, natural Earth phenomena and artificial human operations had caused a great threat to the stability of the lithosphere and consequently, to the life of man as experienced in different parts of the world today. Gravity distribution in either the continents or ocean had been determined using the existing GGM_S. However, modification of these models by the inclusion of a compensation factor η has allowed for the prediction of stability and detection of areas of natural disaster across the ocean-continental margins of West Africa.

5.3 Conclusion

The approach employed by previous existing models has generated results which cannot be applied to both continental and oceanic regions simultaneously. This is due to the fact that the gravity results obtained does not cover all areas of concern where deep exploration and mineral exploitation have taken place. Hence, a better technique as specified in this research work has been employed which produces a more reliable or extended results that can be validated with standard results obtained in any part of the world. This does not imply that existing GGM_S have not performed as there are no models without limitations. Infact, modelling work is gaining more scientific interest since better techniques are now available to produce better results. Software upgrading has also led to the generation of better results. This research employed the use of latest software to upgrade the results obtained by previous models

Also, the new model will adequately monitor future earth events and detect areas of disaster where natural anti earth activities and artificially imposed human operations had caused damages to the body of the earth. Therefore, this research work has been able to solve complicated earth problems (for both continents and ocean) through the use of numerical models to determine lithospheric stability for non-homogeneous layers.

Future earth events and possible activity of the earth subsurface region may adequately be monitored from the available gravity and density data for the region concerned.

5.4 Recommendations

The MGGM is recommended for use in obtaining the geopotential gravity distribution in any part of the world whether the region of concern is separately oceanic or continental or both. This model can solve even complicated earth problems that existing GGM may find difficult to solve. This is because the modified gravity model has taken care of many physical earth parameters such as, the depth, geometry, density, topography, numbers of earth layers and bulk modulus.

With the presence of many physical parameters in the new model, earth internal activities are adequately assessed and possible future earth events can be determined. Infact, this new geopotential gravity model should serve as a baseline or reference upon which judgement on subsequent gravity variations should be based.

5.5 Suggestions for further work

It is suggested that the MGGM used in this research work can still be improved upon. Also, better models can be developed which will cater for other earth parameters such as temperature, pressure young modulus of elasticity etc. These parameters will cater for the thermodynamic nature of the lithospheric earth layers.

5.6 Research Limitations

This research work is limited in some areas. Computation of gravity potential was carried out by using a MATLAB 8.2 software version with release name R2013b. This has led to the generation of gravity results of certain approximations. However, the use of higher versions of MATLAB could lead to improved and more accurate gravity data generation. Latest versions such as MATLAB 16 function f( ) are now available in the electronic market. These higher versions might produce better results of higher approximations. Most version available now seems to be very expensive.

The modified gravity model in this research could be improved upon if another physical parameter is added to the model.

Acquisition of satellite gravity data is expensive. Satellite data is required for validation. Thus, lack of funds to acquire gravity data is also a hindering factor.

REFERENCES

Ahmed Zaki, (2018) Comparison of Satellite Altimetric gravity and global geopotential models with ship borne gravity in the Red Sea

Amos, M.J and Featherstone, W.E (2002) Comparisons of recent global geopotential models with Terrestrial gravity field data over New Zealand and Australia, Geomatics Research Australia, Proceedings of GG2002, Thessaloniki, http://olimpia.topo.auth.gr/GG2002/session6.html

Bernard, B., Kueppers, U. and Ortiz, H. (2015) Revisiting the Statistical Analysis of pyroclast density and porosity data, Copernicus Publication of the European Geosciences Union, Vol. 6 Pp 869-879, Quito, Ecuador

Binks, R.M. and Fairhead, J.D. (1992) A plate tectonic setting for Mesozoic rifts of West and Central Africa, Journal of Tectonophysics, Elsevier Science Publishers, Vol. 213, Pp 141-151 B.V. Amsterdam

Blitzer, L (1969) Handbook of Orbital Perturbations, Astronautics Journal No 453, University of Arizona Pp 1-93 USA

Bullard, E., Everett, J.E. and Smith, A.G. (1965) The fit of the continents around the Atlantic, Symposium on continental drift. Philos. Trans. No 258, Pp 41-52 London

Christina, M. B. and Ludwig, C. (2012) Global geopotential Models from Satellite Laser ranging data with geophysical applications: A Review, South African Journal of Science Vol. 3, No 108, Pp 1-10 South Africa

Cottrell, E., Jaupart, C. and Molnar, P. (2004) Marginal Stability of Thick Continental Lithosphere, Geophysical Research letters (American Geophysical Union) Vol. 31, letter 18612 Pp 1-4, USA

Dayoub, N. et al (2011) The Geoid geopotential value for unification of vertical Datums, A Paper Publication in Tishreen University, Dept. of

Topography, Faculty of Civil Engineering, Lattakia, Syrian Arab Republic

Dietmar, M.R. and Walter, R.R. (1992) Fracture zones in the North Atlantic from combined Geosat and Seasat Data, Journal of Geophysical Research Vol.97, No 83, Pp 3337-3350, Ottawa Canada

Ebun-Oni, A (1986) A Review of kinematics and dynamics of the African Plate, A Paper Presentation at the First International Workshop, University of Ibadan Pp 1-23, Nigeria

Erol, B (2020) An Assessment of the GOCE High-level Processing Facility (HPF) released global geopotential models with regional test results in Turkey, Instanbul Technical University, Civil Engineering Faculty, Geomatics Engineering Department, Turkey, Vol.12 No 3, Pp 586-612

Eshagh, M. et al., (2016) Moho Density Contrast in Central Eurasia from GOCE Gravity Gradients, Journal of Remote Sensing, www.mdpi.com/journal/remotesensing Vol. 8 No. 418, Pp 1-18

Eze, et al. (2011) Mechanical Model for Nigerian Intra-plate Earth Tremors, http://www.earthzine.org An article submitted to The Institute of Geosciences and Space Technology, RSUST Port-Harcourt, Nigeria Pp 1-8

Fairhead, J.D. and Binks, R.M. (1991) Differential Opening of the Central and South Atlantic Oceans and the Opening of the West African rift system, Tectonophysics 187,Pp 191-203

Forsberg, R. and Tscherning, C.C. (1981) The use of height data in gravity field approximation, Journal of Geophysical Research Vol. 86, Pp 7843-7854

Forste, C. et al (2005) A new high resolution global gravity field Model derived from combination of GRACE and CHAMP mission and altimetry/gravimetry surface data. Poster Presentation, European Geosciences Union General Assembly, Vienna.

Geyling, F. T. (1964) Perturbation Methods for Satellite Orbits Journal of Franklin Institute Vol. 275, No 8 Pp 602-641

Hirt, C (2013) RTM Gravity Forward-Modeling using Topography/Bathymetry data to Improve High-degree global geopotential models in the Coastal zone, Marine Geodesy Journal, Vol.36 Issue 2 Pp 183-202

Ibrahim et al. (2010) Evaluation of recent global geopotential models based on GPS/levelling data over Afyonkarahisar Turkey, Scientific Research and Essay, Vol. 5 No 5, Pp 484-493

Jean Marcel et al. (2018) Validation of gravity data from the geopotential field model for subsurface investigation of the Cameroon volcanic line (Western Africa)

Jull, M. and Kelemen, P.B. (2001) On the conditions for lower crustal convective instability, Journal of Geophysical Research Vol. 106, No B4 Pp 6423-6446, U.K.

Kaban, M.K. and Schwintzer, P. (2004) A New isostatic Model of the Lithosphere and Gravity Field, Journal of Geodesy, Vol. 78, Pp 368-385, U.K.

Kaula, W.M (1966) Tesseral Harmonics of the Earth's gravitational field from Camera tracking of Satellites, Journal of Geophysical Research, Vol. 71 Issue 18, Pp 4377-4388

Kendett, B.L.N. (1997) On the density distribution within the Earth, Geophysical Journal International, Vol. 132, Issue 2, Pp 374-390, U.K.

Khan, M.A (1967) Figure of the Earth and Mass Anomalies defined by Satellite Orbital Perturbations, Journal of Geophysical Research, Vol. 62 No 8, Pp 293-304

Khan, M. A. (1972) Figure of the Earth and Mass Anomalies defined by Satellite orbital Perturbations, Journal of Geophysical Research Vol. 52, No. 7, Pp 293-304 Hawaii

Koch, K. and Morrison, F. (1970) A Simple layer Model of the Geopotential from a combination of Satellite and Gravity data, Journal of Geophysical Research Vol.75 No 8, Pp1483-1493 United Kingdom

Koneshov and Nepoklonov (2018)Studying the Representation Accuracy of the Earth's gravity field in the Polar Regions based on the global geopotential models

Korte, M and Mandea, M (2016) Geopotential field Anomalies and Regional Tectonic features in Southern Africa and Germany

Kozai, Y (1967) New Determination of zonal harmonic coefficients of the Earth's gravitational potential, Smithsonian Astrophysical Observatory, Spec. Reprt. 165, Pp B67-B104.

Lenardic, A. and Moresi, L. N. (1999) Some thoughts on the Stability of Cratonic lithosphere: Effects of Bouyancy and Viscosity, Journal of Geophysical Research Vol. 104, No 12 Pp 747-758

Li, X. and Gotze, H. J. (2001) Ellipsoid, geoid, gravity, geodesy and geophysics, Journal of Society of Exploration Geophysicists. Vol. 66, No. 6 Pp 1660-1668 Texas U.S.A.

Marone, F. and Romanowicz, B (2007) The depth distribution of Azimuthal Anisotropy in the Continental Upper Mantle, Web of Science Journal, Nature 447, Pp 198-201

Merry, C. L. (2007) Evaluation of global Geopotential Models in determining the Quasi-geoid for Southern Africa, School of Architecture, Planning and Geomatics, University of Cape Town, Pp 1-4 South Africa.

Mickus, K (2002) Gravity Method: Environmental and Engineering Applications, Journal of Applied Geophysics, Vol. 56 Pp 215-236

Milelli, L., Fourel, L., Jaupart, C. (2012) A lithospheric instability origin for the Cameroon Volcanic line, Earth and Planetary Science letters www.elsevier.com No 335, Pp 80-87

Millar, C.E. and Mitalas, R. (1998) Model of the Earth with a Constant-Density Core and a Constant-Gravity Mantle, Journal of Geoscience Education, Vol. 46, Pp 465-470

Mohammed El-Ashquer et al. (2019) Study on the Selection of Optimal global geopotential models for geoid determination in Kuwait

Mosegaard, K and Sambridge, M (2002) Monte Carlo Analysis of Inverse Problems, Institute of Physics Publishing Vol. 18 Pp 29-54 U.K.

Okiwelu, A et al. (2010) Crustal Structure and Tectonics of the Calabar flank, West Africa based on Residual Gravity Interpretation, European Journal of Scientific Research, Vol. 42 No 2, Pp 195-203

Okiwelu, A. et al (2010) Crustal Structure and Tectonics of the Calabar flank, West Africa, based on Residual Gravity Interpretation, European Journal of Scientific Research Vol. 42, No. 2 Pp 195-203, Nigeria

Onyedim, G.C.(2007) Mapping Faults in Part of the Benue Trough, Nigeria by Cross Correlation Analysis of Gravity data, Journal of Applied Sciences, Vol. 7, Pp 226-231, Nigeria

Peiliang Xu (1992) Determination of surface gravity anomalies using gradiometric observables

Rapp, R.H. and Pavlis, N.K. (1990) The development and Analysis of Geopotential Coefficient Models to Spherical Harmonic degree 360: OSU89A and OSU89B, Journal of Geophysical Research, Vol. 95, No B13, Pp 21855-21911

Rizos, C. (1979) An Efficient computer technique for the Evaluation of geopotential from Spherical Harmonics, Australian Journal of Geodesy Photogrammetry and Surveying, Vol. 31, Pp 161-169, Australia

Samaila, N.K. and Likkason, O.K. (2013) Role of Equatorial Fracture zones on fluid migration across the South Atlantic Margins, Journal of Earth Science and Climatic change S12-004, Pp 1-10

Sankaran, A.V. (2001) Stability of Ancient Cratons and Lithospheric Mantle Composition, Current Science Journal, Vol. 81, No 9, Pp 1158-1160, Bangalore India

Selda, and Abbak, (2017) Regional Analysis of recent global geopotential Models: A case study in Turkey

Senachin, V.N. and Baranov, A.A. (2010) Estimation of the Deep density distribution in the lithosphere of Central and Southern Asia using data about free Mantle surface depth, Published in Fizika Zemli, Vol. 46, No 11, Pp 966-973

Shadini, and Tadjou, (2012) Interpreting gravity anomalies in South Cameroon and Central Africa

Szymkiewicz, A. (2013) Mathematical Models of flow in Porous Media, Earth and Planetary Science Journal Vol.3, No.7 Pp 9-47 Springer Verlag Berlin Heidelberg

Thorsten, W.B. and Boris, J.P.K. (2016) Numerical Modeling of Earth Systems, Lecture Notes for USC GEOL557, Vol.114, Pp1-92

Tenzer, R., Bagherbandi, M. and Vajda, P. (2012) Journal of Geophysical Institute of Slovak Academy of Science, Vol. 42, No. 1 Pp 1-13, Slovak Republic

Timar et al. (2018) A Short overview of the history of gravimetric measurements in Geodesy, Researchgate Journal Vol.6 No. 9 Pp 149-173

Tocho, C and Vergos, G.S (2015) Estimation of the Geopotential value WO for the local vertical datum of Argentina using EGM2008 and GPS/levelling data WO LVD, Geospacial Science, Vol. 10 No 32, Pp 1345-1422

Tomislav et al. (1989) A new geopotential model tailored to gravity data in Europe, A Conference proceedings of the IAG general meeting in Edinburgh.

Turcotte, D.L and Ockendon, J.R (1977) Geoid Anomalies and the Near-surface dipole distribution of Mass, Geophysical Journal Research, Vol 36 Pp 257-260

Turcotte, D.L. and Ockendon, J.R. (1978) Geoid Anomalies and the Near-surface Dipole distribution of Mass, Proceedings of the 9th GEOP conference at The Ohio State University No 280, Pp 257-260 USA

Yoder, C.F et al. (1983) Secular variation of Earth's gravitational harmonic coefficient from Lageos and Nontidal acceleration of Earth rotation, Centre for Space Research, Texas, Vol. 303 No 5920 Pp757-762

Yoder, C. F. et al (1983) Secular Variation of Earth's Gravitational Harmonic J_2 Coefficient from Lageos and non-tidal acceleration of Earth rotation, Macmillan Journals Ltd Vol. 303, No 5920 Pp 757-762, U.S.A

APPENDIX A

PROGRAM A1: To compute the geopotential over West African Sector

```
!-----------------------------------------------------------------
      !
   !  Purpose: To compute geopotential over the West African Region
      !
      !  Inputs:
      !    NMAX  I2 max. order and degree loaded
      !      Nm  I2 desired order and degree (Nm <= NMAX)
      !      Ae  R8 mean equatorial radius of the model [m]
      !      GM  R8 Earth gravitational constant [m**3/s**2]
      !       C  R8 array (0:NMAX,0:Nm) Harmonic coefficients J(n,m)
      !       S  R8 array (0:NMAX,0:Nm) Harmonic coefficients K(n,m)
      !       X  R8 array (3) ECEF cartesian coordinates [m]
      !
      !  Outputs:
      !       V  R8 geopotential value [m**2/s**2]
      !
      !
      !
   !  Refs.:
      !
      !
      !
   !-----------------------------------------------------------------

   subroutine Leg_ForCol_Pot (NMAX, Nm, Ae, GM, C, S, X, V)

      implicit none

   ! Calling parameters
      integer*2 NMAX, Nm
      real*8 Ae, GM, C(0:NMAX,0:Nm), S(0:NMAX,0:Nm), X(3), V

   ! Locals
   integer*2 n, m
   real*8 r, q, t, u, tf, al, sl, cl, Gmr
      real*8 pn(0:Nm), qn(0:Nm)
   real*8 Pnm, anm, bnm
   real*8 am, an, Pnn, Pnm1m, Pnm2m, sm, cm, sml, cml
   real*8 Xc, Xs, Omega

   ! Auxiliary variables
   r = sqrt(x(1)*x(1) + x(2)*x(2) + x(3)*x(3))
      q = Ae / r
      t = x(3) / r          ! sin (lat)
```

```
      u = sqrt (1.d0 - t*t)  ! cos (lat)
      tf = t/u               ! tan (lat)
      al = atan2(x(2), x(1)) ! longitude
      sl = sin (al)          ! sin (long)
    cl = cos (al)          ! cos (long)
      Gmr = GM / r

    ! Summation initialization
    Omega = 0.d0

    ! Pre-Store sectoral polynomials and q(m) = (Ae/r)**m
      pn(0) = 1.d0
      pn(1) = 1.7320508075688773D0 * u ! sqrt(3) * u
      qn(0) = 1.d0
      qn(1) = q
    do m = 2, Nm
     pn(m) = u * sqrt(1.d0+0.5d0/dble(m)) * pn(m-1)
       qn(m) = q * qn(m-1)
    end do

    ! Initialize sin and cos recursions
    sm = 0.d0
      cm = 1.d0

    ! Outer m loop
    do m=0,Nm

     ! init
       am = dble(m)

       ! For m = n
     Pnm = pn(m)            ! m=n sectoral
       Pnm1m = Pnm
       Pnm2m = 0.d0

     ! Init Xc, Xs sums
     Xc = qn(m) * C(m,m) * Pnm
     Xs = qn(m) * S(m,m) * Pnm

     ! Inner n Loop
     do n=m+1,Nm
         an = dble(n)
      anm = sqrt( ((an+an-1.d0)*(an+an+1.d0))
&          / ((an-am)*(an+am)) )
          bnm = sqrt( ((an+an+1.d0)*(an+am-1.d0)*(an-am-1.d0))
&          / ((an-am)*(an+am)*(an+an-3.d0)) )
```

```
   ! Pnm recursion
   Pnm = anm * t * Pnm1m - bnm * Pnm2m

   ! Store
        Pnm2m = Pnm1m
        Pnm1m = Pnm

   ! Inner sum
   if (n .lt. 2) cycle
   Xc = Xc + qn(n) * C(n,m) * Pnm
   Xs = Xs + qn(n) * S(n,m) * Pnm

      end do

  ! Outer sum
      Omega = Omega + (Xc*cm + Xs*sm)

  ! sin and cos recursions to next m
      cml = cl*cm - sm*sl
  sml = cl*sm + cm*sl
  cm = cml ! save to next m
      sm = sml ! save to next m

end do

! Finalization, include n=0 (P00=1),
     ! for n=1 all terms are zero: C,S(1,1), C,S(1,0) = 0
V =  Gmr * (1.d0+Omega)

return
     end
```

PROGRAM A2

To compute the gravity Anomaly of West African Region

```
latbegin=3;
latend=20;
longbegin=-25;
longend=20;

a=6378; % km
r=63712; % km
M=5.975*10^(24); %kg, mass of the Earth
G=6.673*10^(-11); % Newton gravitational constant, Nm2/kg2
J=[-484.1394,-0.1755,2.4839,0.8721,1.5773,0.9314,0.4038].*10^(6); %%% these data
are taken from the table attached.
K=[0,0.0442,-1.1957,0,-0.1050,-0.9212,2.0061].*10^(6);

nlat=0;
for lat=latbegin:latend % geographic latitude
phi=90-lat; % co-latitude
nlat=nlat+1; nlong=0;
for L=longbegin:longend; % geographic longitude
nlong=nlong+1; nm=0;
for n=2:3 %can get to 360
        Pn=legendre(n,sind(phi));
%           Pn=legendre(n,sind(phi)),'norm';
for m=0:n
nm=nm+1; Pnm=Pn(m+1);
inside1(m+1)=((J(nm)*sind(m*L)+K(nm)*cosd(m*L))*Pnm);
end
inside2(n-1)=((a/r)^n)*sum(inside1);
end
V(nlat,nlong)=(G*M/r)*(1-sum(inside2));
end
end

contourf(longbegin:longend, latbegin:latend, V);
xlabel('Longitude'); ylabel('Latitude'); colorbar;
```

PROGRAM A3

To compute the Geopotential over Itakpe Region

```
tic;
mkdir('PLOTS');
latbegin=3;
latend=20;
longbegin=-25;
longend=15;
% z=xlsread('Ruke1.xlsx');
% y=fopen('ewumi.txt', 'wt');
% fprintf(y, '%3.0f\t %3.0f\t %4.11f\t %4.11f\t %7.11f\n',z');
fid=fopen('ewumi.txt');
    a=textscan(fid, '%f %f %f %f %f');
    J=a{3};K=a{4};
a=6378; % km
r=63712; % km
M=5.975*10^(24); %kg, mass of the Earth
G=6.673*10^(-11); % Newton gravitational constant, Nm2/kg2
%    J=[-484.1394,-0.1755,2.4839,0.8721,1.5773,0.9314,0.4038].*10^(6);
%%% these data are taken from the table attached.
% K=[0,0.0442,-1.1957,0,-0.1050,-0.9212,2.0061].*10^(6);

nlat=0;
for lat=latbegin:latend % geographic latitude
phi=90-lat; % co-latitude
nlat=nlat+1; nlong=0;
for L=longbegin:longend; % geographic longitude
nlong=nlong+1; nm=0;
for n=2:360 %can get to 360
%Pn=legendre(n,sind(phi))
            Pn=legendre(n,sind(phi),'norm')
for m=0:n
nm=nm+1; Pnm=Pn(m+1);
inside1(m+1)=((J(nm)*sind(m*L)+K(nm)*cosd(m*L))*Pnm);
                fid2=fopen('ewumivalues.txt', 'wt');
end
inside2(n-1)=((a/r)^n)*sum(inside1);
end
V(nlat,nlong)=(G*M/r)*(1-sum(inside2));
end
end

% contourf(longbegin:longend, latbegin:latend, V);
% xlabel('Longitude'); ylabel('Latitude'); colorbar;
% saveas(gcf, 'PLOTS\Geopotential_Equation.fig');
```

PROGRAM A4

To compute the gravity anomalies over South-south Sector

```
mkdir('PLOTS');
latbegin=3;
latend=15;
longbegin=-30;
longend=15;
% z=xlsread('Ruke1.xlsx');
% y=fopen('ewumi.txt', 'wt');
% fprintf(y, '%3.0f\t %3.0f\t %4.11f\t %4.11f\t %7.11f\n',z');
fid=fopen('ewumi.txt');
a=textscan(fid, '%f %f %f %f %f');
J=a{3};K=a{4};

a=6378; % km
r=63712; % km
M=5.975*10^(24); %kg, mass of the Earth
G=6.673*10^(-11); % Newton gravitational constant, Nm2/kg2
%    J=[-484.1394,-0.1755,2.4839,0.8721,1.5773,0.9314,0.4038].*10^(6);
%%% these data are taken from the table attached.
% K=[0,0.0442,-1.1957,0,-0.1050,-0.9212,2.0061].*10^(6);

nlat=0;
for lat=latbegin:latend % geographic latitude
phi=90-lat; % co-latitude
nlat=nlat+1; nlong=0;
for L=longbegin:longend; % geographic longitude
nlong=nlong+1; nm=0;
for n=2:3 %can get to 360
%              Pn=legendre(n,sind(phi));
              Pn=legendre(n,sind(phi),'norm')
for m=0:n
nm=nm+1; Pnm=Pn(m+1);
inside1(m+1)=((J(nm)*sind(m*L)+K(nm)*cosd(m*L))*Pnm);
end
inside2(n-1)=((a/r)^n)*sum(inside1);
end
deltag(nlat,nlong)=(-G*M/r^2)*(1-sum(inside2));
end
end

contourf(longbegin:longend, latbegin:latend, deltag);
xlabel('Longitude'); ylabel('Latitude'); colorbar;
saveas(gcf, 'PLOTS\Gravity_Anomalies_Equation.fig');
```

PROGRAM A5

To compute the Geoidal Height over the West African Region

```
mkdir('PLOTS');
latbegin=3;
latend=15;
longbegin=-30;
longend=15;
% z=xlsread('Ruke1.xlsx');
% y=fopen('ewumi.txt', 'wt');
% fprintf(y, '%3.0f\t %3.0f\t %4.11f\t %4.11f\t %7.11f\n',z');
fid=fopen('ewumi.txt');
a=textscan(fid, '%f %f %f %f %f');
J=a{3};K=a{4};

a=6378; % km
r=63712; % km
M=5.975*10^(24); %kg, mass of the Earth
G=6.673*10^(-11); % Newton gravitational constant, Nm2/kg2
%    J=[-484.1394,-0.1755,2.4839,0.8721,1.5773,0.9314,0.4038].*10^(6);
%%% these data are taken from the table attached.
% K=[0,0.0442,-1.1957,0,-0.1050,-0.9212,2.0061].*10^(6);
g=9.815; %m/s2, theoretical gravity

nlat=0;
for lat=latbegin:latend % geographic latitude
phi=90-lat; % co-latitude
nlat=nlat+1; nlong=0;
for L=longbegin:longend; % geographic longitude
nlong=nlong+1; nm=0;
for n=2:3 %can get to 360
%Pn=legendre(n,sind(phi))
          Pn=legendre(n,sind(phi),'norm')
for m=0:n
nm=nm+1; Pnm=Pn(m+1);
inside1(m+1)=((J(nm)*sind(m*L)+K(nm)*cosd(m*L))*Pnm);
end
inside2(n-1)=((a/r)^n)*sum(inside1);
end
N(nlat,nlong)=1/g*(-G*M/r)*(1-sum(inside2));
end
end

contourf(longbegin:longend, latbegin:latend, N);
xlabel('Longitude'); ylabel('Latitude'); colorbar;
saveas(gcf, 'PLOTS\Geoidal_Undulations_Equation.fig');
```

PROGRAM A6

MARKOV CHAIN MONTE-CARLO PROGRAMME (MCMC)

R CODE

5.1 Geopotential

```
normgibbs = function(N,n,a,b,cc,d,xbar,ssquared)
{
mat = matrix(ncol=2, nrow=N)
mu = cc
tau = a/b

mat[1,] = c(mu,tau)
for (i in 2 : N) {
muprec = n*tau+d
mumean = (d*cc+n*tau*xbar)/muprec
mu = rnorm(1,mumean,sqrt(1/muprec))
taub = b+0.5*((n-1)*ssquared+n*(xbar-mu)^2)
tau = rgamma(1, a+n/2,taub)
mat[i, ] = c(mu,tau)
}
mat
}
postmat = normgibbs(N=11000, n =length(x),a=3, b = 11, cc = 10, d=1/100, xbar =
mean(x), postmat = postmat[1001:11000,]
op = par(mfrow=c(3,3))
plot(postmat,col=1:10000,main="joint posterior")
plot(postmat,type = "l", main="joint posterior")
plot.new()
plot(ts(postmat[,1]),main= expression("Marginal for" ~mu))
plot(ts(postmat[,2]),main=expression("Marginal for" ~tau))
plot(ts(sqrt(1/postmat[,2])),main=expression("Marginal for" ~sigma))
hist(postmat[,1],40,main=expression("Marginal for" ~mu))
hist(postmat[,2],40,main=expression("Marginal for" ~tau))
hist(sqrt(1/postmat[,2]),40,main=expression("Marginal for" ~sigma))
par(op)
rm(list=ls())
rran<-read.table("C:/Users/Obisesan/Desktop/physic phd/AGP.txt",header = TRUE)
x<-rran[,1]
```

5.2 Geoidal Height

```
normgibbs = function(N,n,a,b,cc,d,xbar,ssquared)
{
```

```
mat = matrix(ncol=2, nrow=N)
mu = cc
tau = a/b

mat[1,] = c(mu,tau)
for (i in 2 : N) {
muprec = n*tau+d
mumean = (d*cc+n*tau*xbar)/muprec
mu = rnorm(1,mumean,sqrt(1/muprec))
taub = b+0.5*((n-1)*ssquared+n*(xbar-mu)^2)
tau = rgamma(1, a+n/2,taub)
mat[i, ] = c(mu,tau)
}
mat
}
postmat = normgibbs(N=11000, n =length(x),a=3, b = 11, cc = 10, d=1/100, xbar =
mean(x), postmat = postmat[1001:11000,]
op = par(mfrow=c(3,3))
plot(postmat,col=1:10000,main="joint posterior")
plot(postmat,type = "l", main="joint posterior")
plot.new()
plot(ts(postmat[,1]),main= expression("Marginal for" ~mu))
plot(ts(postmat[,2]),main=expression("Marginal for" ~tau))
plot(ts(sqrt(1/postmat[,2])),main=expression("Marginal for" ~sigma))
hist(postmat[,1],40,main=expression("Marginal for" ~mu))
hist(postmat[,2],40,main=expression("Marginal for" ~tau))
hist(sqrt(1/postmat[,2]),40,main=expression("Marginal for" ~sigma))
par(op)
rm(list=ls())
rran<-read.table("C:/Users/Obisesan/Desktop/physic phd/AGH.txt",header = TRUE)
x<-rran[,1]
```

5.3 Gravity Anomaly

```
normgibbs = function(N,n,a,b,cc,d,xbar,ssquared)
{
mat = matrix(ncol=2, nrow=N)
mu = cc
tau = a/b
mat[1,] = c(mu,tau)

for (i in 2 : N) {
muprec = n*tau+d
mumean = (d*cc+n*tau*xbar)/muprec
mu = rnorm(1,mumean,sqrt(1/muprec))
```

```
taub = b+0.5*((n-1)*ssquared+n*(xbar-mu)^2)
tau = rgamma(1, a+n/2,taub)
mat[i, ] = c(mu,tau)
}
mat
}
postmat = normgibbs(N=11000, n =length(x),a=3, b = 11, cc = 10, d=1/100, xbar =
mean(x), postmat = postmat[1001:11000,]
op = par(mfrow=c(3,3))
plot(postmat,col=1:10000,main="joint posterior")
plot(postmat,type = "l", main="joint posterior")
plot.new()
plot(ts(postmat[,1]),main= expression("Marginal for" ~mu))
plot(ts(postmat[,2]),main=expression("Marginal for" ~tau))
plot(ts(sqrt(1/postmat[,2])),main=expression("Marginal for" ~sigma))
hist(postmat[,1],40,main=expression("Marginal for" ~mu))
hist(postmat[,2],40,main=expression("Marginal for" ~tau))
hist(sqrt(1/postmat[,2]),40,main=expression("Marginal for" ~sigma))
par(op)
rm(list=ls())
rran<-read.table("C:/Users/Obisesan/Desktop/physic phd/GAA.txt",header = TRUE)
x<-rran[,1]
```

APPENDIX B

Table B1: The Geoidal Height data of Itakpe, computed from models (MGGM and GGM) and compared with available In-situ data of the area.

Latitude (deg)	Longitude (deg)	Geoidal Height (m) MGGM (W/A)	Geoidal Height (m) GGM (W/A)	Geoidal Height (m) Itakpe (W/A)
6.264	5.027	32.8	55.7	40.4
6.267	5.033	47.6	61.9	68.9
6.269	5.038	86.3	109.2	91.5
6.273	5.044	51.7	63.4	75.2
6.280	5.051	128.2	142.6	134.1
6.285	5.057	36.4	22.9	-13.3
6.291	5.062	43.5	67.2	31.8
6.298	5.069	-22.9	-43.6	-35.6
6.304	5.073	49.1	56.3	38.7
6.310	5.078	27.6	-12.8	45.9
6.316	5.084	-54.7	-31.4	-29.3
6.322	5.089	-36.4	-42.8	-57.5
6.328	5.095	28.3	30.7	46.4
6.331	5.101	92.5	86.8	79.1
6.335	5.107	-33.9	-45.6	-65.8
6.342	5.116	27.4	36.8	43.2

Table B1 continued

Latitude (deg)	Longitude (deg)	Geoidal Height (m) MGGM (W/A)	Geoidal Height (m) GGM (W/A)	Geoidal Height (m) Itakpe (W/A)
6.347	5.121	-45.2	-29.7	-39.5
6.353	5.128	32.5	41.8	26.7
6.359	5.134	57.8	29.3	35.2
6.364	5.139	80.6	102.5	97.8
6.370	5.145	-33.5	-28.7	-41.6
6.376	5.152	52.4	49.3	65.9
6.381	5.160	37.2	21.8	42.6
6.388	5.167	-45.9	-55.2	-38.3
6.395	5.173	64.7	52.9	80.4
6.402	5.178	56.5	61.8	75.5
6.409	5.184	-58.8	-43.6	-60.7
6.414	5.190	-42.2	-39.2	-55.6
6.417	5.196	38.6	29.3	47.9
6.423	5.204	50.1	42.5	36.3
6.428	5.211	127.4	139.7	144.2
6.435	5.217	93.7	68.8	85.4
6.442	5.222	39.9	46.2	27.8
6.449	5.226	-41.5	-28.5	-39.2

Table B1 continued

Latitude (deg)	Longitude (deg)	Geoidal Height (m) MGGM (W/A)	Geoidal Height (m) GGM (W/A)	Geoidal Height (m) Itakpe (W/A)
6.456	5.234	65.8	47.2	58.5
6.463	5.240	43.6	36.9	51.9
6.467	5.248	-37.3	28.4	-65.7
6.472	5.253	78.2	49.5	21.5
6.478	5.259	-43.4	-51.6	-38.4
6.485	5.267	91.7	64.8	85.2
6.491	5.272	56.9	78.3	39.7
6.494	5.275	122.5	113.6	101.4
6.501	5.282	-36.2	-53.7	-48.6
6.509	5.286	69.8	39.5	56.3
6.513	5.294	43.1	28.2	37.5
6.517	5.298	-52.6	-49.4	-23.7
6.524	5.305	71.3	65.9	54.2
6.528	5.312	-38.7	-50.6	-42.6
6.535	5.316	26.4	47.5	35.8
6.542	5.324	44.9	39.8	65.7
6.547	5.329	59.5	76.2	43.4
6.553	5.337	-62.8	-49.6	-57.1

Table B1 continued

Latitude (deg)	Longitude (deg)	Geoidal Height (m) MGGM (W/A)	Geoidal Height (m) GGM (W/A)	Geoidal Height (m) Itakpe (W/A)
6.560	5.341	56.2	17.3	39.3
6.564	5.348	-33.6	-28.5	-42.5
6.569	5.353	95.1	84.6	78.4
6.572	5.356	44.3	37.2	50.9
6.576	5.362	127.8	45.9	34.2
6.583	5.369	-54.5	-32.8	-46.8
6.588	5.37 4	201.4	176.5	188.7
6.595	5.378	54.2	42.9	63.1
6.601	5.385	88.7	62.5	75.6
6.609	5.397	-35.3	-28.6	-42.7
6.614	5.403	73.6	81.6	60.2
6.620	5.409	42.9	39.4	45.8
6.627	5.414	-34.8	-25.1	-49.3
6.632	5.420	61.5	58.6	75.4
6.638	5.426	-43.3	-38.9	-50.5
6.643	5.435	72.6	44.4	69.9
6.649	5.441	69.3	86.4	72.6
6.655	5.447	-37.2	-53.6	-46.4

Table B1 continued

Latitude (deg)	Longitude (deg)	Geoidal Height (m) MGGM (W/A)	Geoidal Height (m) GGM (W/A)	Geoidal Height (m) Itakpe (W/A)
6.662	5.453	52.4	63.9	35.7
6.668	5.459	61.1	58.7	49.3
6.673	5.465	35.5	63.2	56.1
6.679	5.472	-38.4	49.9	47.6
6.684	5.478	56.7	72.1	65.8
6.687	5.486	29.6	40.3	36.4
6.695	5.494	-47.8	57.9	-37.2
6.701	5.498	-33.5	69.7	-26.9
6.706	5.503	49.6	52.3	63.5

Table B2: The gravity anomaly data of Itakpe from models (MGGM and GGM) and compared with the aero-gravity data of the area

Latitude (deg)	Longitude (deg)	Theoretical Gravity (m/s^2) West Africa	Gravity Anomaly(gals) (M GGM)	Gravity Anomaly(gals) (GGM)	Gravity Anomaly(gals) (In-situ)
2	-8	9.7916	84.52	93.64	87.15
2	-6	9.7956	-81.17	75.23	-80.96
2	-4	9.7909	72.96	84.18	69.25
2	-2	9.7867	-63.54	-92.46	84.39
2	0	9.7927	86.28	87.03	91.76
2	2	9.7849	79.63	-85.89	-82.31
2	4	9.7797	-82.97	-81.97	-84.44
2	6	9.7786	63.24	72.02	75.96
2	8	9.7792	-76.59	85.14	-69.72
2	10	9.7787	91.03	76.97	82.83
4	-8	9.7952	85.66	91.72	-79.65
4	-6	9.7822	-75.38	-82.46	-87.19
4	-4	9.7801	-92.14	-85.48	-63.57
4	-2	9.7807	68.25	76.09	87.41
4	0	9.7811	79.84	90.31	82.56
4	2	9.7811	85.73	81.62	74.32
4	4	9.7798	-72.34	-76.59	-80.19
4	6	9.7807	83.05	82.96	86.64
4	8	9.7807	95.86	94.33	82.57
4	10	9.7798	74.32	77.95	76.61
6	-8	9.7966	-87.53	69.48	-84.59
6	-6	9.7835	81.05	78.36	88.69
6	-4	9.7829	72.96	80.42	67.25
6	-2	9.7829	85.21	89.30	83.44
6	0	9.7829	74.83	92.75	86.56

Table B2: continued

Latitude (deg)	Longitude (deg)	Theoretical Gravity (m/s^2) West Africa	Gravity Anomaly(gals) (M GGM)	Gravity Anomaly(gals) (GGM)	Gravity Anomaly(gals) (In-situ)
6	2	9.7829	84.26	75.09	81.12
6	4	9.7823	90.84	83.37	85.93
6	6	9.7827	86.92	79.65	67.29
6	8	9.7826	73.19	80.28	83.74
6	10	9.7803	92.46	85.73	86.93
8	-8	9.7974	-76.65	-79.24	-75.22
8	-6	9.7861	-86.71	-82.49	-84.86
8	-4	9.7849	93.28	96.83	91.05
8	-2	9.7852	82.54	88.76	85.63
8	0	9.7856	79.25	76.18	80.24
8	2	9.7848	84.07	83.95	89.72
8	4	9.7841	72.96	75.38	82.49
8	6	9.7849	86.59	81.40	85.73
8	8	9.7846	93.74	90.62	87.84
8	10	9.7843	85.52	87.35	83.46
10	-8	9.8021	79.69	74.13	75.58
10	-6	9.7895	88.57	86.94	82.82
10	-4	9.7885	93.42	96.85	94.26
10	-2	9.7886	-86.19	-83.52	-81.19
10	0	9.7887	72.55	76.94	73.74
10	2	9.7866	84.26	87.31	82.94
10	4	9.7855	75.39	81.46	76.78
10	6	9.7877	80.54	86.92	87.53
10	8	9.7879	89.72	85.34	82.96
10	10	9.7879	76.85	83.69	79.04
30	-12	9.8077	-82.67	-87.25	-84.16

Table B2: continued

Latitude (deg)	Longitude (deg)	Theoretical Gravity (m/s^2) West Africa	Gravity Anomaly(gals) (M GGM)	Gravity Anomaly(gals) (GGM)	Gravity Anomaly(gals) (In-situ)
12	-6	9.8039	-77.93	-75.86	-79.92
12	-4	9.7947	85.54	84.23	81.58
12	-2	9.7912	-91.86	-87.29	-90.53
12	0	9.7928	84.52	83.64	89.06
12	2	9.7921	76.39	81.28	74.29
12	4	9.7916	82.87	79.16	73.45
12	6	9.7919	89.56	85.93	82.76
12	8	9.7929	77.23	72.58	78.90
12	10	9.7929	83.11	78.36	86.52
0	-8	9.7931	64.97	75.10	79.84
0	-6	9.7907	85.26	83.75	81.97
0	-4	9.7935	72.35	74.09	76.58
0	-2	9.7957	86.17	89.28	85.55
0	0	9.7945	93.64	84.25	92.61
0	2	9.7927	-86.29	-87.36	-83.49
0	4	9.7802	-75.31	-76.84	-80.02
0	6	9.7789	-96.27	-89.62	-95.34
0	8	9.7793	82.58	85.17	86.69
0	10	9.7791	87.25	79.43	83.64
-2	-8	9.7962	75.68	80.21	75.92
-2	-6	9.7927	-82.16	-85.95	-88.56
-2	-10	9.7911	-84.72	-91.36	-82.49
-2	-2	9.7953	-78.39	-86.50	-89.73
-2	0	9.7946	-92.85	-87.94	-81.16
-2	2	9.7962	76.38	79.82	82.58
-2	4	9.7909	83.62	86.03	85.67

Table B2: continued

Latitude (deg)	Longitude (deg)	Theoretical Gravity (m/s^2) West Africa	Gravity Anomaly(gals) (M GGM)	Gravity Anomaly(gals) (GGM)	Gravity Anomaly(gals) (In-situ)
-2	6	9.7791	79.54	75.48	86.94
-2	8	9.779	85.17	82.99	79.32
-2	10	9.7787	94.86	87.57	81.79

Statistics

Minimum Gravity (m/s^2)	9.7786
Maximum Gravity(m/s^2)	9.8077
Average Gravity(m/s^2)	9.7874
Mode Gravity(m/s^2)	9.7829
Standard Deviation	0.0070

Table B3: The Geopotential values computed from Modified Model (MGGM) over Itakpe and compared with existing GGM (Wiechert, 2008) and observed/In-situ data.

Latitude (deg)	Longitude (deg)	Geopotential(m^2/s^2) Wiechert W/A (GGM)	Geopotential (m^2/s^2) Itakpe W/A	Geopotential(m^2/s^2) West Africa (MGGM)
6.264	5.027	26.67	38.55	43.84
6.267	5.033	85.01	69.27	77.26
6.269	5.039	68.33	46.13	59.22
6.273	5.044	116.83	92.49	86.91
6.281	5.051	24.83	-35.28	-15.85
6.285	5.057	59.24	21.75	-33.36
6.291	5.062	-40.53	59.23	38.22
6.298	5.069	62.02	48.96	-25.42
6.304	5.073	49.73	57.14	69.45
6.310	5.078	-16.50	-24.82	-46.73
6.316	5.084	62.43	37.87	52.89

Table B3: continued

Latitude (deg)	Longitude (deg)	Geopotential(m^2/s^2) Wiechert W/A (GGM)	Geopotential (m^2/s^2) Itakpe W/A	Geopotential(m^2/s^2) West Africa (MGGM)
6.322	5.089	18.76	49.03	-27.55
6.328	5.095	79.45	56.14	68.64
6.331	5.101	-28.85	-46.27	33.90
6.335	5.107	57.16	29.63	42.11
6.342	5.116	-16.25	-38.39	-22.58
6.347	5.121	59.03	67.84	42.56
6.353	5.128	81.15	53.94	75.86
6.359	5.134	-47.33	-28.56	-31.64
6.364	5.139	-39.02	-46.83	-57.02
6.370	5.145	56.84	27.91	43.27
6.376	5.152	-23.89	-39.68	-10.55
6.381	5.160	-31.90	-57.42	-49.99
6.388	5.167	45.61	63.17	76.84

Table B3: continued

Latitude (deg)	Longitude (deg)	Geopotential(m^2/s^2) Wiechert W/A (GGM)	Geopotential (m^2/s^2) Itakpe W/A	Geopotential(m^2/s^2) West Africa (MGGM)
6.395	5.173	34.45	29.53	47.24
6.402	5.178	62.89	55.02	82.09
6.409	5.184	-20.14	-36.97	-29.12
6.414	5.190	-39.02	-16.94	-27.83
6.417	5.196	98.22	68.19	75.34
6.423	5.204	52.97	41.53	62.69
6.428	5.211	67.04	88.16	59.32
6.435	5.217	61.36	92.54	78.07
6.442	5.222	80.65	73.03	94.21
6.449	5.226	-57.90	-46.25	-30.41
6.456	5.234	61.26	73.84	88.15
6.463	5.240	23.07	18.09	46.23
6.467	5.248	-42.56	-54.92	-39.71

Table B3: continued

Latitude (deg)	Longitude (deg)	Geopotential(m^2/s^2) Wiechert W/A (GGM)	Geopotential (m^2/s^2) Itakpe W/A	Geopotential(m^2/s^2) W/Africa (MGGM)
6.472	5.253	98.59	85.73	79.67
6.478	5.259	62.03	51.48	46.15
6.485	5.267	-21.67	-33.19	-40.52
6.491	5.272	73.14	59.26	68.99
6.494	5.275	-30.92	-48.17	-23.22
6.501	5.282	-67.10	55.86	-31.69
6.509	5.286	98.33	72.51	84.45
6.513	5.294	56.24	49.06	68.38
6.517	5.298	42.81	28.93	31.62
6.524	5.305	69.77	53.46	-3.64
6.528	5.312	53.68	49.88	61.74
6.535	5.316	67.06	82.15	42.93
6.542	5.324	39.28	55.09	27.35

Table B3: continued

Latitude (deg)	Longitude (deg)	Geopotential(m^2/s^2) Wiechert W/A (GGM)	Geopotential (m^2/s^2) Itakpe W/A	Geopotential(m^2/s^2) West Africa (MGGM)
6.547	5.329	85.26	91.73	103.63
6.553	5.337	93.63	79.46	65.51
6.560	5.341	79.31	88.52	94.32
6.564	5.348	46.90	56.38	67.29
6.569	5.353	31.44	29.26	40.53
6.572	5.356	79.66	52.07	63.64
6.576	5.362	84.50	92.34	59.22
6.583	5.369	48.14	63.28	75.39
6.588	5.374	72.43	85.35	64.16
6.595	5.378	52.67	49.06	38.99
6.601	5.385	83.15	92.72	62.65
6.609	5.397	46.97	75.31	58.04
6.614	5.403	97.93	65.64	84.31
6.620	5.409	106.37	87.91	79.53
6.627	5.414	46.43	53.24	61.82
6.632	5.420	35.12	48.75	56.35
6.638	5.426	92.57	76.19	84.98

6.643	5.435	115.25	82.04	91.27
6.649	5.441	56.09	49.73	62.85
6.655	5.447	24.86	39.62	48.50
6.662	5.453	82.35	74.17	93.43
6.669	5.459	79.50	65.23	58.16
6.673	5.465	43.40	52.86	74.35
6.679	5.472	86.25	93.77	72.63
6.691	5.477	79.38	65.42	58.43
6.695	5.491	45.46	39.03	22.83
6.702	5.496	93.74	105.26	84.69
6.706	5.503	62.80	75.49	59.23
6.712	5.509	75.93	63.08	91.45
6.720	5.514	86.22	74.75	63.48

Table B4: The Density distribution for varying Latitude ϕ and Longitude λ computed over the West African Region.

Lat ϕ (deg)	Long λ (deg)	N(m)	ρ (g/cm³)
0	-10	58.7	-5.127
2	-10	72.2	2.074
4	-10	-22.5	-1.244
6	-10	96.9	3.691
8	-10	35.8	7.705
0	-8	79.1	-3.849
2	-8	66.6	-2.957
4	-8	-54.3	12.957
6	-8	-20.4	8.251
8	-8	-88.2	5.652
0	-6	-12.7	-8.313
2	-6	58.3	-7.822
4	-6	39.9	5.604
6	-6	-77.2	9.015
8	-6	-14.5	3.181
0	-4	55.6	6.005
2	-4	71.9	-18.316
4	-4	83.1	-4.031
6	-4	-11.7	16.074
8	-4	-84.0	5.523
0	-2	-28.5	-13.546
2	-2	59.2	21.154
4	-2	23.8	10.176
6	-2	44.3	-19.532
8	-2	-33.9	-7.934
0	0	77.5	13.212
2	0	36.7	10.469
4	0	-18.2	-5.699
6	0	39.8	8.197

Lat ϕ (deg)	Long λ (deg)	N(m)	ρ (g/cm³)
0	2	17.1	-15.867
2	2	46.8	8.321
4	2	29.3	10.784
6	2	39.9	-15.692
8	2	-66.1	-10.674
0	4	-38.6	-14.834
2	4	-63.4	-13.713
4	4	35.5	18.154
6	4	58.8	8.299
8	4	-22.7	-10.821
0	6	-48.2	7.207
2	6	63.6	-3.646
4	6	57.9	-11.757
6	6	-12.7	4.623
8	6	-59.7	-5.982
0	-8	27.3	-3.728
2	-8	75.5	-8.998
4	-8	-44.4	8.652
6	-8	11.7	-3.315
8	-8	36.8	9.803
0	-8	-91.0	8.762
2	-8	28.5	-9.172
4	-8	94.4	-4.168
6	-8	-32.8	-3.269
8	-8	-51.3	12.706
0	-6	47.6	6.384
2	-6	29.9	-3.987
4	-6	-23.3	4.514
6	-6	18.1	-13.863
8	-6	-13.7	15.559
0	-4	31.5	-11.974
2	-4	64.2	-4.451

Lat ϕ (deg)	Long λ (deg)	N(m)	ρ (g/cm³)
6	-4	57.4	-8.919
8	-4	40.3	-9.422
0	-2	62.0	16.026
2	-2	85.6	9.923
6	-2	47.4	20.818
8	-2	12.9	-13.427
0	-2	38.8	-10.899
0	0	105.2	8.181
2	0	45.7	10.803
4	0	19.3	5.688
6	0	69.8	10.355
8	0	80.5	11.829
0	2	-41.2	12.208
2	2	76.2	10.462
4	2	31.4	-11.284
6	2	16.7	9.689
8	2	-22.5	8.547
0	4	75.1	6.301
2	4	59.3	10.536
4	4	16.6	-8.531
6	4	-26.8	5.284
8	4	53.4	-7.083
0	6	30.2	-6.723
2	6	88.7	-11.951
4	6	-32.6	9.842
6	6	47.5	10.529
8	6	82.2	8.313
0	-8	-39.9	15.573
2	-8	-12.3	-7.896
4	-8	-47.4	-14.476
6	-8	17.5	-6.687
8	-8	56.9	8.323

Lat ϕ (deg)	Long λ (deg)	N(m)	ρ (g/cm³)
2	-8	38.1	26.253
4	-8	83.8	15.348
6	-8	51.3	9.515
8	-8	-69.5	8.037
0	-6	-27.2	9.825
2	-6	58.4	7.968
4	-6	46.8	12.849
6	-6	33.6	8.704
8	-6	-37.4	5.015
0	-4	-82.9	6.018
2	-4	92.7	13.307
4	-4	75.3	11.829
6	-4	15.5	10.565
8	-4	-41.1	7.499
0	-2	-11.8	9.581
2	-2	34.4	-5.652
4	-2	58.7	-4.603
6	-2	18.3	8.746
8	-2	-60.9	15.502
0	0	22.2	5.126
2	0	-19.8	18.522
4	0	91.6	3.975
6	0	21.5	9.284
8	0	130.7	-4.698
0	2	55.0	-5.318
2	2	-77.4	-6.248
4	2	63.1	8.132
6	2	17.3	8.657
8	2	57.0	10.803
0	4	-65.5	-10.899
2	4	-18.2	5.827
4	4	13.7	-9.756

Lat ϕ (deg)	Long λ (deg)	N(m)	ρ (g/cm³)
8	4	127.6	6.296
0	6	-78.7	8.323
2	6	35.2	-8.156
4	6	20.8	-10.279
6	6	44.1	-13.427
8	6	-61.5	-9.546
0	-4	58.3	-6.578
2	-4	-60.9	-10.613
4	-4	-32.7	12.687
6	-4	62.4	7.854
8	-4	49.2	13.308
0	-8	-31.6	10.875
2	-8	87.8	-12.951
4	-8	-10.5	8.045
6	-8	42.2	13.618
8	-8	33.9	15.621
0	-6	-26.4	23.396
2	-6	34.3	11.321
4	-6	-90.7	19.413
6	-6	19.5	6.074
8	-6	-49.8	10.946
0	-4	56.1	7.875
2	-4	94.5	13.756
4	-4	21.0	9.953
6	-4	-50.6	7.902
8	-4	83.2	15.979
0	-2	109.7	11.098
2	-2	-74.1	8.987
4	-2	42.8	10.736
6	-2	96.5	26.236
8	-2	46.4	14.654
0	0	-59.3	8.749

Lat ϕ (deg)	Long λ (deg)	N(m)	ρ (g/cm³)
4	0	88.0	28.252
6	0	63.5	15.444
8	0	12.6	8.848
0	2	-15.1	7.991
2	2	-66.8	10.353
4	2	58.9	16.926
6	2	21.5	5.258
8	2	70.3	13.445
0	4	35.8	9.112
2	4	-43.2	3.005
4	4	19.4	43.427
6	4	91.6	27.522
8	4	33.2	16.576
0	6	73.9	39.158
2	6	-38.4	8.848
4	6	-14.0	7.875
6	6	12.7	9.946
8	6	65.4	12.186
0	-10	95.5	24.258
2	-10	-19.8	6.377
4	-10	37.2	10.762
6	-10	51.5	12.546
8	-10	-56.3	6.782
0	-8	29.6	9.853
2	-8	-31.1	8.901
4	-8	28.7	13.498
6	-8	44.2	9.158
8	-8	-48.0	7.247
0	-6	62.4	27.921
2	-6	-83.6	10.632
4	-6	28.9	8.425
6	-6	90.1	22.616

Lat ϕ (deg)	Long λ (deg)	N(m)	ρ (g/cm³)
0	-4	-72.5	14.667
2	-4	25.0	9.403
4	-4	37.2	13.578
6	-4	89.7	-10.803
8	-4	-30.8	4.576
0	-2	11.4	13.524
2	-2	-99.7	7.045
4	-2	50.5	16.461
6	-2	-41.3	9.214
8	-2	79.6	21.566
0	0	10.1	6.842
2	0	-58.7	8.906
4	0	-13.2	7.457
6	0	22.5	11.894
8	0	-43.9	9.709
0	2	90.6	24.104
2	2	57.4	12.385
4	2	-47.8	6.729
6	2	58.0	13.641
8	2	12.3	9.532
0	4	65.9	18.845
2	4	-28.1	6.578
4	4	44.6	14.273
6	4	-34.7	9.284
8	4	63.9	6.062
0	6	76.2	15.688
2	6	52.8	13.449
4	6	32.3	9.759
6	6	103.9	23.264
8	6	-31.7	8.229
0	-10	-14.0	4.831
2	-10	58.5	19.537

Lat ϕ (deg)	Long λ (deg)	N(m)	ρ (g/cm³)
6	-10	14.6	8.429
8	-10	23.8	12.454
0	-8	85.1	14.968
2	-8	-48.4	6.884
4	-8	62.3	9.854
6	-8	95.7	17.255
8	-8	-29.5	6.508
0	-6	71.6	13.994
2	-6	61.9	10.245
4	-6	93.2	12.894
6	-6	15.8	8.142
8	-6	-49.9	9.224
0	-4	36.4	3.928
2	-4	83.6	12.766
4	-4	126.3	19.123
6	-4	37.2	9.451
8	-4	-30.9	6.992
0	-2	-53.5	12.191
2	-2	19.7	6.789
4	-2	46.8	11.167
6	-2	-51.6	7.388
8	-2	82.2	16.054
0	0	64.1	12.171
2	0	-16.5	7.584
4	0	118.3	18.605
6	0	-80.9	6.932
8	0	33.7	11.478
0	2	17.4	9.019
2	2	59.2	13.615
4	2	-97.8	8.867
6	2	-39.6	6.193
8	2	69.1	12.532

Lat ϕ (deg)	Long λ (deg)	N(m)	ρ (g/cm³)
2	4	-55.9	6.227
4	4	81.6	15.715
6	4	37.0	8.293
8	4	61.3	10.376
0	6	31.8	7.203
2	6	-18.4	5.079
4	6	25.0	7.869
6	6	-44.2	3.496
8	6	70.7	21.817
0	-10	38.5	9.534
2	-10	-43.6	5.506
4	-10	89.4	14.223
6	-10	-13.3	5.135
8	-10	72.1	9.878
0	-8	45.7	3.269
2	-8	-31.0	6.781
4	-8	17.5	8.975
6	-8	56.5	11.942
8	-8	93.9	23.968
0	-6	-24.3	7.716
2	-6	48.7	9.263
4	-6	22.2	6.236
6	-6	70.6	15.277
8	-6	-67.9	7.239
0	-4	99.4	14.977
2	-4	51.1	12.551
4	-4	-32.8	6.536
6	-4	-84.5	8.843
8	-4	29.3	9.326
0	-2	16.7	5.529
2	-2	33.0	10.384
4	-2	-66.4	7.606

Lat ϕ (deg)	Long λ (deg)	N(m)	ρ (g/cm³)
8	-2	-51.2	7.915
0	0	122.8	8.697
2	0	73.9	13.393
4	0	47.6	9.688
6	0	-38.0	8.614
8	0	-22.5	6.895
0	2	60.1	12.677
2	2	49.7	9.785
4	2	-31.4	7.576
6	2	83.2	22.954
8	2	-26.9	7.429
0	4	16.3	9.036
2	4	39.6	11.962
4	4	-37.5	6.966
6	4	55.3	17.732
8	4	-44.8	8.276
0	6	71.0	6.813
2	6	122.5	14.145
4	6	-18.7	9.488
6	6	31.2	8.404
8	6	50.6	12.061
0	-10	-32.9	10.023
2	-10	23.4	6.529
4	-10	97.1	12.776
6	-10	-56.3	7.021
8	-10	-45.2	5.594
0	-8	101.8	8.635
2	-8	60.5	13.241
4	-8	98.4	18.838
6	-8	52.6	9.206
8	-8	-22.1	5.048
0	-6	71.6	23.491

Lat ϕ (deg)	Long λ (deg)	N(m)	ρ (g/cm³)
4	-6	-50.9	6.627
6	-6	26.4	9.761
8	-6	66.7	12.641
0	-4	-19.3	6.618
2	-4	-86.5	7.767
4	-4	39.2	11.731
6	-4	65.0	19.787
8	-4	-41.9	6.325
0	-2	38.3	8.361
2	-2	54.7	12.956
4	-2	-16.1	7.614
6	-2	36.5	11.816
8	-2	-24.4	5.919
0	0	-11.6	7.345
2	0	100.3	29.402
4	0	-83.9	8.478
6	0	-28.7	2.074
8	0	-52.1	3.379
0	2	37.4	4.648
2	2	92.5	5.337
4	2	20.2	5.506
6	2	66.8	5.119
8	2	-43.6	12.212
0	4	17.3	5.545
2	4	-80.9	6.644
4	4	69.5	10.042
6	4	81.4	8.003
8	4	-25.7	7.093
0	6	74.9	16.365
2	6	56.3	12.136
4	6	85.0	9.492
6	6	-57.6	7.194

Table B5: Density distribution across the West African Region

Countries	Capital	Lat ϕ (deg)	Long λ (deg)	Density Range(g/cm^3)
Rep of Benin	Porto-Novo	06^o 23$^{'}$N	02^o 42$^{'}$E	8.491 – 25.947
Burkina Faso	Ouagadougou	12^o 15'N	01^o 30'W	13.165 - 31.863
Cameroon	Yaounde	03^o 50'N	11^o 35'E	9.824 – 23.215
Cape Verde	Praia	15^o 02'N	23^o 34'W	7.303 – 27.694
Cote d'Ivoire	Yamoussoukro	06^o 49'N	05^o 17'W	10.546 – 30.179
Gambia	Banjul	13^o 28'N	16^o 40$^{'}$W	12.722 – 29.632
Ghana	Accra	05^o 35'N	00^o 06'W	11.689 – 28.051
Guinea	Conakry	09^o 29'N	13^o 49'W	9.286 – 25.836
Guinea-Bissau	Bissau	11^o 45'N	15^o 45'W	14.597 – 33.758
Liberia	Monrovia	06^o 18'N	10^o 47'W	9.094 – 27.643
Mali	Bamako	12^o 34'N	07^o 55'W	11.753 – 29.526
Mauritania	Nouakchott	20^o 10'S	57^o 30'E	8.216 – 31.945
Niger	Niamey	13^o 27'N	02^o 06'E	12.937 – 28.101

Table B5 continued

Countries	Capital	Lat ϕ (deg)	Long λ (deg)	Density Range(g/cm^3)
Nigeria	Abuja	09^o 05'N	07^o 32'E	9.868 – 33.264
Senegal	Dakar	14^o 34'N	17^o 29'W	10.524 – 26.752
Sierra Leone	Freetown	08^o 30'N	13^o 17'W	7.203 – 30.563
Togo	Lome	06^o 21'N	04^o 23'W	8.317 – 25.49

Table B6: Density data of Itakpe (continental) region computed from model and compared with the observed and satellite values

Latitude ϕ(deg)	Longitude λ(deg)	Gravity data (Gals)	Depth Z (km)	Density(Observed) (kg/m³)	Density(Model) (kg/m³)	Density(satellite) (kg/m³)
6.023	5.057	980.235	15.708	3096.21	2944.94	3062.85
6.025	5.084	980.146	06.527	2705.33	3122.87	2935.96
6.028	5.093	980.378	11.269	2944.94	2683.61	7284.44
6.031	5.116	979.874	20.514	3122.87	4785.39	5573.29
6.033	5.132	979.672	09.728	2683.61	3371.74	2628.59
6.036	5.158	977.551	14.052	6785.39	2862.52	3179.72
6.039	5.179	978.265	18.231	3371.74	6410.78	4603.38
6.042	5.191	977.536	22.443	2862.52	3647.49	2988.94
6.045	5.206	978.612	10.725	4410.78	4657.82	3251.03
6.047	5.227	980.023	08.526	3647.49	2811.56	4104.67
6.049	5.249	977.836	11.038	2657.82	3259.37	5694.95
6.051	5.265	977.725	17.186	2811.56	2973.63	3218.49
6.052	5.282	978.964	26.249	3259.37	5168.41	2775.36
6.054	5.314	979.428	12.395	2973.63	3582.96	6026.13
6.056	5.336	977.869	06.889	5168.41	2736.45	3592.84
6.058	5.359	978.231	16.374	3582.96	3467.38	4001.38
6.061	5.371	980.264	13.216	4736.45	2805.12	5972.51
6.063	5.395	977.795	25.922	3467.38	6640.78	3726.37
6.065	5.412	979.382	14.036	2805.12	3062.85	2854.25
6.067	5.437	980.507	09.458	3640.78	2935.96	4166.63
6.069	5.456	977.956	20.025	5062.85	5284.44	4482.48
6.072	5.474	979.218	37.183	2935.96	3573.29	3515.12
6.073	5.499	979.364	25.835	3284.44	2628.59	2964.39
6.076	5.513	978.553	12.472	3573.29	3179.72	3628.48
6.078	5.537	978.532	28.994	2628.59	3603.38	4165.74
6.080	5.552	977.836	15.101	3179.72	2988.94	3987.67

Table B6 (continued)

Latitude ϕ(deg)	Longitude λ(deg)	Gravity data (Gals)	Depth Z (km)	Density(Observed) (kg/m³)	Density(Model) (kg/m³)	Density(satellite) (kg/m³)
6.085	5.595	980.314	19.485	2988.94	4104.67	2592.36
6.087	5.604	977.869	22.846	3251.03	3694.95	3386.56
6.089	5.623	977.765	17.029	4104.67	3218.49	3857.28
6.091	5.641	977.901	30.812	3694.95	2775.36	3154.95
6.093	5.658	978.256	24.337	3218.49	3026.13	2944.43
6.095	5.673	978.339	09.528	2775.36	3592.84	3175.49
6.098	5.687	977.564	21.832	3026.13	4001.38	4823.84
6.102	5.705	977.805	13.694	3592.84	3972.51	3566.21
6.104	5.722	977.278	22.659	4001.38	3726.37	4234.55
6.106	5.745	977.693	14.385	3972.51	2854.25	3712.43
6.108	5.763	978.658	32.127	3726.37	3166.63	2987.68
6.112	5.785	978.692	26.836	2854.25	3482.48	4035.17
6.115	5.794	978.912	15.319	3166.63	3515.12	3298.54
6.117	5.815	977.786	23.044	3482.48	2964.39	3434.62
6.119	5.839	977.895	11.128	3515.12	3628.48	4185.93
6.122	5.858	978.863	29.529	2964.39	4165.74	3976.28
6.124	5.882	978.642	35.715	3628.48	3987.67	2765.35
6.127	5.907	979.216	38.426	4165.74	4423.15	3147.02
6.129	5.929	979.538	40.653	3987.67	2592.36	3652.54
6.131	5.954	980.249	46.197	4423.15	3386.56	4396.45
6.135	5.983	980.314	32.622	2592.36	3857.28	4672.92
6.138	6.016	979.855	37.014	3386.56	3154.95	3166.53
6.141	6.039	979.689	50.331	3857.28	2944.43	3839.84
6.142	6.063	979.462	22.769	3154.95	3583.02	4527.67
6.145	6.094	977.628	36.253	2944.43	2746.56	4953.59
6.147	6.113	977.604	38.984	3583.02	3423.79	3508.26
6.149	6.139	977.786	35.152	2746.56	2706.35	4219.81

Table B6 (continued)

Latitude ϕ(deg)	Longitude λ(deg)	Gravity data (Gals)	Dept Z (km)	Density (Observed) (kg/m³)	Density (Model) (kg/m³)	Density (satellite) (kg/m³)
6.157	6.204	979.473	42.032	3188.69	2876.38	2863.94
6.161	6.231	977.784	48.578	3621.57	3492.94	3482.13
6.163	6.259	978.342	39.184	2876.38	3900.26	3753.69
6.165	6.288	978.659	30.622	3492.94	4172.27	4218.85
6.167	6.302	978.812	25.679	3900.26	3485.66	4627.93
6.169	6.325	977.623	22.591	4172.27	2954.31	2984.52
6.171	6.335	977.816	28.586	3485.66	3253.75	3796.19
6.173	6.378	977.695	26.452	2954.31	2634.69	3243.78
6.176	6.391	980.347	39.624	3253.75	3352.93	3500.26
6.178	6.412	980.259	35.453	2634.69	4503.86	2716.29
6.182	6.436	979.624	37.794	3352.93	3857.24	4185.83
6.184	6.462	978.392	31.342	4503.86	4139.18	4428.57
6.186	6.489	977.739	45.926	3857.24	4611.63	4916.39
6.189	6.508	979.261	42.024	4139.18	3694.27	4645.21
6.193	6.526	979.856	40.159	4611.63	3175.49	5187.46
6.195	6.557	979.363	49.835	3694.27	4823.84	4522.53
6.197	6.582	979.405	35.547	3175.49	3566.21	4853.08
6.201	6.611	980.102	31.154	4823.84	4234.55	3364.96
6.203	6.633	980.273	35.567	3566.21	3712.43	5076.82
6.207	6.659	980.269	39.078	4234.55	2987.68	5417.34
6.209	6.681	977.736	25.618	3712.43	4035.17	4692.15
6.212	6.702	977.892	20.965	2987.68	3298.54	4724.86
6.218	6.753	980.372	21.012	3298.54	4185.93	4293.58
6.221	6.776	980.416	32.034	3434.62	3976.28	4475.36
6.224	6.794	977.389	29.245	4185.93	2765.35	3622.49
6.227	6.813	980.235	27.095	3976.28	3147.02	3915.73
6.231	6.837	980.146	30.237	2765.35	3652.54	4326.07
6.234	6.863	980.378	24.047	3147.02	4396.45	5515.45
6.236	6.889	979.874	26.753	3652.54	4672.92	5169.38

Table B6 (continued)

Latitude ϕ(deg)	Longitude λ(deg)	Gravity data (Gals)	Depth Z (km)	Density(Observed) (kg/m³)	Density(Model) (kg/m³)	Density(satellite) (kg/m³)
6.245	6.941	978.265	40.012	3166.53	4527.67	2683.75
6.247	6.973	977.536	43.184	3839.84	4953.59	4294.82
6.251	6.992	978.612	45.816	4527.67	3508.26	4937.15
6.253	7.031	980.023	47.091	4953.59	4219.81	5376.63
6.255	7.053	977.836	32.132	3508.26	4036.37	6123.46
6.258	7.084	977.725	34.098	4219.81	3925.05	4758.32
6.261	7.105	978.964	36.951	4036.37	2863.94	4682.65
6.264	7.126	979.428	37.304	3925.05	3482.13	5038.29
6.267	7.148	977.869	31.945	2863.94	3753.69	4647.81
6.269	7.184	978.231	30.187	3482.13	4218.85	3829.34
6.271	7.216	980.264	22.904	3753.69	4627.93	4103.66
6.283	7.281	980.507	17.984	2984.52	3243.78	3914.65
6.285	7.321	977.956	14.278	3796.19	3500.26	4172.23
6.289	7.349	979.218	19.824	3243.78	2716.29	3528.46
6.294	7.366	979.364	25.321	3500.26	4185.83	3837.59
6.297	7.389	978.553	27.854	2716.29	4428.57	3915.07
6.301	7.412	978.532	29.152	4185.83	4916.39	2799.63
6.305	7.435	977.836	34.159	4428.57	4645.21	3424.51
6.308	7.458	980.223	39.543	4916.39	5187.46	3164.85
6.311	7.479	980.314	27.895	4645.21	4522.53	4238.36
6.314	7.493	977.869	14.901	5187.46	4853.08	4594.75
6.317	7.516	977.765	17.267	4522.53	3364.96	4984.48
6.319	7.525	977.901	29.953	4853.08	5076.82	5207.53
6.324	7.548	978.256	22.095	3364.96	5417.34	5033.62
6.326	7.569	978.339	20.784	5076.82	4692.15	4724.86
6.328	7.572	977.564	34.946	5417.34	4724.86	4325.31
6.331	7.593	977.805	32.056	4692.15	3856.24	3682.59
6.334	7.608	977.278	33.095	4724.86	4293.58	3897.44

Table B6 (continued)

Latitude ϕ(deg)	Longitude λ(deg)	Gravity data (Gals)	Depth Z (km)	Density(Observed) (kg/m³)	Density(Model) (kg/m³)	Density(satellite) (kg/m³)
6.345	7.661	978.692	24.315	4475.36	3915.73	5923.72
6.347	7.678	978.912	26.815	3622.49	4326.07	4219.38
6.349	7.696	977.786	22.675	3915.73	5515.45	6234.74
6.352	7.713	977.895	45.987	4326.07	5169.38	6015.96
6.355	7.734	978.863	41.658	5515.45	4824.67	6732.25
6.358	7.751	978.642	39.374	5169.38	3191.25	6483.48
6.361	7.772	979.216	50.423	4824.67	2683.75	7235.03
6.363	7.785	979.538	45.557	3191.25	4294.82	6922.52
6.365	7.803	980.249	23.768	2683.75	4937.15	6316.27
6.377	7.882	979.462	34.908	6123.46	4682.65	4638.91
6.378	7.901	977.628	31.895	4758.32	5038.29	5527.46
6.382	7.916	977.604	23.987	4682.65	4647.81	6493.72
6.384	7.937	977.786	19.876	5038.29	3829.34	6725.81
6.385	7.959	979.392	26.475	4647.81	4103.66	6239.95
6.388	7.973	979.511	29.812	3829.34	4497.85	7006.32
6.394	7.992	979.473	34.813	4103.66	4735.29	7324.94
6.398	8.034	977.784	42.971	4497.85	3914.65	7682.56
6.405	8.067	978.342	24.781	4735.29	4172.23	5254.82
6.409	8.089	978.659	26.658	3914.65	3528.46	5735.41
6.413	8.117	978.812	21.563	4172.23	3837.59	4693.28
6.417	8.135	977.623	39.971	3528.46	3915.07	6053.47
6.422	8.159	977.816	22.981	3837.59	2799.63	6386.95
6.425	8.183	977.695	31.875	3915.07	3424.51	5625.29
6.428	8.201	980.347	27.654	2799.63	3164.85	5184.36
6.434	8.234	980.259	14.986	3424.51	4238.36	5739.12
6.436	8.254	979.624	23.103	3164.85	4594.75	5982.53
6.439	8.279	978.392	28.143	4238.36	5917.28	7495.27

Table B6 (continued)

Latitude ϕ(deg)	Longitude λ(deg)	Gravity data (Gals)	Depth Z (km)	Density(Observed) (kg/m³)	Density(Model) (kg/m³)	Density(satellite) (kg/m³)
6.451	8.331	979.856	34.987	5207.53	4969.53	8526.85
6.456	8.358	979.363	28.234	5033.62	5255.02	8793.64
6.459	8.377	979.405	20.122	4724.86	5621.49	8425.93
6.462	8.392	980.102	34.987	4325.31	6101.35	8206.71
6.466	8.421	980.273	29.096	3682.59	4682.67	8052.26
6.469	8.461	980.269	24.158	3897.44	4926.34	7635.49
6.474	8.489	977.736	18.452	4326.23	3964.31	7286.18
6.479	8.502	977.892	44.756	5710.65	5104.94	7846.53
6.486	8.532	980.264	31.908	5923.72	5827.52	7154.39
6.505	8.629	978.642	24.986	6732.25	3847.63	6452.65
6.509	8.662	979.216	35.824	6483.48	4234.99	6693.47
6.514	8.693	979.538	28.734	7235.03	4618.02	8179.26
6.517	8.703	980.249	46.839	6922.52	5262.34	8452.33
6.521	8.725	980.314	38.082	6316.27	6004.53	7928.54
6.524	8.758	979.855	20.345	6289.53	5462.55	7316.28
6.528	8.774	979.689	12.893	5814.39	2736.45	7694.83
6.535	8.791	979.462	29.084	5276.22	3467.38	7024.62
6.556	8.893	979.392	41.032	6725.81	2935.96	8524.67
6.559	8.922	979.511	37.234	6239.95	3284.44	9485.34
6.564	8.945	979.473	26.653	7006.32	3573.29	10653.86
6.568	8.961	977.784	14.987	7324.94	2628.59	10924.55
6.571	8.988	978.342	37.092	7682.56	3179.72	10728.45
6.575	8.995	978.659	29.875	5254.82	3603.38	8251.69
6.579	9.026	978.812	31.126	5735.41	2988.94	9034.73

Table B6 (continued)

ϕ(deg)	Longitude λ(deg)	Latitude (Gals)	Depth Z (km)	Density(Observed) (kg/m³)	Density(Model) (kg/m³)	Density(satellite) (kg/m³)
6.588	9.097	977.695	39.623	6386.95	3694.95	7955.19
6.592	9.116	980.347	22.483	5625.29	3218.49	8052.64
6.596	9.138	980.259	34.832	5184.36	2775.36	8379.52
6.612	9.203	979.261	29.983	7926.15	3972.51	7649.33
6.615	9.214	979.856	50.734	8364.42	3726.37	6893.78
6.618	9.237	979.363	23.892	8526.85	2854.25	6126.42
6.624	9.263	979.405	18.984	8793.64	3166.63	5947.32
6.629	9.284	980.102	27.846	8425.93	3482.48	5201.56
6.635	9.302	980.273	31.109	8206.71	3515.12	5683.33
6.638	9.334	980.269	45.874	8052.26	2964.39	6225.79
6.646	9.359	977.736	24.982	7635.49	3628.48	6138.17
6.671	9.375	977.892	38.834	7286.18	4165.74	7246.92
6.676	9.394	980.264	17.983	7846.53	3987.67	7785.83
6.679	9.417	980.372	50.872	7154.39	4423.15	4398.66
6.683	9.435	980.416	43.453	6822.76	2592.36	3895.25
6.688	9.462	977.389	37.243	6209.42	3386.56	5214.03
6.694	9.488	980.235	28.342	5973.81	3857.28	6117.38
6.701	9.503	980.146	19.784	6452.65	3154.95	3096.21
6.703	9.514	980.378	23.984	6693.47	2944.43	3215.76
6.707	9.536	979.874	48.904	8179.26	3583.02	4724.86
6.711	9.557	979.672	28.234	8452.33	2746.56	3856.24
6.714	9.571	977.551	12.848	7928.54	3423.79	4293.58
6.716	9.593	978.265	45.976	7316.28	2706.35	4475.36
6.719	9.614	977.536	32.124	7694.83	3188.69	3622.49
6.726	9.639	978.612	40.214	7024.62	3621.57	3915.73
6.732	9.652	980.023	50.934	9126.45	2876.38	4326.07
6.739	9.676	977.836	28.134	9367.38	3492.94	5515.45

Table B6 (continued)

Latitude ϕ(deg)	Longitude λ(deg)	Gravity data (Gals)	Depth Z (km)	Density(Observed) (kg/m³)	Density(Model) (kg/m³)	Density(satellite) (kg/m³)
6.756	9.722	979.428	32.154	9485.34	3485.66	3191.25
6.763	9.748	977.869	20.222	10653.86	2954.31	2683.75
6.769	9.761	978.231	29.091	10924.55	3253.75	4294.82
6.774	9.793	980.264	36.756	10728.45	2634.69	4937.15
6.778	9.825	977.795	44.591	8251.69	3352.93	5376.63
6.781	9.853	979.382	40.021	9034.73	4503.86	6123.46
6.786	9.891	980.507	32.321	10138.29	3857.24	4758.32
6.789	9.926	977.956	24.598	7643.26	4139.18	4682.65
6.793	9.957	979.218	16.199	7955.19	4611.63	5038.29
6.797	9.976	979.364	20.846	8052.64	3694.27	4647.81
6.805	9.993	978.553	45.985	8379.52	3175.49	3829.34
6.809	10.046	978.532	24.985	8853.13	4823.84	4103.66
6.816	10.089	977.836	34.983	9106.46	3566.21	4497.85
6.822	10.105	980.223	40.775	9448.51	4234.55	4735.29
6.828	10.137	980.314	23.987	7649.33	3712.43	3914.65
6.837	10.159	977.869	49.984	6893.78	2987.68	4172.23
6.843	10.182	977.765	34.228	6126.42	4035.17	3528.46
6.849	10.199	977.901	21.356	5947.32	3298.54	3837.59
6.857	10.226	978.256	53.865	5201.56	3434.62	3915.07
6.861	10.243	978.339	45.678	5683.33	4185.93	2799.63
6.866	10.278	977.564	30.334	6225.79	3976.28	3424.51
6.889	10.378	978.658	37.895	4398.66	4396.45	5917.28
6.895	10.396	978.692	45.342	3895.25	4672.92	5062.16
6.902	10.411	978.912	55.896	5214.03	3166.53	4733.94
6.909	10.439	977.786	43.975	6117.38	3839.84	4969.53
6.911	10.455	977.895	29.567	3096.21	4527.67	5255.02
6.918	10.473	978.863	40.897	3215.76	4953.59	5621.49

Table B6 (continued)

Latitude ϕ(deg)	Longitude λ(deg)	Gravity data (Gals)	Depth Z (km)	Density(Observed) (kg/m³)	Density(Model) (kg/m³)	Density(satellite) (kg/m³)
6.937	10.526	979.538	16.358	2683.61	4036.37	4926.34
6.945	10.543	980.249	32.069	2785.39	3925.05	3964.31
6.952	10.571	980.314	25.187	3371.74	2863.94	5104.94
6.959	10.596	979.855	16.158	2862.52	3482.13	5827.52
6.968	10.623	979.689	24.975	3410.78	3753.69	6086.48
6.974	10.644	979.462	20.783	3647.49	4218.85	4834.28
6.978	10.676	977.628	38.499	2657.82	4627.93	3769.25
6.983	10.683	977.604	30.458	2811.56	2984.52	3847.63
6.989	10.702	977.786	29.356	3259.37	3796.19	4234.99
6.992	10.735	979.392	11.852	2973.63	3243.78	4618.02
6.995	10.761	979.511	52.631	3168.41	3500.26	5262.34
7.011	10.846	978.659	27.725	2805.12	4916.39	2935.96
7.023	10.858	978.812	15.583	3640.78	4645.21	3284.44
7.032	10.871	977.623	28.419	3062.85	5187.46	3573.29
7.046	10.894	977.816	31.162	2935.96	4522.53	2628.59
7.055	10.911	977.695	26.425	3284.44	4853.08	3179.72
7.064	10.936	980.347	17.656	3573.29	3364.96	3603.38
7.073	10.955	980.259	23.104	2628.59	5076.82	2988.94
7.085	10.978	979.624	39.572	3179.72	5417.34	3251.03
7.092	10.998	978.392	49.835	3603.38	4692.15	4104.67
7.107	11.023	977.739	51.739	2988.94	4724.86	3694.95
7.114	11.057	979.261	42.847	3251.03	3856.24	3218.49
7.119	11.089	979.856	33.621	4104.67	4293.58	2775.36
7.126	11.111	979.363	28.146	3694.95	4475.36	3026.13
7.135	11.147	979.405	46.837	3218.49	3622.49	3592.84
7.141	11.172	980.102	22.554	2775.36	3915.73	4001.38
7.153	11.195	980.273	19.832	3026.13	4326.07	3972.51

Table B6 (continued)

Latitude ϕ(deg)	Longitude λ(deg)	Gravity data (Gals)	Depth Z (km)	Density(Observed) (kg/m³)	Density(Model) (kg/m³)	Density(satellite) (kg/m³)
7.183	11.251	977.892	16.374	3647.49	4824.67	3166.63
7.191	11.274	980.264	13.216	2657.82	3191.25	3482.48
7.206	11.296	980.372	25.922	2811.56	2683.75	3515.12
7.215	11.322	980.416	14.036	3259.37	4294.82	2964.39
7.228	11.358	977.389	9.458	2973.63	4937.15	3628.48
7.239	11.377	979.462	20.025	3168.41	5376.63	4165.74
7.247	11.394	977.628	37.183	3582.96	6123.46	3987.67
7.255	11.413	977.604	25.835	2736.45	4758.32	4423.15
7.264	11.437	977.786	12.472	3467.38	4682.65	2592.36
7.271	11.458	979.392	28.994	2805.12	5038.29	3386.56
7.283	11.474	979.511	15.101	3640.78	4647.81	3857.28
7.296	11.492	979.473	26.673	3062.85	3829.34	3154.95
7.305	11.518	977.784	19.485	2935.96	4103.66	2944.43
7.314	11.533	978.342	22.846	3284.44	4497.85	3175.49
7.342	11.601	977.816	9.528	3603.38	3528.46	3712.43
7.354	11.622	977.695	21.832	2988.94	3837.59	2987.68
7.360	11.647	980.347	13.694	3251.03	3915.07	4035.17
7.367	11.665	980.259	22.659	4104.67	2799.63	3298.54
7.375	11.695	979.624	14.385	3694.95	3424.51	3434.62
7.383	11.726	978.392	32.127	3218.49	3164.85	4185.93
7.391	11.741	977.739	26.836	2775.36	4238.36	3976.28
7.402	11.763	979.261	15.319	3026.13	4594.75	2765.35
7.414	11.788	979.856	23.044	3592.84	5917.28	3147.02
7.426	11.804	979.363	11.128	4001.38	5062.16	3652.54
7.435	11.829	979.405	29.529	3972.51	4733.94	4396.45
7.449	11.843	980.102	35.715	3726.37	4969.53	4672.92
7.453	11.861	980.273	38.426	2854.25	5255.02	3166.53

Table B6 (continued)

Latitude ϕ(deg)	Longitude λ(deg)	Gravity data (Gals)	Depth Z (km)	Density(Observed) (kg/m³)	Density(Model) (kg/m³)	Density(satellite) (kg/m³)
7.486	11.929	977.892	32.622	3515.12	4682.67	4953.59
7.497	11.957	980.264	37.014	2964.39	4926.34	3508.26
7.503	11.981	980.372	50.331	3628.48	3964.31	4219.81
7.519	12.003	980.416	22.769	4165.74	5104.94	4036.37
7.524	12.034	977.389	36.253	3987.67	5827.52	3925.05
7.535	12.056	978.642	38.984	4423.15	6086.48	2863.94
7.541	12.088	979.216	35.152	2592.36	4834.28	3482.13
7.553	12.096	979.538	30.284	3386.56	3769.25	3753.69
7.567	12.135	980.249	27.995	3857.28	3847.63	4218.85
7.574	12.162	980.314	42.032	3154.95	4234.99	4627.93
7.585	12.189	979.855	48.578	2944.43	4618.02	2984.52
7.592	12.212	979.689	39.184	3583.02	5262.34	3796.19
7.603	12.243	979.462	30.622	2746.56	6004.53	3243.78
7.617	12.268	977.628	25.679	3423.79	5462.55	3500.26
7.628	12.283	977.604	22.591	2706.35	2746.56	2716.29
7.696	12.386	979.473	35.453	3492.94	3621.57	4645.21
7.715	12.412	977.784	37.794	3900.26	2876.38	5187.46
7.749	12.432	978.342	31.342	4172.27	3492.94	4522.53
7.762	12.456	978.659	45.926	3485.66	3900.26	4853.08
7.781	12.478	978.812	42.024	2954.31	4172.27	3364.96
7.803	12.491	977.623	40.159	3253.75	3485.66	5076.82
7.822	12.522	977.816	49.835	2634.69	2954.31	5417.34
7.859	12.548	977.695	35.547	3352.93	3253.75	4692.15
7.874	12.567	980.347	31.154	4503.86	2634.69	4724.86
7.895	12.591	980.259	35.567	3857.24	3352.93	3856.24
7.913	12.621	979.624	39.078	4139.18	4503.86	4293.58
7.936	12.643	978.392	25.618	4611.63	3857.24	4475.36

Table B6 (continued)

Latitude ϕ(deg)	Longitude λ(deg)	Gravity data (Gals)	Depth Z (km)	Density(Observed) (kg/m³)	Density(Model) (kg/m³)	Density(satellite) (kg/m³)
7.993	12.712	979.856	21.012	4823.84	3694.27	4326.07
8.037	12.736	979.363	32.034	3566.21	3175.49	5515.45
8.068	12.758	979.405	29.245	4234.55	4823.84	5169.38
8.092	12.781	980.102	27.095	3712.43	3566.21	4824.67
8.115	12.815	980.273	30.237	2987.68	4234.55	3191.25
8.149	12.838	980.269	24.047	4035.17	3712.43	2683.75
8.164	12.859	977.736	26.753	3298.54	2987.68	4294.82
8.198	12.873	977.892	21.958	3434.62	4035.17	4937.15
8.213	12.891	980.264	32.147	4185.93	3298.54	5376.63
8.245	12.926	980.372	40.012	3976.28	3434.62	6123.46
8.267	12.947	980.416	43.184	2765.35	4185.93	4758.32
8.288	12.962	977.389	45.816	3147.02	3976.28	4682.65
8.323	12.985	980.235	47.091	3652.54	2765.35	5038.29
8.359	12.993	980.146	32.132	4396.45	3147.02	4647.81
8.371	13.016	980.378	34.098	4672.92	3652.54	3829.34
8.395	13.045	979.874	36.951	3166.53	4396.45	4103.66

Table B7: A table of Longitude, Latitude and the Satellite derived parameters J_{nm} and K_{nm}

longitude(x)	latitude(y)	Jnm	Knm
		-	
-30	3	0.0004842	0.00E+00
-29.875	3.0333	-2.52E-10	1.46E-09
-29.75	3.0667	2.44E-06	-1.40E-06
-29.625	3.1	9.57E-07	0.00E+00
-29.5	3.1333	2.03E-06	2.48E-07
-29.375	3.1667	9.05E-07	-6.19E-07
-29.25	3.2	7.21E-07	1.41E-06
-29.125	3.2333	5.40E-07	0.00E+00
-29	3.2667	-5.36E-07	-4.74E-07
-28.875	3.3	3.50E-07	6.62E-07
-28.75	3.3333	9.91E-07	-2.01E-07
-28.625	3.3667	-1.88E-07	3.09E-07
-28.5	3.4	6.87E-08	0.00E+00
-28.375	3.4333	-6.29E-08	-9.44E-08
-28.25	3.4667	6.52E-07	-3.23E-07
-28.125	3.5	-4.52E-07	-2.15E-07
-28	3.5333	-2.95E-07	4.98E-08
-27.875	3.5667	1.75E-07	-6.69E-07
-27.75	3.6	-1.50E-07	0.00E+00
-27.625	3.6333	-7.59E-08	2.65E-08
-27.5	3.6667	4.86E-08	-3.74E-07
-27.375	3.7	5.72E-08	8.94E-09
-27.25	3.7333	-8.60E-08	-4.71E-07
-27.125	3.7667	-2.67E-07	-5.36E-07
-27	3.8	9.47E-09	-2.37E-07
-26.875	3.8333	9.05E-08	0.00E+00
-26.75	3.8667	2.81E-07	9.51E-08
-26.625	3.9	3.30E-07	9.30E-08
-26.5	3.9333	2.50E-07	-2.17E-07
-26.375	3.9667	-2.75E-07	-1.24E-07

Table B7 continued

longitude(x)	latitude(y)	Jnm	Knm
-26.25	4	1.66E-09	1.79E-08
-26.125	4.0333	-3.59E-07	1.52E-07
-26	4.0667	1.52E-09	2.41E-08
-25.875	4.1	4.95E-08	0.00E+00
-25.75	4.1333	2.32E-08	5.89E-08
-25.625	4.1667	8.00E-08	6.53E-08
-25.5	4.2	-1.94E-08	-8.60E-08
-25.375	4.2333	-2.44E-07	6.98E-08
-25.25	4.2667	-2.57E-08	8.92E-08
-25.125	4.3	-6.60E-08	3.09E-07
-25	4.3333	6.73E-08	7.49E-08
-24.875	4.3667	-1.24E-07	1.21E-07
-24.75	4.4	2.80E-08	0.00E+00
-24.625	4.4333	1.42E-07	2.14E-08
-24.5	4.4667	2.14E-08	-3.17E-08
-24.375	4.5	-1.61E-07	-7.43E-08
-24.25	4.5333	-9.37E-09	1.99E-08
-24.125	4.5667	-1.63E-08	-5.40E-08
-24	4.6	6.28E-08	2.23E-07
-23.875	4.6333	-1.18E-07	-9.69E-08
-23.75	4.6667	1.88E-07	-2.99E-09
-23.625	4.7	-4.76E-08	9.69E-08
-23.5	4.7333	5.33E-08	0.00E+00
-23.375	4.7667	8.38E-08	-1.31E-07
-23.25	4.8	-9.40E-08	-5.13E-08
-23.125	4.8333	-7.02E-09	-1.54E-07
-23	4.8667	-8.45E-08	-7.90E-08
-22.875	4.9	-4.93E-08	-5.06E-08
-22.75	4.9333	-3.76E-08	-7.98E-08
-22.625	4.9667	8.26E-09	-3.05E-09

Table B7 continued

longitude(x)	latitude(y)	Jnm	Knm
-22.25	5.0667	1.00E-07	-2.39E-08
-22.125	5.1	-5.08E-08	0.00E+00
-22	5.1333	1.56E-08	-2.71E-08
-21.875	5.1667	2.01E-08	-9.90E-08
-21.75	5.2	-3.06E-08	-1.49E-07
-21.625	5.2333	-3.80E-08	-6.38E-08
-21.5	5.2667	3.74E-08	4.96E-08
-21.375	5.3	-1.56E-09	3.43E-08
-21.25	5.3333	4.66E-09	-8.98E-08
-21.125	5.3667	-6.30E-09	2.45E-08
-21	5.4	-3.11E-08	4.21E-08
-20.875	5.4333	-5.22E-08	-1.84E-08
-20.75	5.4667	4.62E-08	-6.97E-08
-20.625	5.5	3.64E-08	0.00E+00
-20.5	5.5333	-5.36E-08	-4.32E-08
-20.375	5.5667	1.43E-08	3.11E-08
-20.25	5.6	3.96E-08	2.51E-08
-20.125	5.6333	-6.77E-08	3.84E-09
-20	5.6667	3.09E-08	7.60E-09
-19.875	5.7	3.13E-09	3.90E-08
-19.75	5.7333	-1.90E-08	3.57E-08
-19.625	5.7667	-2.59E-08	1.69E-08
-19.5	5.8	4.19E-08	2.50E-08
-19.375	5.8333	-6.20E-09	3.09E-08
-19.25	5.8667	1.14E-08	-6.39E-09
-19.125	5.9	-2.43E-09	-1.11E-08
-19	5.9333	4.17E-08	0.00E+00
-18.875	5.9667	-5.14E-08	3.87E-08
-18.75	6	5.53E-08	-6.27E-08
-18.625	6.0333	-2.16E-08	9.77E-08

Table B7 continued

longitude(x)	latitude(y)	Jnm	Knm
-18.5	6.0667	-3.65E-09	-1.18E-08
-18.375	6.1	5.84E-08	6.72E-08
-18.25	6.1333	-3.50E-08	-6.27E-09
-18.125	6.1667	3.02E-09	-7.32E-09
-18	6.2	-1.01E-08	-9.86E-09
-17.875	6.2333	2.48E-08	4.59E-08
-17.75	6.2667	4.11E-08	-3.68E-08
-17.625	6.3	-4.45E-08	-4.84E-09
-17.5	6.3333	-3.13E-08	8.79E-08
-17.375	6.3667	-6.12E-08	6.81E-08
-17.25	6.4	-2.27E-08	0.00E+00
-17.125	6.4333	-1.88E-08	2.89E-08
-17	6.4667	-3.59E-08	-4.05E-09
-16.875	6.5	3.65E-08	1.97E-08
-16.75	6.5333	1.60E-09	-2.27E-08
-16.625	6.5667	2.93E-08	-1.68E-08
-16.5	6.6	-1.91E-08	2.46E-09
-16.375	6.6333	3.76E-08	-3.93E-09
-16.25	6.6667	-3.49E-08	-1.54E-08
-16.125	6.7	3.20E-08	2.85E-08
-16	6.7333	3.88E-08	-1.29E-09
-15.875	6.7667	1.56E-08	-3.90E-08
-15.75	6.8	8.46E-09	-3.11E-08
-15.625	6.8333	3.22E-08	4.51E-08
-15.5	6.8667	-5.19E-08	-4.81E-09
-15.375	6.9	2.20E-09	0.00E+00
-15.25	6.9333	9.43E-09	1.05E-08
-15.125	6.9667	-2.05E-08	-3.03E-08
-15	7	5.34E-08	1.77E-08
-14.75	7.0667	1.22E-08	7.62E-09

Table B7 continued

longitude(x)	latitude(y)	Jnm	Knm
-14.625	7.1	3.28E-08	-3.65E-08
-14.5	7.1333	5.97E-08	5.08E-09
-14.375	7.1667	-3.21E-08	2.22E-08
-14.25	7.2	1.33E-08	3.80E-08
-14.125	7.2333	1.03E-08	1.47E-08
-14	7.2667	-1.30E-09	1.85E-08
-13.875	7.3	-3.24E-08	1.56E-08
-13.75	7.3333	-2.84E-08	-4.58E-09
-13.625	7.3667	5.20E-09	-2.44E-08
-13.5	7.4	-1.90E-08	-4.70E-09
-13.375	7.4333	-4.71E-09	0.00E+00
-13.25	7.4667	2.62E-08	3.33E-08
-13.125	7.5	-2.45E-08	2.80E-08
-13	7.5333	-3.39E-08	-2.13E-08
-12.875	7.5667	4.09E-08	4.80E-08
-12.75	7.6	-1.21E-08	-3.44E-09
-12.625	7.6333	1.39E-08	-3.56E-08
-12.5	7.6667	-8.06E-09	-8.65E-09
-12.375	7.7	-2.12E-08	5.41E-09
-12.25	7.7333	-2.24E-08	- 3.97E-08
-12.125	7.7667	-1.18E-08	1.15E-08
-12	7.8	1.91E-08	-3.20E-09
-11.875	7.8333	1.96E-08	6.72E-09
-11.75	7.8667	1.38E-08	1.05E-09
-11.625	7.9	-1.93E-08	-3.86E-08
-11.5	7.9333	-1.44E-08	-3.28E-08
-11.375	7.9667	-3.83E-08	2.97E-09
-11.25	8	1.92E-08	0.00E+00
-11.125	8.0333	-2.54E-08	-3.17E-08
-11	8.0667	-2.01E-08	6.82E-09
-10.875	8.1	6.31E-09	5.08E-09
-10.75	8.1333	6.48E-09	2.53E-08

Table B7 continued

longitude(x)	latitude(y)	Jnm	Knm
-6.75	9.2	2.99E-09	-1.09E-08
-6.625	9.2333	-3.30E-09	0.00E+00
-6.5	9.2667	-8.97E-09	1.19E-09
-6.375	9.3	3.57E-08	-2.37E-09
-6.25	9.3333	-7.56E-09	1.11E-09
-6.125	9.3667	1.58E-08	-8.14E-09
-6	9.4	1.04E-08	2.75E-08
-5.875	9.4333	-4.80E-09	1.88E-08
-5.75	9.4667	5.64E-09	-8.74E-09
-5.625	9.5	2.99E-08	-9.99E-09
-5.5	9.5333	3.29E-09	7.24E-09
-5.375	9.5667	-3.39E-08	-7.58E-09
-5.25	9.6	1.63E-08	1.04E-08
-5.125	9.6334	-2.44E-09	9.46E-09
-5	9.6667	-7.55E-09	-2.85E-08
-4.875	9.7	-4.74E-09	-1.29E-08
-4.75	9.7334	-1.76E-08	-1.41E-08
-4.625	9.7667	-2.17E-08	-7.10E-09
-4.5	9.8	2.88E-08	-1.53E-08
-4.375	9.8334	3.50E-08	-9.69E-09
-4.25	9.8667	-2.71E-09	5.20E-09
-4.125	9.9	2.16E-08	0.00E+00
-4	9.9334	5.57E-09	7.03E-09
-3.875	9.9667	2.03E-08	1.72E-08
-3.75	10	-4.75E-09	3.89E-08
-3.625	10.0334	4.27E-09	-2.26E-08
-3.5	10.0667	-1.01E-08	-8.26E-09
-3.375	10.1	1.22E-08	-4.36E-09
-3.25	10.1334	-2.12E-08	-7.04E-10
-3.125	10.1667	5.10E-09	2.15E-09
-3	10.2	1.72E-08	-7.01E-09
-2.875	10.2334	-3.23E-08	-4.79E-09

Table B7 continued

longitude(x)	latitude(y)	Jnm	Knm
-2.75	10.2667	1.44E-08	-1.92E-08
-2.625	10.3	-6.47E-09	1.81E-08
-2.5	10.3334	2.74E-08	6.76E-09
-2.375	10.3667	1.15E-08	-1.44E-08
-2.25	10.4	-2.58E-08	-8.68E-10
-2.125	10.4334	-1.24E-08	-3.44E-10
-2	10.4667	4.50E-09	-1.37E-08
-1.875	10.5	1.54E-08	-8.83E-10
-1.75	10.5334	-3.03E-09	1.09E-08
-1.5	10.6	6.25E-09	0.00E+00
-1.375	10.6334	-1.62E-08	2.87E-08
-1.25	10.6667	-5.62E-09	4.18E-09
-1.125	10.7	1.91E-08	2.27E-08
-1	10.7334	-5.11E-09	1.90E-08
-0.875	10.7667	2.61E-09	1.10E-09
-0.75	10.8	-1.35E-08	1.57E-11
-0.625	10.8334	-6.61E-09	2.52E-09
-0.5	10.8667	-1.72E-08	2.15E-09
-0.375	10.9	1.59E-08	9.08E-09
-0.25	10.9334	-1.14E-08	-1.14E-09
-0.125	10.9667	6.89E-09	-3.56E-08
0	11	-3.33E-09	1.48E-08
0.125	11.0334	-1.94E-08	1.39E-08
0.25	11.0667	2.03E-08	7.35E-09
0.375	11.1	1.76E-08	1.04E-08
0.5	11.1334	7.48E-09	-6.65E-09
0.75	11.2	2.65E-08	-1.11E-08
0.875	11.2334	-2.72E-08	1.66E-08
1	11.2667	-2.69E-08	1.59E-08
1.125	11.3	8.46E-09	-3.66E-09
1.25	11.3334	-1.08E-08	0.00E+00

Table B7 continued

longitude(x)	latitude(y)	Jnm	Knm
1.375	11.3667	1.57E-08	-3.84E-09
1.5	11.4	-2.65E-08	-1.17E-09
1.625	11.4334	1.13E-08	1.01E-08
1.75	11.4667	-3.62E-09	1.87E-08
1.875	11.5	9.77E-11	-3.20E-10
2	11.5334	1.02E-08	-5.51E-09
2.125	11.5667	1.75E-08	4.75E-09
2.25	11.6	-2.35E-08	3.82E-09
2.375	11.6334	6.68E-09	8.38E-09
2.5	11.6667	5.63E-09	2.24E-08
2.625	11.7	-4.82E-09	-1.76E-08
2.75	11.7334	2.42E-09	-8.21E-09
2.875	11.7667	-1.72E-08	1.95E-08
3	11.8	1.09E-08	8.33E-09
3.125	11.8334	2.58E-08	4.71E-09
3.25	11.8667	1.11E-10	-7.29E-09
3.375	11.9	8.56E-09	-1.46E-08
3.5	11.9334	1.02E-08	-1.62E-08
3.625	11.9667	1.41E-08	-3.36E-09
3.75	12	-1.68E-08	1.96E-08
3.875	12.0334	-2.53E-08	2.40E-08
4	12.0667	-1.01E-08	2.33E-09
4.125	12.1	-2.23E-08	0.00E+00
4.25	12.1334	9.18E-09	1.62E-08
4.375	12.1667	-1.44E-08	-4.58E-09
4.5	12.2001	-2.41E-08	-1.75E-08
4.625	12.2334	-2.39E-08	8.29E-09
4.75	12.2667	-8.84E-10	1.66E-10
4.875	12.3001	-1.19E-08	1.61E-08
5	12.3334	-6.89E-09	-1.91E-09
			1.83E-10
5.125	12.3667	7.36E-09	1.83E-10

Table B7 continued

longitude(x)	latitude(y)	Jnm	Knm
5.25	12.4001	1.82E-09	-1.28E-08
5.375	12.4334	1.69E-08	-2.27E-09
5.5	12.4667	9.23E-09	1.43E-08
5.625	12.5001	1.65E-08	-1.20E-08
5.75	12.5334	-1.16E-08	-5.21E-09
5.875	12.5667	6.96E-09	-1.47E-09
6	12.6001	1.89E-08	-3.59E-09
6.125	12.6334	5.90E-09	1.11E-08
6.25	12.6667	-5.46E-09	-1.29E-08
6.375	12.7001	8.55E-09	-1.48E-08
6.5	12.7334	-5.48E-09	1.07E-08
6.625	12.7667	7.97E-09	-5.45E-09
6.75	12.8001	1.57E-08	1.17E-08
6.875	12.8334	-1.80E-08	4.73E-09
7	12.8667	3.05E-09	-1.20E-08
7.125	12.9001	-7.26E-11	0.00E+00
7.25	12.9334	-2.73E-09	-1.53E-09
7.375	12.9667	9.59E-10	1.52E-08
7.5	13.0001	-4.81E-09	-9.73E-09
7.625	13.0334	5.97E-09	5.09E-09
7.75	13.0667	-7.12E-09	-2.14E-08
7.875	13.1001	3.62E-09	1.36E-09
8	13.1334	-6.07E-09	4.92E-09
8.125	13.1667	1.54E-08	-3.61E-09
8.25	13.2001	-1.16E-08	-1.78E-08
8.375	13.2334	1.10E-08	2.13E-08
8.5	13.2667	1.52E-08	1.78E-08
8.625	13.3001	1.15E-08	-6.18E-09
8.75	13.3334	-3.02E-09	2.93E-09
8.875	13.3667	-2.00E-08	-2.04E-09
9	13.4001	6.36E-09	-1.60E-08
9.125	13.4334	8.45E-09	2.72E-09

Table B7 continued

longitude(x)	latitude(y)	Jnm	Knm
9.25	13.4667	-1.19E-08	-6.44E-09
9.375	13.5001	-3.64E-10	-1.03E-08
9.5	13.5334	-4.44E-09	-8.67E-09
9.625	13.5667	-5.66E-09	8.64E-09
9.75	13.6001	5.54E-09	1.41E-08
9.875	13.6334	3.99E-09	-3.93E-09
10	13.6667	-6.19E-09	-8.82E-09
10.125	13.7001	1.27E-08	-3.69E-09
10.25	13.7334	3.20E-09	0.00E+00
10.375	13.7667	6.37E-09	-9.16E-09
10.5	13.8001	2.27E-08	9.35E-09
10.625	13.8334	-9.68E-09	-1.43E-08
10.75	13.8667	1.02E-08	2.98E-10
10.875	13.9001	-1.10E-08	-4.10E-10
11	13.9334	1.63E-08	1.64E-10
11.125	13.9667	9.59E-09	-6.62E-09
11.25	14.0001	2.08E-09	1.85E-10
11.375	14.0334	-3.04E-08	2.30E-08
11.5	14.0667	9.00E-09	-4.42E-09
11.625	14.1001	1.89E-09	1.03E-08
11.75	14.1334	-7.76E-09	1.16E-08
11.875	14.1667	7.96E-09	-1.17E-08
12	14.2001	-1.99E-08	6.56E-09
12.125	14.2334	-4.44E-09	-7.41E-09
12.25	14.2667	1.30E-09	-1.29E-08
12.375	14.3001	-1.55E-08	-3.70E-09
12.5	14.3334	1.54E-09	-1.49E-08
12.625	14.3667	7.76E-09	9.81E-09
12.75	14.4001	-7.99E-09	-9.63E-10
12.875	14.4334	1.07E-08	7.76E-09
13	14.4667	-1.41E-08	3.86E-09

Table B7 continued

longitude(x)	latitude(y)	Jnm	Knm
13.125	14.5001	8.59E-09	-1.26E-08
13.25	14.5334	4.24E-09	-8.40E-09
13.375	14.5667	1.05E-08	4.94E-09
13.5	14.6001	5.89E-09	0.00E+00
13.625	14.6334	-1.45E-10	-6.65E-09
13.75	14.6668	-1.59E-09	1.15E-08
13.875	14.7001	1.51E-08	4.05E-09
14	14.7334	1.91E-08	-2.02E-08
14.125	14.7668	1.32E-08	7.82E-09
14.25	14.8001	9.60E-09	-1.05E-08
14.375	14.8334	-1.59E-09	4.45E-09
14.5	14.8668	3.47E-09	1.78E-09
14.625	14.9001	-1.31E-08	7.14E-10
14.75	14.9334	-1.50E-08	-5.66E-09
14.875	14.9668	-4.63E-09	1.67E-09
15	15.0001	-1.70E-08	2.33E-09